NUREG/CR-7274

U.S.NRC
United States Nuclear Regulatory Commission
Protecting People and the Environment

Validation of a Computational Fluid Dynamics Method Using Horizontal Dry Cask Simulator Data

Office of Nuclear Regulatory Research

AVAILABILITY OF REFERENCE MATERIALS IN NRC PUBLICATIONS

NRC Reference Material

As of November 1999, you may electronically access NUREG-series publications and other NRC records at the NRC's Library at www.nrc.gov/reading-rm.html. Publicly released records include, to name a few, NUREG-series publications; *Federal Register* notices; applicant, licensee, and vendor documents and correspondence; NRC correspondence and internal memoranda; bulletins and information notices; inspection and investigative reports; licensee event reports; and Commission papers and their attachments.

NRC publications in the NUREG series, NRC regulations, and Title 10, "Energy," in the *Code of Federal Regulations* may also be purchased from one of these two sources:

1. **The Superintendent of Documents**
   U.S. Government Publishing Office
   Washington, DC 20402-0001
   Internet: www.bookstore.gpo.gov
   Telephone: (202) 512-1800
   Fax: (202) 512-2104

2. **The National Technical Information Service**
   5301 Shawnee Road
   Alexandria, VA 22312-0002
   Internet: www.ntis.gov
   1-800-553-6847 or, locally, (703) 605-6000

A single copy of each NRC draft report for comment is available free, to the extent of supply, upon written request as follows:

Address: **U.S. Nuclear Regulatory Commission**
Office of Administration
Multimedia, Graphics, and Storage & Distribution Branch
Washington, DC 20555-0001
E-mail: distribution.resource@nrc.gov
Facsimile: (301) 415-2289

Some publications in the NUREG series that are posted at the NRC's Web site address www.nrc.gov/reading-rm/doc-collections/nuregs are updated periodically and may differ from the last printed version. Although references to material found on a Web site bear the date the material was accessed, the material available on the date cited may subsequently be removed from the site.

Non-NRC Reference Material

Documents available from public and special technical libraries include all open literature items, such as books, journal articles, transactions, *Federal Register* notices, Federal and State legislation, and congressional reports. Such documents as theses, dissertations, foreign reports and translations, and non-NRC conference proceedings may be purchased from their sponsoring organization.

Copies of industry codes and standards used in a substantive manner in the NRC regulatory process are maintained at—

The NRC Technical Library
Two White Flint North
11545 Rockville Pike
Rockville, MD 20852-2738

These standards are available in the library for reference use by the public. Codes and standards are usually copyrighted and may be purchased from the originating organization or, if they are American National Standards, from—

American National Standards Institute
11 West 42nd Street
New York, NY 10036-8002
Internet: www.ansi.org
(212) 642-4900

Legally binding regulatory requirements are stated only in laws; NRC regulations; licenses, including technical specifications; or orders, not in NUREG-series publications. The views expressed in contractor prepared publications in this series are not necessarily those of the NRC.

The NUREG series comprises (1) technical and administrative reports and books prepared by the staff (NUREG–XXXX) or agency contractors (NUREG/CR–XXXX), (2) proceedings of conferences (NUREG/CP–XXXX), (3) reports resulting from international agreements (NUREG/IA–XXXX),(4) brochures (NUREG/BR–XXXX), and (5) compilations of legal decisions and orders of the Commission and the Atomic and Safety Licensing Boards and of Directors' decisions under Section 2.206 of the NRC's regulations (NUREG–0750).

NUREG/CR-7274

U.S.NRC
United States Nuclear Regulatory Commission
Protecting People and the Environment

Validation of a Computational Fluid Dynamics Method Using Horizontal Dry Cask Simulator Data

Manuscript Completed: November 2020
Date Published: December 2020

Prepared by:
Kimbal Hall, P.E.

Alden Research Laboratory, Inc.
Holden, MA 01541

Abdelghani Zigh, Senior Technical Advisor, U.S. NRC

Michelle Bales, NRC Project Manager

Office of Nuclear Regulatory Research

ABSTRACT

Applicants submit spent nuclear fuel dry storage cask designs to the U.S. Nuclear Regulatory Commission (NRC) for certification under Title 10 of the *Code of Federal Regulations* Part 72, "Licensing requirements for the independent storage of spent nuclear fuel, high-level radioactive waste, and reactor-related greater than Class C waste" [1]. The NRC staff performs its technical review of these designs in accordance with 10 CFR Part 72 and NUREG-2215, "Standard Review Plan for Spent Fuel Dry Storage Systems and Facilities," issued April 2020 [2]. To ensure that the cask and fuel material temperatures of the dry cask storage system remain within the allowable limits or criteria for normal, off normal, and accident conditions, the NRC staff performs a thermal review as part of the technical review.

Recent applications have increasingly used thermal-hydraulic analyses using computational fluid dynamics (CFD) codes (e.g., ANSYS-Fluent) to demonstrate the adequacy of the thermal design. The applicants are also looking to license casks with decay heat close to 50 kilowatts (kW), resulting in a peak cladding temperature (PCT) close to the temperature limit of 400 degrees Celsius (C) (752 degrees Fahrenheit (F)) suggested in NUREG-2215 [2]. It is part of CFD best practice guidelines to present CFD predictions for the PCT or any other target variable supported by an uncertainty quantification (UQ) to provide assurance and confidence that the obtained margin is adequate. For this reason, the NRC Office of Nuclear Material Safety and Safeguards asked the NRC Office of Nuclear Regulatory Research to be part of a dry cask storage system numerical modeling validation study to assist it in making regulatory decisions to ensure adequate protection for storage and transportation casks [3].

The NRC recognizes that CFD using finite volume is one of the methods for the applicants to perform dry cask thermal modeling and to demonstrate adequate margins with the temperature limits suggested in NUREG-2215 [2]. Additionally, when demonstrating the thermal margins, it is valuable to quantify the uncertainty in the simulation result as a function of the computational mesh and simulation inputs. When finite volume CFD is applied carefully through the use of CFD best practice guidelines in NUREG-2152, "Computational Fluid Dynamics Best Practice Guidelines for Dry Cask Applications," issued March 2013 [4], and UQ, there will be confidence and certainty in the obtained margins. As a participant in this CFD validation exercise, the NRC led the effort to include UQ and followed the CFD best practice guidelines in NUREG-2152 [4].

The numerical modeling validation study was based on data collected at Sandia National Laboratories (SNL) in an experiment sponsored by the U.S. Department of Energy (DOE) on a horizontal dry cask simulator (HDCS) [3]. The HDCS simulates one prototypic 9x9 boiling-water reactor fuel assembly, which uses electrical resistance heaters to simulate the decay heat. The power input in the experiment ranged from 0.5 kW to 5 kW. The fill gas was either helium or air. The fill gas pressure was either 100 kilopascals or 800 kilopascals (helium only). Extensive temperature measurements were made throughout the cask, including throughout the axial length of the fuel assembly and on different wall surfaces of the HDCS inside and outside the pressure vessel representing the dry cask canister. The measurements also included PCT and induced air mass flow rate.

Ten tests were conducted in the HDCS at SNL. Two tests were considered "open," in that the measured temperatures and airflow rates were provided to the participant modelers to benchmark and validate their CFD models. Following submission of the results of these two open cases, modelers predicted the air mass flow rate and temperature at 21 locations within

the case for the other eight cases. The simulation of these eight cases was considered "blind" in that the modelers submitted their simulation results before the experimental results were released.

This report discusses the validation and UQ of the HDCS CFD model using the experimental data gathered by SNL. Uncertainty quantification follows the procedures outlined in American Society of Mechanical Engineers (ASME) Verification and Validation (V&V) 20-2009, "Standard for Verification and Validation in Computational Fluid Dynamics and Heat Transfer" [5]. Sources of uncertainty examined in the analysis include iterative uncertainty, spatial discretization, experimental uncertainty, and uncertainty due to eight input parameters including ambient temperature, emissivity values, decay heat, fuel region porous media hydraulic resistance (i.e., a porous media model was used to model the fuel region), ventilated air straighteners porous media hydraulic resistance (i.e., porous media were used to model straighteners that were applied to obtain uniform airflow before mass flow rate measurements), sensitivity to certain gaps, orientation angle with respect to gravity, and external heat transfer coefficients. This report documents the HDCS CFD model validation exercise and is not intended to be used for regulatory guidance.

The CFD results and experimental data for PCT and location of PCT agreed very favorably for all the collected cases within the calculated validation uncertainty using best estimate CFD analysis that includes the most likely scenario analysis supplemented by UQ. The uncertainty in the wall emissivity values, and hence radiation heat transfer between surfaces within the fuel assembly and the pressure vessel, was found to be the principal source of uncertainty in the HDCS experiment. The PCT validation uncertainty was calculated to be higher for the air fill cases than for the helium fill cases. This result is attributed to the larger role that radiation heat transfer plays with air fill gas than it does with helium fill gas. Air thermal conductivity is almost one order of magnitude less than the conductivity of helium, so radiative heat transfer contributes more to the overall heat exchange to compensate for the minimal heat conduction of the air. The PCT validation uncertainty in helium cases varied between 6 to 20 degrees C (11 to 36 degrees F) for decay heat varying between 0.5 to 5 kW respectively. In the air fill cases, the PCT validation uncertainty varied between 8 to 40 degrees C (14 to 72 degrees F) for decay heat between 0.5 to 5 kW respectively.

Even though the validation uncertainty in this experiment is much less than the one obtained for the DOE cask demonstration documented in NUREG/CR-7260, "CFD Validation of Vertical Dry Cask Storage System," issued May 2019 [6], a smaller value would be preferred, especially for the air fill cases. Cask vendors have been submitting applications within PCT margins of approximately 10–20 degrees C (18–36 degrees F) from the specified temperature limit of 400 degrees C (752 degrees F) in NUREG-2215 [2]. To demonstrate that the CFD modeling process can produce this level of accuracy, the validation uncertainty should be minimized to the desired margin of 10–20 degrees C (18–36 degrees F) or less. Therefore, it is difficult to classify this experiment as CFD-grade for this explicit purpose with such a low temperature margin, particularly for the cases with air fill gas. If the cask vendors use a worst-case scenario and proven documented conservative input to perform their CFD predictions, they can avoid the UQ for input CFD variables. As such, the margins obtained by applicants would be compared with only the numerical uncertainty. The CFD predictions presented in analyses of this report, using CFD best practice guidelines documented in NUREG-2152 [4], showed that numerical uncertainty for all the cases varied between 0.4–4.9 degrees C (1–9 degrees F). Consequently, thermal models using documented conservative input parameters as usually used by applicants using CFD modeling guidelines documented in NUREG-2152 [4] would generally be deemed acceptable with adequately demonstrated thermal margins.

The results show that an ANSYS-Fluent thermal model using NUREG-2152 CFD best practice guidelines [4], including simulating the fuel assembly using a porous media approach, can demonstrate the safety of the storage of spent nuclear fuel by accurately predicting the PCT with accurate model inputs. This report also looks at the quality of the data collected in the HDCS experiment document [3] using the calculated validation uncertainty. The HDCS experiment was designed to minimize the validation uncertainty—a key factor and the basis for thermal model validation. Consequently, a well-validated thermal model will enable thermal reviewers to have confidence in the predictions, even with decreased margins.

The discussions and conclusion section of the Electric Power Research Institute (EPRI) DOE cask demonstration (demo) project report validation exercise [7] indicated that "CFD dry cask thermal models are generally conservative." However, the NRC cask demonstration CFD analysis as documented in NUREG/CR-7260 [6] showed that the EPRI report statement is acceptable only when conservative analysis is used. NUREG/CR-7260 [6] showed that if a best estimate model (i.e., most likely or base case scenario supplemented by UQ as done in this report) was used, the PCT and temperature field overpredictions can be explained in detail. In that thermal model round robin involving the DOE cask demonstration project [6] [7], geometrical uncertainties (i.e., gaps) were the main reasons for temperature prediction deviations as explained in detail by NUREG/CR-7260 [6], which showed a PCT validation uncertainty of 62 degrees C (112 degrees F) for the DOE cask demonstration exercise. This unusually high validation uncertainty was mainly caused by the uncertainty in the knowledge of the fluid gaps existing in the cask geometry. The validation exercise contained in this report, NUREG-2238, "Validation of a Computational Fluid Dynamics Method using Vertical Dry Cask Simulator Data," issued June 2020 [8], NUREG/CR-7260 [6], and the SNL validation synthesis report [9] [10] showed that CFD thermal model as described in this report, using CFD best practice guidelines as documented in NUREG-2152 [4] resulted in PCT predictions that agreed very favorably with the experimental data within the calculated validation uncertainty.

Three different modeling groups participated in the numerical validation and benchmarking exercise, including the NRC, Pacific Northwest National Laboratory, and Empresa Nacional del Uranio, S.A., S.M.E. [9]. The SNL validation synthesis report [9] states the following about the models used to validate the HDCS cases as presented in this report: "Based on the combined RMS error results, NRC model offered the best overall fit to the experimental data." The report also adds the following:

> NRC was the only institution that accompanied the base case model with uncertainty quantification…the NRC submission was an extensive effort that captures the effect of introducing simulation uncertainty bounds in the comparison of model results to experimental data. The method, which is derived from the ASME verification and validation approach in ASME V&V 20-2009, "Standard for Verification and Validation in Computational Fluid Dynamics and Heat Transfer" [5], is explored in the validation uncertainty section in Chapter 3 of the synthesis report [9], which shows how the uncertainty quantification can be used to provide a better measure of model prediction accuracies. Overall, this model validation method takes both measurement and simulation uncertainties into account and serves as an example of how the model validation uncertainty quantification can be further explored. By definition, NRC thermal model is considered validated if the combined RMS error normalized by the validation uncertainty is less than 1, and this was shown to be the case.

TABLE OF CONTENTS

LIST OF FIGURES

LIST OF TABLES

EXECUTIVE SUMMARY

The field of computational fluid dynamics (CFD) applications and technologies is rapidly expanding, with a large database of proven capabilities. The driving force for program development generally is not the nuclear community, as it was for the classical thermal-hydraulic system codes. Nevertheless, many CFD capabilities overlap with those required by the nuclear industry and, in particular, dry cask applications: flows in complex geometries, mixing in stratified fluids, flow separation and reattachment, turbulence, multiphase phenomena, chemical species interaction, and fire scenarios. Consequently, practitioners in areas related to dry cask applications can benefit from advances in CFD technology taking place in other industries. However, because of the complexity of modern commercial CFD packages, it is essential that care is taken with the inputs and equations used to avoid errors.

Dry cask storage is playing an ever-increasing role in storage of spent nuclear fuel. With no licensed repository for offsite waste storage and fuel pools that are filled far beyond their intended storage capacity, there is a push towards onsite dry cask storage. Additionally, the decay heat of the fuel that is to be placed in dry cask storage is increasing, which brings dry cask storage system temperatures closer to their limits. The accuracy afforded by CFD modeling is a useful tool for demonstrating compliance with thermal performance and, in particular, the temperature limit of 400 degrees Celsius (C) (752 degrees Fahrenheit (F)) specified for cladding in NUREG-2215, "Standard Review Plan for Spent Fuel Dry Storage Systems and Facilities," issued April 2020 [2].

The NRC is responsible for ensuring that applicants meet compliance standards such as Title 10 of the *Code of Federal Regulations* Part 72, "Licensing requirements for the independent storage of spent nuclear fuel, high-level radioactive waste, and reactor-related greater than Class C waste" [1], and NUREG-2215 [2]. Increasingly, this includes reviewing the applicant's CFD analysis to demonstrate compliance. Often, applicants will submit designs for consideration that have a margin of only 10–20 degrees C (18–36 degrees F), and sometimes less, between the predicted peak cladding temperature (PCT) value and the NUREG-2215 [2] specified cladding temperature limit of 400 degrees C (752 degrees F). This requires demonstrating that the simulation uncertainty is less than this margin, which can be a difficult task.

The introduction of the Electric Power Research Institute's phenomena identification and ranking table for thermal modeling [11] states that there are engineering simulations used for the design and licensing of spent fuel systems and other simulations used for improving the state of the art in computational research. The distinction is that the former provides decision makers with the necessary information about a system's performance and safety, whereas the latter aims at improving modeling and simulation codes and methods. The first approach takes a "conservative" approach with conservative model inputs, and the second approach uses a best estimate, "most likely or base case plus uncertainty" approach.

The conservative approach—which is to say using an accurate model (i.e., physics modeled correctly) with conservative geometric assumptions and boundary conditions—is useful for applicants. This approach minimizes the number of sensitivity runs needed to quantify the input uncertainty. However, it is still necessary to quantify the numerical uncertainty and to use a modeling process following CFD best practice guidelines as in NUREG-2152, "Computational Fluid Dynamics Best Practice Guidelines for Dry Cask Applications," issued March 2013 [4],

which has been demonstrated to have low uncertainty when validated against experimental data in problems with all of the same physical processes. Some applications contained CFD predictions that were within a margin of 10–20 degrees C (18–36 degrees F). To demonstrate that the modeling approach is accurate to that desired margin, there must be a model validation using best estimate analysis that includes a most likely base case supplemented by uncertainty quantification that demonstrates that the modeling approach to be used is capable of matching experimental data to within an accuracy of that margin.

Looking for validation experiments for CFD application to dry cask simulation for both design and safety studies, it appears that available data often suffer from a lack of local measurements, an insufficient number of measured flow variables, a lack of well-defined initial and boundary conditions, and a lack of information on experimental uncertainty. A working group on CFD application to nuclear safety of the Organisation for Economic Co-operation and Development-Nuclear Energy Agency-Committee on Safety of Nuclear Installations-Working Group on the Analysis and Management of Accidents (OECD-NEA-CSNI-WGAMA) established some requirements for CFD-grade experiments able to validate properly the single-phase CFD tools [12] [13] using existing information and based in ASME V&V 20-2009 [5]. These reports [5] [12] [13] found that the quality of the experiment used for the validation was a concern because many input parameters of value to the modeler were lacking. The discussion of this topic establishes whether this experiment is of a CFD grade. CFD-grade experiments should be able to validate a CFD model, and the main concern is to minimize the validation uncertainty on some selected figures of merit or target variable such as PCT.

Clear objectives should be first defined in an experimental program designed to validate a computational method. The success of the validation hinges on the constant collaboration between the experimentalist and the CFD specialist. This discussion should include the definition of the test section geometry, initial and boundary conditions, and the requirement for the measurement uncertainty. Agreement is necessary on what to measure, where it will be measured, and with which measurement technique. Acceptance criteria may be defined for the sensitivity of the measured parameters to the process of interest, or for the required accuracy of some selected physical quantity, or for both. Preliminary code simulations are necessary to define appropriate model boundaries and measurement locations, with sensitivity tests to determine the uncertainty of initial and boundary conditions and of measured field parameters. Iterations may be necessary to optimize the design.

The HDCS experiments that were performed by Sandia National Laboratories and discussed in this report provide valuable data for the dry cask storage system CFD model validation. The model inputs, temperatures, and flow rates were carefully measured, along with associated uncertainties, so that a full verification, validation, and uncertainty quantification analysis could be conducted, which resulted in a reasonable level of validation uncertainty. Perhaps the results of this study cannot justify modeling uncertainties of PCT prediction to within 10 degrees C (18 degrees F), especially when using air as the fill gas, but the overall accuracy of the modeling approach can be demonstrated.

In the HDCS validation effort, the largest source of uncertainty was found to result from the uncertainty in emissivity values of the various materials—particularly the Inconel cladding, the Zircaloy channel box, and the painted steel of the basket and pressure vessel. These are the hottest components within the HDCS experiment, and the emissivity value was found to vary spatially in addition to the uncertainty of the measurement at each location. Since radiation is the primary means of heat transfer within the fuel assembly at elevated temperatures and power levels, the emissivity values contributed the most to the uncertainty in the calculated PCT value.

For the 10 cases analyzed, 77 percent of individual temperature measurements were found to be within the simulation uncertainty band, and 9 out of the 10 cases predicted the PCT within the simulation uncertainty band. The air mass flow rate was not predicted as well, with 4 out of the 10 cases predicted within the uncertainty band of the experimental measurements. However, the calculated uncertainty band associated with mass flow rate was relatively small, at between 4–8 percent.

Overall, the dry cask modeling approach, including the use of porous media as a simplification of the detailed fuel assembly, was demonstrated to be an accurate way of simulating the heat transfer within the HDCS experiment.

ABBREVIATIONS AND ACRONYMS

2D	two-dimensional
3D	three-dimensional
ASME	American Society of Mechanical Engineers
BWR	boiling-water reactor
C	Celsius
CFD	computational fluid dynamics
DCS	dry cask simulator
DCSS	dry cask storage system
DOE	Department of Energy
EPRI	Electric Power Research Institute
F	Fahrenheit
GCI	grid convergence index
HDCS	horizontal dry cask simulator
HTC	heat transfer coefficient
K	kelvin
kg	kilogram
kPa	kilopascal
kW	kilowatt
k_{eff}	effective thermal conductivity
m	meter
MgO	magnesium oxide
mm	millimeter
NRC	Nuclear Regulatory Commission
PCT	peak cladding temperature
PIRT	phenomena identification and ranking table
PNNL	Pacific Northwest National Laboratory
RMS	root mean square
s	second
SIMPLE	Semi-Implicit Method for Pressure-Linked Equations
SNL	Sandia National Laboratories
TC	thermocouple
UQ	uncertainty(ies) quantification
V&V	verification and validation
VVUQ	verification, validation, and uncertainty quantification

1 INTRODUCTION

The U.S. Nuclear Regulatory Commission (NRC), along with two other modeling groups, participated in a blind benchmark study sponsored by the U.S. Department of Energy (DOE), aimed at assessing and improving the accuracy of computational fluid dynamics (CFD) simulations for dry cask storage systems (DCSS). Sandia National Laboratories (SNL) measured temperature data throughout the horizontal dry cask simulator (HDCS), along with induced air mass flow rate under steady-state conditions. Ten test cases were collected with the HDCS with fill gas of either helium or air and fill pressures of 100 kilopascals (kPa) to 800 kPa (helium only). Heating power input ranged from 0.5 kilowatts (kW) to 5 kW.

The NRC participated in this rare opportunity to validate and verify the CFD method used to simulate DCSS. This method used CFD best practice guidelines from NUREG-2152, "Computational Fluid Dynamics Best Practice Guidelines for Dry Cask Applications," issued March 2013 [4], and American Society of Mechanical Engineers (ASME) Verification and Validation (V&V) 20-2009, "Standard for Verification and Validation in Computational Fluid Dynamics and Heat Transfer" [5], to thoroughly quantify the simulation uncertainty for the temperatures and induced airflow through the cask.

Uncertainties quantification (UQ) starts by clearly identifying the various sources of uncertainties. The deficiencies or inaccuracies of CFD simulations can be attributed to many errors and uncertainties. These errors and uncertainties consist of two main broad categories. The first category is related to modeling physics, while the second is concerned with numerical aspects of the solution. The first category includes simplification of physical complexity, boundary and initial conditions, and physical boundary conditions. The second category includes computer programming, round-off, spatial discretization, temporal discretization, and iterative convergence.

The ASME V&V 20-2009 standard for verification and validation in CFD and heat transfer clearly states that the scope of V&V is the quantification of the degree of accuracy of the simulation of a specified validation variable at a specified validation point for cases in which the conditions of the actual experiment are simulated. Practically, ASME V&V 20-2009 affirms that, "The ultimate goal of V&V is to determine the degree to which a model is an accurate representation of the real world." This standard is strongly based on the use of experimental data for V&V and consequently for UQ. With this approach, the ASME standard strongly links V&V and UQ.

The ASME V&V 20-2009 standard methodology for uncertainty analysis underlines the role of V&V in evaluating the confidence in CFD results. Uncertainties have to be evaluated step by step, using clearly defined numerical aspects of the model such as time and space discretization (time step and mesh convergence) or physical models (turbulence models, physical assumptions) with associated evaluation of error.

The ASME V&V 20-2009 standard conforms to NRC regulatory practices, procedures, and methods for licensing dry cask systems as embodied in the *U.S. Code of Federal Regulations* and other pertinent documents such as Regulatory Guide 1.203, "Transient and Accident Analysis Methods," issued December 2005 [14], and NUREG-0800, "Standard Review Plan for the Review and Safety Analysis Reports for Nuclear Power Plants: LWR Edition," issued March 2017 [15].

The data from 2 of the 10 HDCS test cases were made open for the purpose of model validation. These two cases both had an input power of 2.50 kW, with a fill gas pressure of 100 kPa. One case had a fill gas of helium, and the other had a fill gas of air.

Following model validation with the two open cases, eight additional blind test cases were simulated without sharing of the data beforehand. Following submission of the simulation results of these eight conditions, with their associated simulation uncertainty, SNL released the temperature and airflow rate measurements to the modelers. The following report outlines the HDCS experiment, the CFD model used to simulate it, a detailed description of the model validation, and the findings from this process.

2 COMPUTATIONAL MODEL DESCRIPTION

This chapter describes the settings and boundary conditions that were used to simulate the HDCS.

2.1 Description of the Horizontal Dry Cask Simulator Experiment

Run by SNL, the experimental setup used for CFD validation is called the horizontal dry cask simulator (HDCS). Three different modeling groups participated in the numerical validation and benchmarking exercise, including the NRC, Pacific Northwest National Laboratory, and Empresa Nacional del Uranio, S.A., S.M.E. [9].

The HDCS consists of one prototypic 9x9 boiling-water reactor (BWR) assembly that is electrically heated. The fuel rod assembly is housed in a Zircaloy channel box, inside a painted steel basket, and surrounded by a painted steel cylindrical pressure vessel as shown in Figure 2-1. A stainless-steel vault surrounding the pressure vessel was designed with air vents as shown in Figure 2-2. The SNL report contains details of the HDCS geometry and design [3]. The HDCS system from the center to the periphery consists of the following:

- An existing electrically heated prototypic 9x9 BWR assembly has 74 fuel rods that span the first two-thirds of the assembly length and 66 fuel rods that span the last one-third of the assembly length, two water rods, seven grid spacers, bottom tie plate, and top tie plate. The fuel rods were instrumented with 97 thermocouples (TCs) along and across the fuel rods as shown in Figure 2-3. As shown in Figure 2-3 an alpha-alpha grid is used to identify fuel rods TCs. Also, the fuel assembly cross section plan view is identified by 4 quadrants as shown in Figure 2-3. Pin rod CS TC and water rod WEU TC locations are illustrated in Figure 2-3.
- Fuel rods are made of Incoloy cladding and filled with compacted magnesium oxide (MgO) powder to mimic the fuel pellets. Nichrome wire running through the middle of the MgO powder was used to supply a uniform electrical heat source along the length of the fuel rods. Both MgO powder and nichrome wire properties were chosen to match the thermal properties of the fuel pellet in a nuclear fuel rod.
- The channel box is made of Zircaloy surrounding the assembly instrumented with 25 TCs along the length.
- The storage basket is made of painted carbon steel and surrounds the channel box, instrumented with 26 TCs along the length of the basket.
- The pressure vessel is made of 10-inch Schedule 40 (10 in. Sch. 40) painted carbon steel pipe, with an inside diameter (ID) of 254.5 mm (10.02 in) with a maximum allowable working pressure (MAWP) of 2,400 kPa at 400 degrees Celsius (C) (752 degrees F) and is instrumented with 27 TCs along its length. The pressure vessel surrounds the storage basket as shown in Figure 2-1.
- The vault enclosure surrounding the pressure vessel is made of stainless steel and insulation material and is instrumented with 106 TCs.
- Air ducts feed the bottom of the vault with ambient air, and outlet vents at the top of the vault promote natural circulation through the vault.

- Flow straighteners at the four air duct inlets are used to induce uniform air across the air duct for easy measurement using hot wire anemometers.

The HDCS tests included heat input between 0.5 kW and 5 kW using either helium or air as a fill gas. The pressure of the fill gas was either 100 kPa or 800 kPa (helium only).

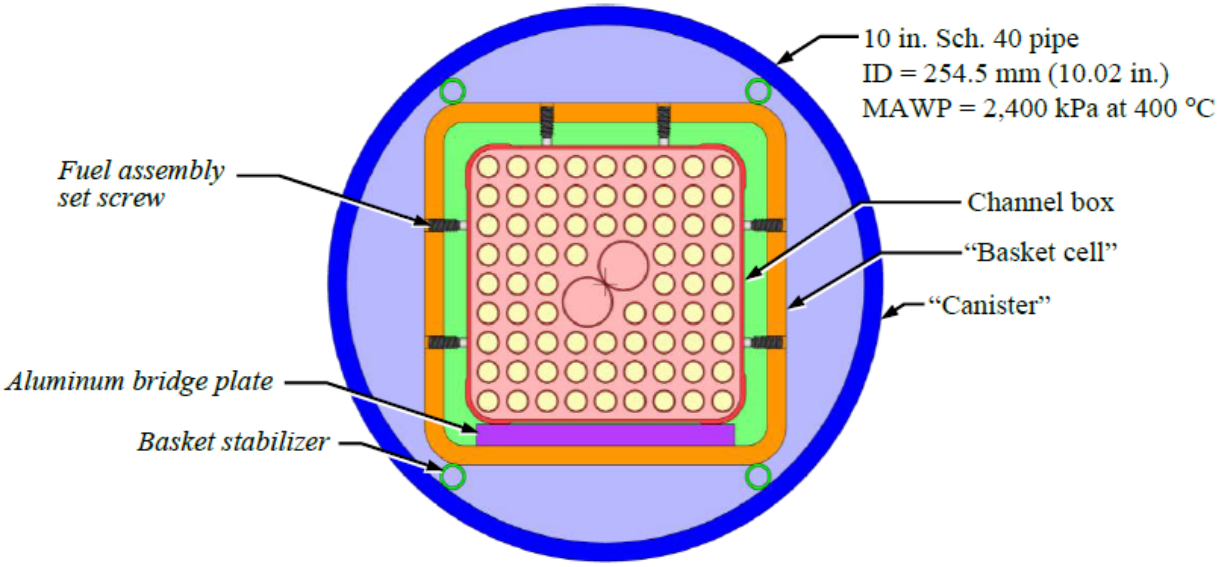

Figure 2-1 General design details of the HDCS [3]

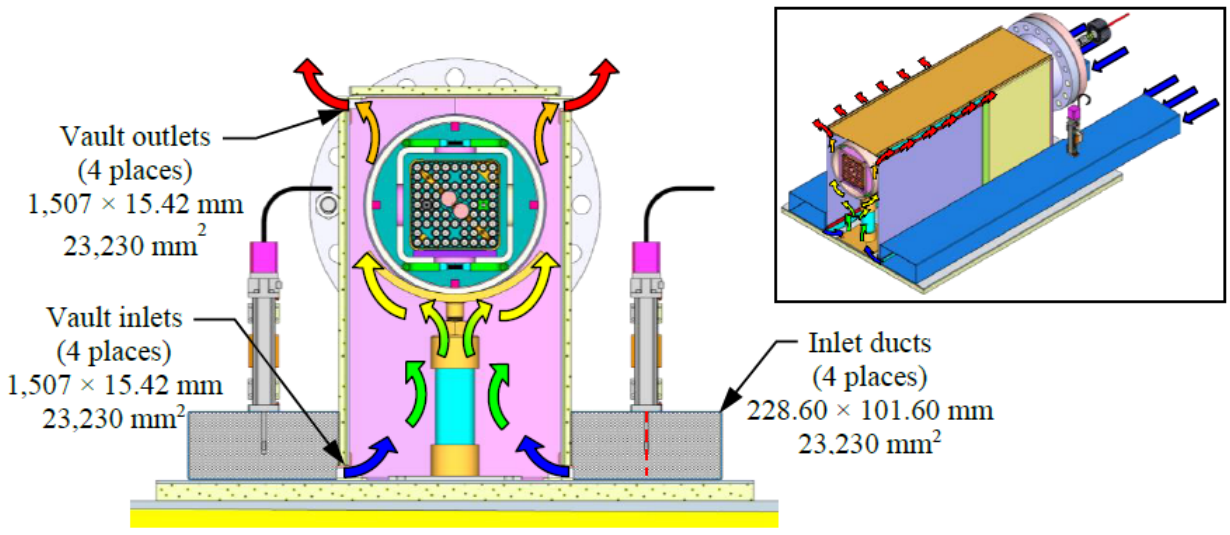

Figure 2-2 Airflow pattern in the HDCS from natural convection [3]

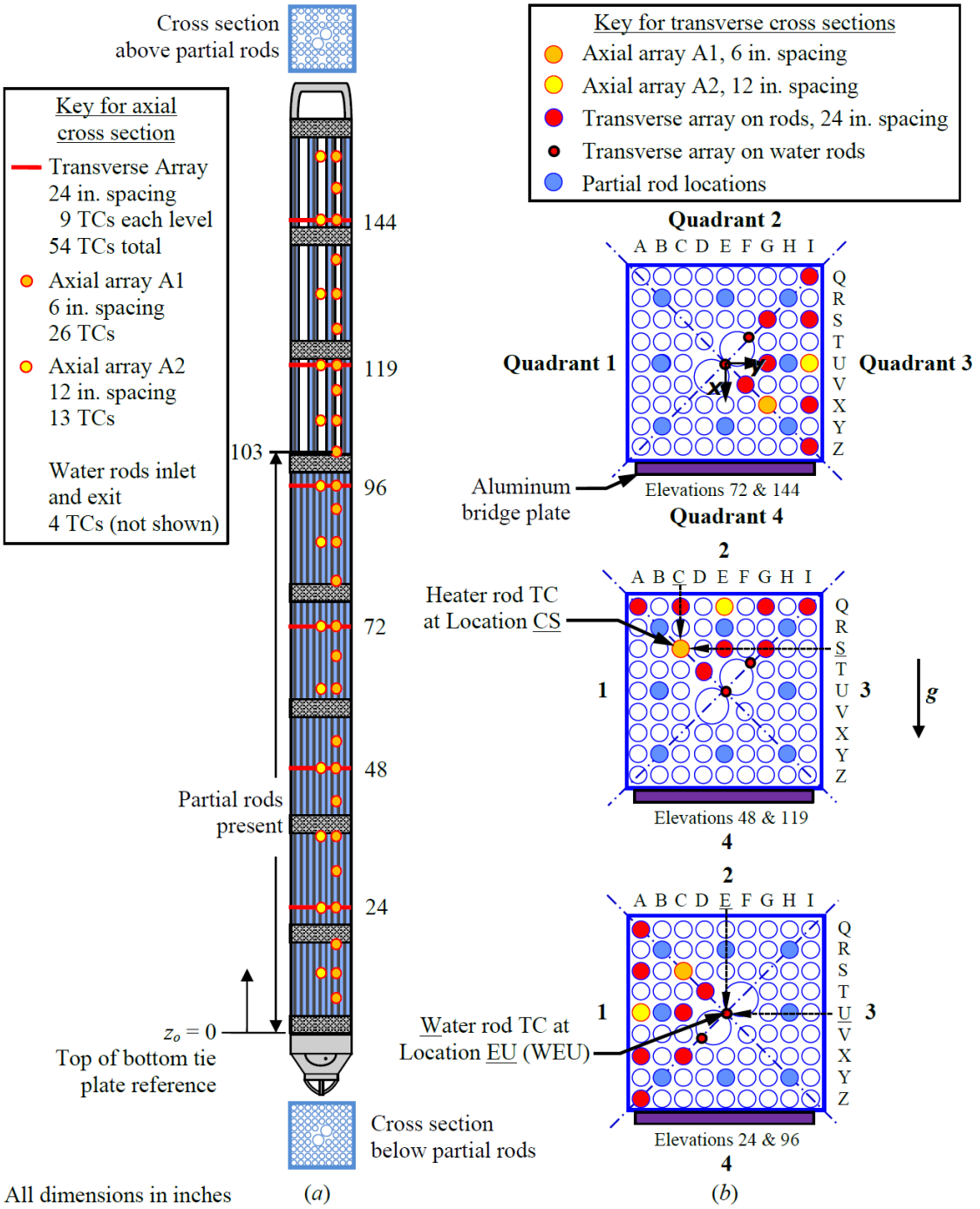

Figure 2-3 Experimental BWR assembly showing as-built *a*) axial and *b*) transverse thermocouple locations [3]

The cask was tested indoors in a cylindrical boiling test facility at SNL. Ten tests were recorded as explained in the Validation Results section of this report (Section 3). Of the 10 tests, 2 were open, and results were provided to modelers for use in validating their CFD models. SAND2019-11688R, "Update on the Thermal Hydraulic Investigations of a Horizontal Dry Cask Simulator," issued September 2019 [3], presents the results of these test cases.

The test consisted of a "thermal soak," in which the cask was allowed to reach steady-state temperatures over a period of time. The steady state was considered reached when the first derivative of all TCs was less than or equal to 0.3 Kelvin/hour (K/h). Once steady state was reached, transverse and axial temperature profiles, including peak cladding temperature (PCT) along with induced cooling airflow, were measured for a wide range of input heating levels and canister pressures using backfills of helium or air. These are the values that the modelers were asked to simulate.

2.2 HDCS Computational Fluid Dynamics Model Domain and Boundary Conditions for the Horizontal Dry Cask Simulator

A one-half symmetry three-dimensional (3D) CFD model of the HDCS apparatus was created, with the symmetry plane on the vertical, longitudinal axis of the fuel bundle assembly. The entire model domain was simulated in one model, which included the features both inside and outside the pressure vessel. To simplify the details of the fuel bundle assembly, a porous media approach was used to simulate the heat generation, hydraulic resistance, and thermal conductivity of the actual assembly. The boundary conditions and model inputs used in the CFD model were representative of those present during the experiment, as documented in the HDCS test description [3].

Figure 2-4 depicts the model domain, with a closer view of the inlet vent and pressure vessel internals shown in Figure 2-5.

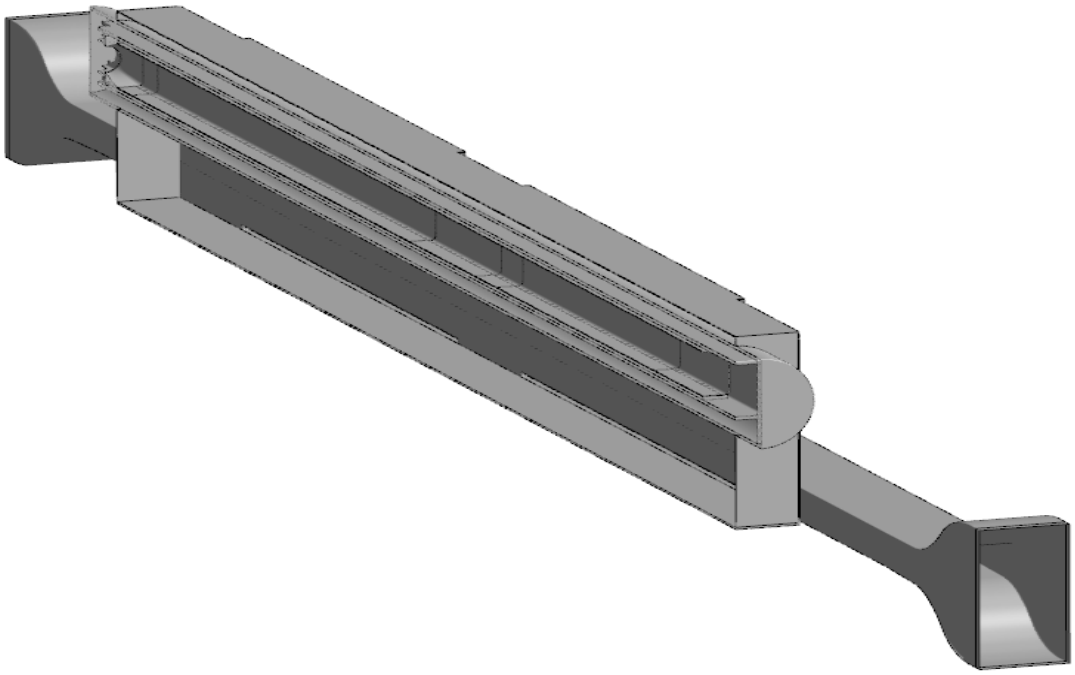

Figure 2-4 HDCS CFD model domain

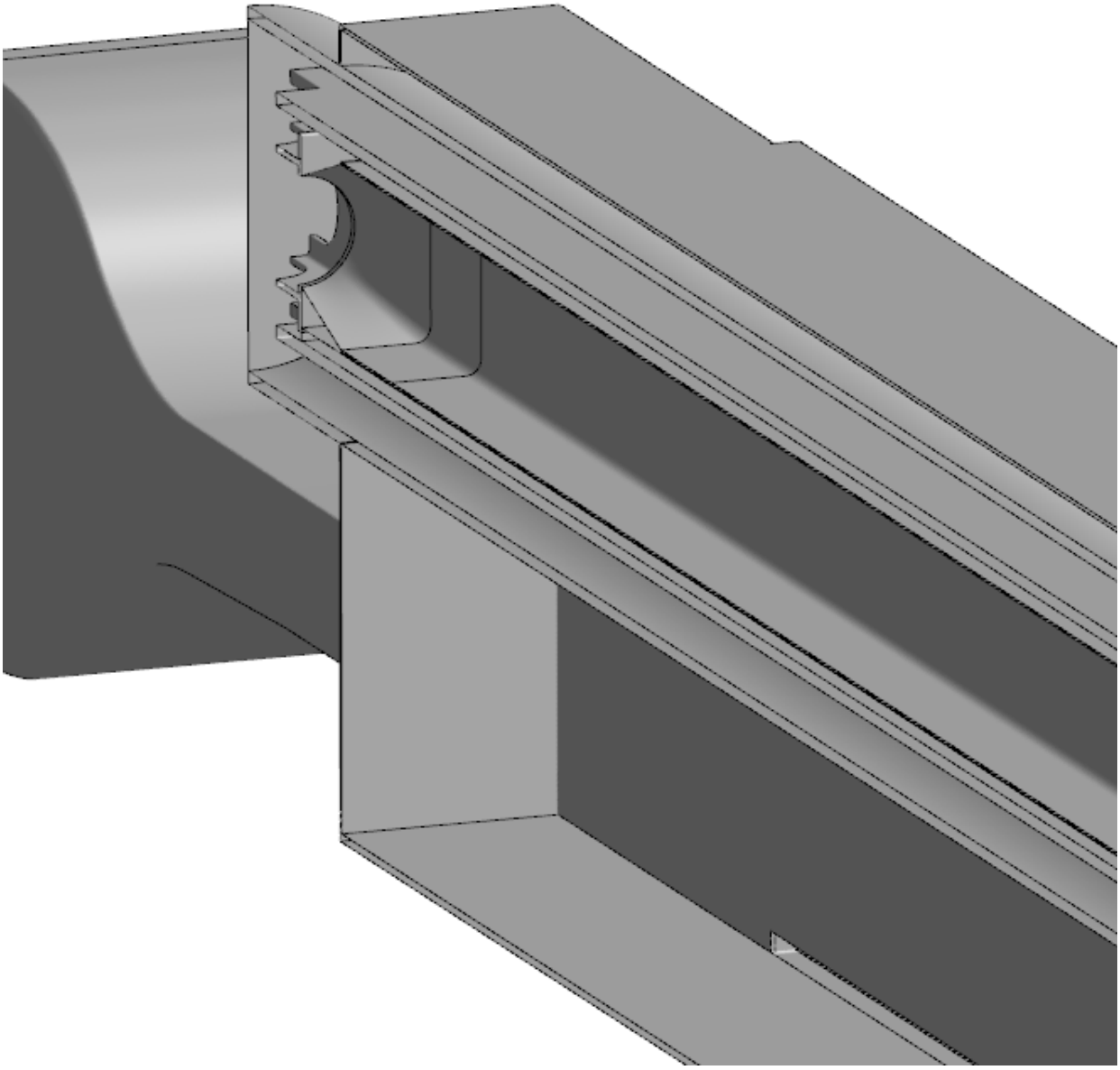

Figure 2-5 HDCS model domain—View of nozzle and inlet vent

2.2.1 Inflow Boundary Condition

The model inflow boundary was located at the inlet to the flow straighteners, with a constant pressure inflow boundary set to an ambient pressure of 83 kPa for all tests. The background turbulence was assumed to be negligible, and the inlet temperature was set to the ambient temperature measured for each test condition. The ambient density was calculated using the ideal gas law with ambient density, ambient temperature, and molecular weight of air equal to 28.966 gram/gram-mole (g/mol).

2.2.2 Inlet Flow Straighteners

The 25.8-millimeter (mm) (1-inch) thick honeycomb inlet flow straighteners at the inlet duct were modeled using porous media. The viscous loss through the inlet straightener in the axial direction was 2.7×10^6 m^{-2} as instructed in the test description [3], with two orders of magnitude higher resistance in the transverse directions to limit flow from one honeycomb cell to the next.

The viscous resistance of the honeycomb is calculated based on the open area and length of the honeycomb cells and does not include any inlet or outlet losses or any potential deformities that may influence the resistance to flow. An uncertainty in the viscous resistance of 30 percent is attributed to this calculated value for the input sensitivity calculations.

2.2.3 Outflow Boundary Condition

The model outflow boundary was located at the downstream end of the outlet vents and was simulated as a constant pressure boundary at the same ambient pressure as the inflow boundary (83 kPa). By specifying the model "operating density" as the ambient density external to the model domain, the simulation calculated the appropriate mass flow of air through the vault. This includes the chimney effect of having hotter gas within the vault than outside and works in conjunction with the constant ambient pressure boundary conditions at the CFD model domain inlets and outlets.

2.2.4 Material Properties

Temperature-dependent material properties for solids and fluids were implemented in the model, including density, thermal conductivity, and specific heat. These properties were obtained from [10] and [16].

Both helium and air were modeled using the ideal gas law, which applies the local temperature, pressure, and gas molecular weight to compute the local gas density. The molecular weight of helium was taken to be 4.04 g/mol, and the molecular weight of air was taken to be 28.966 g/mol. Viscosity, specific heat, and thermal conductivity were all assumed to be dependent on temperature and independent of pressure.

The pressure inside the pressure vessel was initialized to the correct value for each case analyzed (100 kPa or 800 kPa), and being a closed volume, the solution was always found to maintain the correct pressure while solving.

2.2.5 Solid Structures

All solid structures within the model domain were meshed and were included as volumes in the simulation. There was a 0.9-mm gap caused by a recess in the Zircaloy channel box, where it meets the aluminum bridge plate. SNL highlighted this gap as being of interest for a sensitivity study because of the effect that this gap had on heat transfer and the measured cladding temperatures. To facilitate this, the 0.9-mm gap was meshed as an independent fluid volume. This permitted the capability to turn this volume into solid Zircaloy to remove the gap and increase the rate of conductive heat transfer between the channel box and bridge plate.

Because of natural convection and the specific design of the HDCS, there is some differential heating of the channel box. Heat rising within the channel box can cause the top of the box to be hotter, whereas a conductive heat path through the aluminum bridge plate beneath the

channel box causes the bottom to be cooler. The effect of differential heating along the length of the channel box was investigated to see if there would be any bowing due to the top of the channel box being approximately 30 degrees C (54 degrees F) hotter than the bottom, as measured in the experimental data in the open cases. If this were the case, a gap would open up between the channel box and the bridge plate that the relatively small fuel assembly set screws may not be able to keep closed. However, it was determined that the weight of the channel box and heater rods was enough to overcome any deformation due to differential heating and maintain contact between the channel box and the bridge plate. The CFD model was run assuming there was intimate contact between the channel box and the aluminum bridge plate and also between the aluminum bridge plate and the painted steel basket.

The line contact between the basket stabilizer tubes and the pressure vessel was expanded into a narrow surface to facilitate meshing. The intermittently welded contact between the basket and the stabilizer tubes was similarly expanded. The top basket stabilizer tube was assumed not to be in contact with the pressure vessel, and a small gap was included in this area.

Items that were omitted from the domain include fuel assembly set screws, pressure vessel support posts, vault inlet and outlet vent vertical dividers, and the T-shaped pressure vessel structure below the pressure vessel lower flange.

2.2.6 Emissivity

The emissivity values used for each surface in the simulation were measured at room temperature for this experiment [3]. A number of replicate measurements were taken with different sensors, and this range of values, along with the published sensor uncertainty, was taken to be the uncertainty in the emissivity measurement at each location. For many of the components, especially the high-temperature components (Inconel cladding, Zircaloy channel box, painted steel basket and pressure vessel, and stainless-steel vault), the emissivity was measured in several locations. The spatial variation that was found added another degree of uncertainty to the emissivity measurements. While the emissivity at each location was fairly consistent with replicate measurements, the variation from one location to another was significantly greater in many cases. Many of the components in the HDCS have been used for several years in previous studies and have been exposed to surface oxidation at high temperature, which affects the local emissivity according to its temperature history. Since the emissivity measurements represented only a small fraction of the total surface area of these components, the spatial variation in emissivity measurements leads to a significant uncertainty in emissivity in areas that were not measured.

The average emissivity values used in the baseline case were taken as the average of all the measured values for each component. The emissivity uncertainty was taken as the difference between the average value and the end of the uncertainty band for the emissivity values with the greatest deviation from the average. Given the lack of spatial resolution of emissivity measurements, it is possible that this approach underestimates the uncertainty in emissivity values for the surface.

Emissivity values were assumed not to vary over the temperature range of the experiment. Table 2-1 lists the average emissivity values for each material, which were used in the baseline simulations. The table also lists minimum and maximum values, which were used in the emissivity sensitivity analysis.

In the case of Inconel, the maximum emissivity suggested [3] was not used. Instead, a maximum value of 0.90 was used, which is representative of a fully oxidized surface after extended exposure to air at elevated temperatures.

Emissivity measurements of the channel box indicate a stratification in Zircaloy emissivity along the axial length of the channel box at an approximate location of z = 2 m. The lower (full) portion of the fuel bundle was split at an axial coordinate of z = 2 m, to demark the boundary on the Zircaloy channel box where the emissivity goes from approximately 0.56 ± 0.11 below z = 2 m, to approximately 0.70 ± 0.09 above 2 m. The effective thermal conductivity (k_{eff}) values for the porous media inputs were calculated using the appropriate emissivity properties according to their location, and these emissivity values were also used on the exterior surface of the channel box.

The uncertainty in emissivity values was found to be the greatest source of uncertainty in the simulation. This is particularly true for the cases that used air as the fill gas since the primary mode of heat transfer within the pressure vessel is radiation, owing to the low thermal conductivity of air relative to helium.

Table 2-1 Emissivity Values

Material:	Average:	Minimum:	Maximum:
Aluminum	**0.20**	0.15	0.25
Inconel	**0.61**	0.54	0.90
Insulation	**0.90**	0.85	0.95
Painted Steel	**0.52**	0.45	0.59
Vault Base	**0.45**	0.40	0.50
Vault Sides	**0.28**	0.27	0.29
Zircaloy (Lower)	**0.56**	0.45	0.67
Zircaloy (Upper)	**0.70**	0.61	0.79

2.2.7 Heat Dissipation to the Environment

The outer surfaces bounding the control volume were allowed to exchange heat with the surroundings using both convection and radiation. An external convection coefficient was applied to these surfaces, which was calculated using a Nusselt number correlation for natural convection at the average wall temperature and orientation.

The outer surfaces were also allowed to radiate heat to the environment. The vault was covered in a 6-mm-thick layer of insulation, which had an emissivity of 0.90. Portions of the pressure vessel extended through the ends of the vault, and these sections were uninsulated. Their emissivity was set to that of painted steel at 0.52.

The heat transfer coefficient (HTC) from the top of the vault enclosure was calculated to be 6.0 W/m^2-K, the HTC from the sides of the vault enclosure vault and uninsulated sections of pressure vessel was calculated to be 4.0 W/m^2-K, and the external HTC from the bottom of the vault was calculated to be 2.0 W/m^2-K. The uncertainty in these Nusselt number calculations for the input sensitivity analysis was assumed to be ± 33 percent.

Ambient temperatures were measured during testing, and the measured ambient temperature was used as the heat sink temperature for both convection and radiation boundary conditions.

2.3 Modeling the Fuel Bundle Assembly Using Porous Media

To model the fuel region, porous media were used to approximate the complex arrangement of fuel rods inside the channel box by representing the components inside the assembly with an equivalent hydraulic resistance, thermal conductivity, and volumetric heat source. In the NRC's experience, all dry cask applicants favor the use of the porous media method because it greatly simplifies the configuration of the CFD model and saves on processing time. In NUREG-2208, "Validation of Computational Fluid Dynamics Methods Using Prototypic Light Water Reactor Spent Fuel Assembly Thermal-Hydraulic Data," issued March 2017 [17], the use of the porous media was validated and shown to give results comparable to those of the detailed model where fuel rods and grid spacers were represented. Section 3.1 of this document further characterizes the HDCS.

2.3.1 Hydraulic Resistance

Hydraulic resistance is set in the porous media in the axial and transverse directions to simulate the resistance that gas experiences when it flows around the fuel rods, water rods, and spacers within the assembly. The hydraulic resistance is made up of both viscous and inertial components and has different magnitudes in the axial and transverse directions. Although both directions are important, the flow patterns are most sensitive to whichever direction is aligned with gravity. In this case, with a horizontal arrangement of the fuel assembly, the simulation will be most sensitive to the transverse hydraulic resistance.

The equivalent viscous and inertial hydraulic losses in the transverse direction were obtained based on a two-dimensional (2D) CFD analysis of flow through the cross section of the full and partial fuel assembly sections. A range of superficial velocities across the tube bundles was analyzed, and a resulting pressure loss was found, which was converted to an equivalent resistance value.

Uncertainty in fuel hydraulic resistance was assumed to be ±50 percent, which contributed very little to the uncertainty of the simulation for the open cases because of the low circulation velocities in the fuel bundles. This indicates that very little of the heat within the fuel bundle is transferred via convection. Rather, heat is primarily transferred via conduction and radiation. This is preferred, as the k_{eff} calculation discussed next is based on the assumption that heat transfer is primarily by conduction and radiation, so high levels of convective heat transfer may introduce additional uncertainty into the calculation.

2.3.2 Effective Thermal Conductivity

The effective thermal conductivity (k_{eff}) represents radiation and conduction through the gas inside the assembly, as well as conduction through the fuel rods. The k_{eff} value is a strong function of temperature and has different magnitudes in the axial and transverse directions.

This approach also allows for heat convection within the assembly by transport of gas within the fuel bundle. The TRW Environmental Safety Systems, Inc. (TRW) report, "Spent Nuclear Fuel Effective Thermal Conductivity Report," dated July 11, 1996 [18], describes the k_{eff} approach in detail. In NUREG-2208 [17], calculations in the TRW report were confirmed by the developed model using CFD ANSYS-Fluent, which was then used to obtain the k_{eff} for the BWR 9x9 assembly.

To calculate the radial components of k_{eff}, a 2D CFD model representing the detailed cross section of an assembly was used, which included the water rods, heating elements, and fuel rod cladding. Heat transfer from the heating elements to the wall of the channel box is calculated via conduction and radiation only—no convection is included in the calculation. The k_{eff} was calculated for different boundary conditions including heating rate, channel box temperature, and emissivity values of Inconel and Zircaloy. The k_{eff} values were calculated as a function of temperature, and different values were computed for the partial (upper) and full (lower) sections of the fuel bundle because of the different internal geometry.

Axial components of k_{eff} were calculated using an area-weighted average of thermal conductivity of all the components in the fuel bundle, including the MgO heating elements, Inconel cladding, Zircaloy water rods, and the fill gas (either air or helium). Radiation is omitted from the calculation of the axial k_{eff} values. NUREG-2208 [17] explains in further detail how to obtain the proper porous media inputs.

Uncertainty in k_{eff} values was calculated based on the uncertainty in the emissivity values of Inconel and Zircaloy. New k_{eff} values were calculated for the full fuel rod section both above and below the 2 m axial location where the Zircaloy emissivity changed, as well as the partial fuel rod section. There is also a short length between the full and partial fuel rod sections where the partial fuel rods are still present, but not generating heat. In this section, the k_{eff} of the full fuel rods was used, but the heat generation rate of the partial fuel rods was applied.

2.3.3 Decay Heat

SNL provided the experimentally measured heat input value for each test, along with the associated uncertainty. The experimentally measured power input (in watts (W)) was uniformly distributed within each of two different sections of the fuel bundle assembly according to the number of heating rods in each section. The lower (full) section had 74 heating rods and a correspondingly higher heat generation rate (W/m^3). The upper (partial) section had 66 rods and a correspondingly lower heating rate (W/m^3).

2.4 Description of Mesh

The model geometry was built and created using Gambit version 2.4, and the same software was also used to create the mesh. The mesh was created using the best practice guidelines described in NUREG-2152 [4]. The fine mesh, which was used for the baseline evaluation and all the sensitivity simulations, had 12.8 million cells, with the vast majority being hexahedral cells. Tetrahedral cells were used in a very limited area around the nozzle and pedestal at the lower end of the fuel bundle assembly. Triangular prisms were also used in a few selected locations.

A coarse and medium mesh were also created to determine the numerical uncertainty due to spatial discretization, or the grid convergence index (GCI) as described in Section 3.4.4.2 of this document.

In the airflow region, a y+ close to unity was used to appropriately use the Low Reynolds k-epsilon turbulence model. CFD best practice guidelines were used for expansion ratio for successive volume meshing and mesh skewness.

Figure 2-6 shows a sample of the surface mesh on the channel box, bridge plate, basket, stabilizer tubes, pressure vessel, and vault for the baseline simulation. Figure 2-7 shows a cross sectional view of the baseline mesh at an axial location of z = 1 m, along with a temperature contour plot.

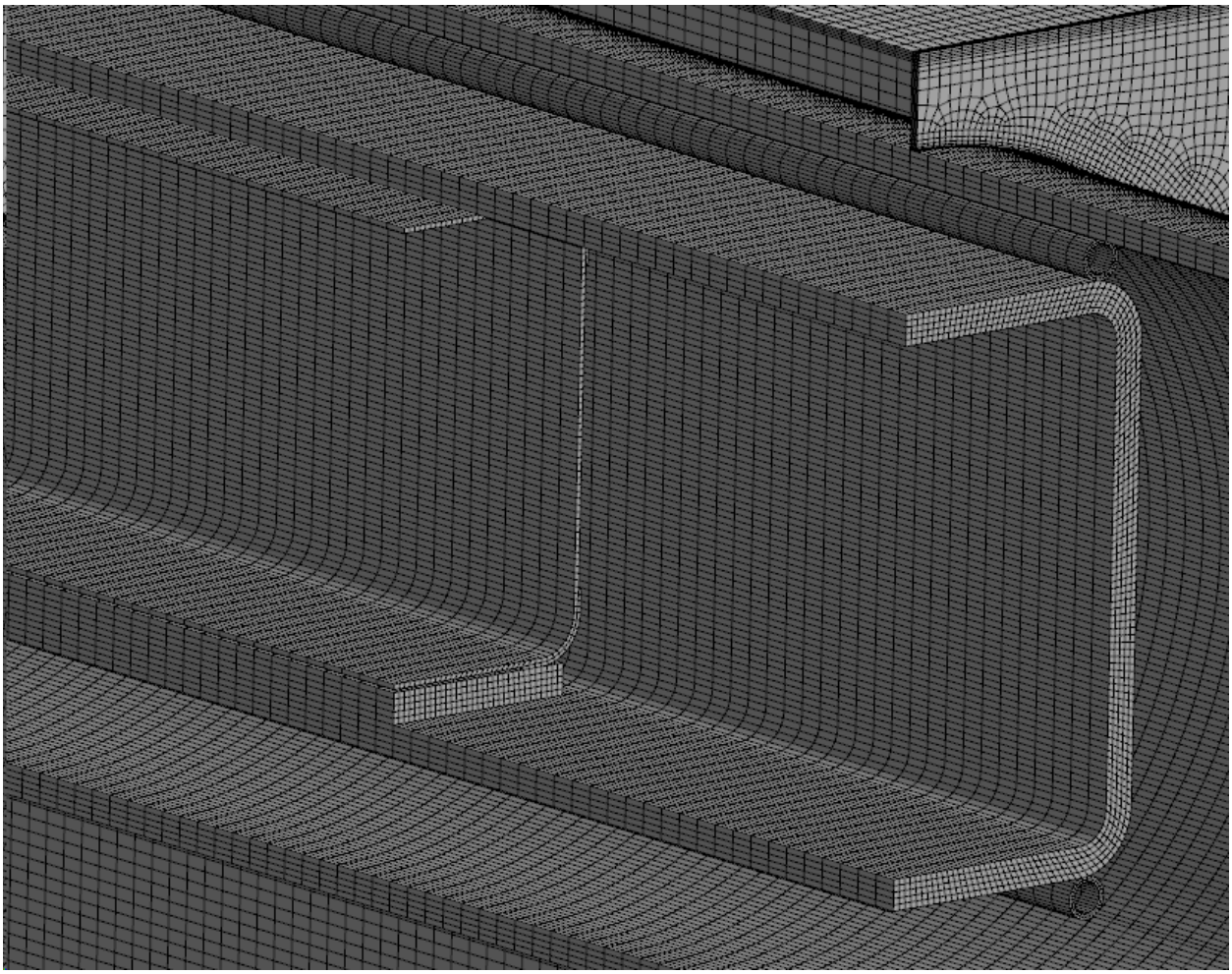

Figure 2-6 Surface mesh of channel box, bridge plate, basket, basket stabilizers, vessel, and vault at the upper end of the DCS apparatus

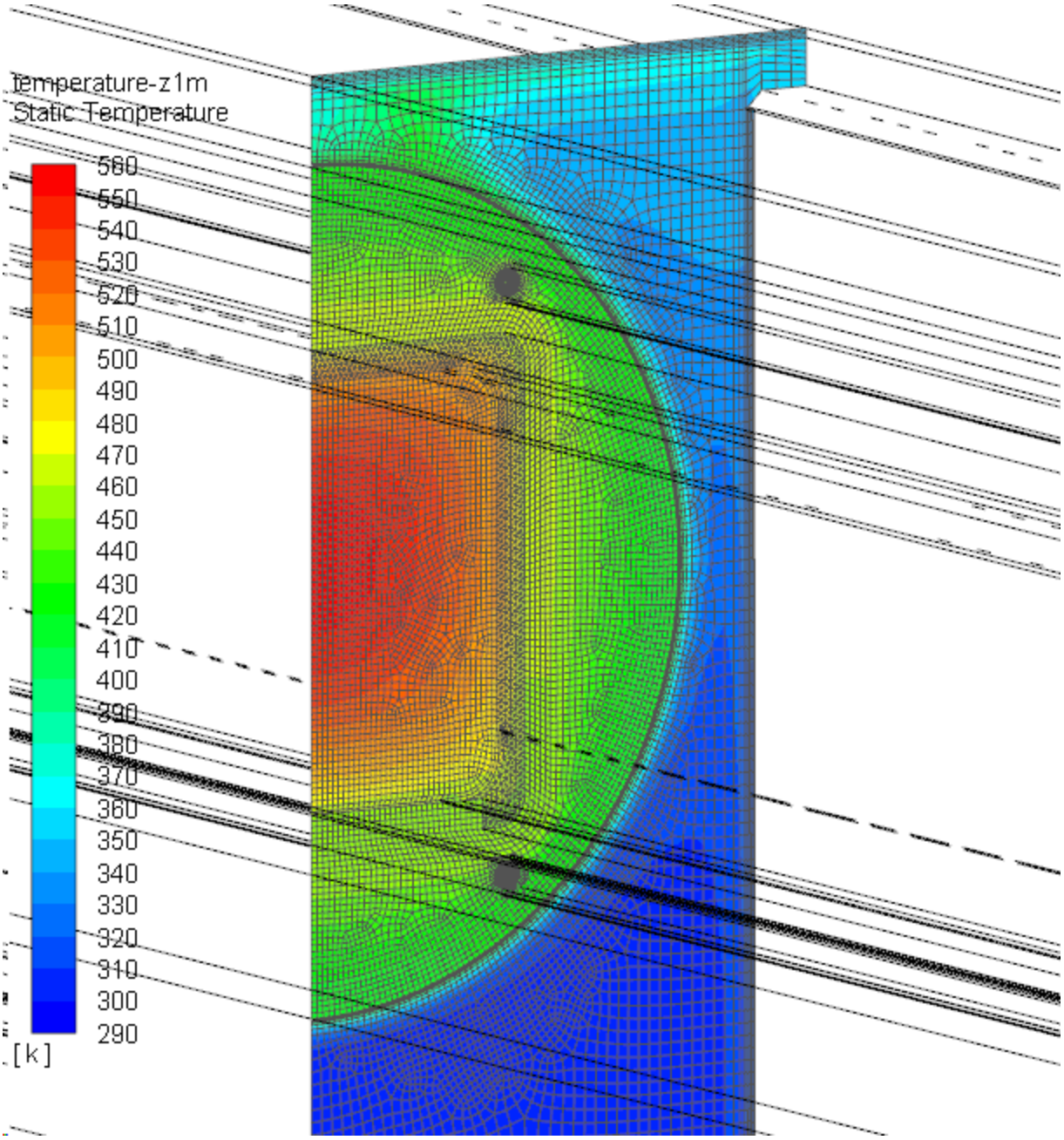

Figure 2-7 Contours of temperature (K) and view of mesh at z = 1m for the 2,500-W, 100-kPa, helium case

2.5 Solver Settings

The commercially available, finite-volume, computational fluid dynamics (CFD) code ANSYS-Fluent version 19.0 was used to simulate the 3D heat and flow patterns within the HDCS.

The gas inside the pressure vessel (helium or air) was assumed to be laminar, while the air outside the pressure vessel was assumed to behave according to the Low Reynolds k-epsilon turbulence model with full buoyancy effect on both the k and epsilon equations, available within the ANSYS-Fluent solver. No wall function model was used to integrate the turbulence equations all the way to the wall. Second order upwind discretization was used for all the conservation equations. Radiation heat transfer was modeled using the discrete ordinates model using second order upwind discretization. A pressure-based solver was used with the Semi-Implicit Method for Pressure-Linked Equations (SIMPLE) to link the conservation of momentum equation to the continuity equation. The Green-Gauss node-based method was used for gradient discretization. Body force weighted pressure interpolation was used.

Table 2-2 presents the solver settings used for all cases.

Table 2-2 CFD Solver Settings

CFD Solver Settings:	Input Value:
Solver Code	ANSYS-Fluent v19.0
Solver Type	Pressure-Based
Viscous	Laminar/Low Reynolds k-epsilon
Radiation	Discrete Ordinates, Gray Model
Pressure-Velocity Coupling Scheme	SIMPLE
Time Discretization	Steady-State
Spatial Discretization:	
Gradient	Green-Gauss Node Based
Pressure	Body-Force Weighted
Momentum	Second Order Upwind
Energy	Second Order Upwind
Discrete Ordinates	Second Order Upwind

3 VALIDATION RESULTS

The HDCS CFD model was validated with two open cases provided by SNL with complete experimental results, which were available to all modelers. Both cases had a total heat input of 2.5 kW, and a fill gas pressure of 100 kPa. The difference between the two open cases was the fill gas in the pressure vessel. One case used helium, and the other used air.

In addition to the two open cases, there were eight blind cases where the experimental results were not provided until after the CFD results were submitted. The uncertainty for all cases was rigorously calculated using the same process according to ASME V&V 20-2009. This section describes in detail the validation effort undertaken for the two open cases and compares the results to the experimental data. Section 4 of this document discusses the results of the blind simulations—although the blind cases were subject to the same level of uncertainty quantification (UQ), the description of the process will be much briefer.

3.1 Two-Dimensional Comparison of Porous Media Approach with Explicit Modeling

As an initial validation effort, the accuracy of the porous media approach for this application was evaluated as a 2D simulation of the HDCS for both open cases. The boundary conditions for the 2D model were similar to the two open cases with 100-kPa fill gas pressure, and 2.5 kW of heat applied, so the temperatures are expected to be representative of the full 3D geometry at the peak temperature location, where the axial temperature gradient is zero.

The explicit case with fuel rods fully resolved had the heat uniformly applied to the MgO heating elements, whereas the porous media case had the heat uniformly applied to the entire volume inside the channel box. Since the 2D model is simulating the location of axial peak temperature, which occurs in the lower full fuel rod section, the explicit model has the full complement of heater rods, and the heat generation rate corresponds to the lower full fuel rod section as well.

The 2D simulation does not include an inlet flow straightener with associated resistance. Instead, a reduced inlet pressure boundary condition of -0.15 pascal gauge was used inside the inlet duct, which was taken from the baseline 3D CFD results at the same location.

The vertical and horizontal temperature profiles through the centerline of the vault are plotted for the porous and explicit 2D simulations over the experimental results that were provided for the open helium case [3] in Figure 3-1 and Figure 3-2. Also, Figure 3-3 provides contour plots comparing the temperature profiles in the porous and explicit 2D simulations.

Outside of the channel box, the mesh for the porous and explicit CFD cases is identical. The results for the porous and explicit cases are also nearly identical outside the channel box, and match very well with experimental data. The horizontal and vertical transects of experimental data are taken at two different axial locations (z = 1.219 m for vertical, and z = 1.829 m for horizontal); however, this is in a region of very little axial variation in temperature.

Inside the channel box, the meshes for the porous and explicit 2D CFD models are different, but they both give similar temperature results, which closely match the experimental data. The explicit mesh exhibits a stepwise temperature profile, as each fuel rod is nearly isothermal, and the primary thermal resistance is the heat transfer between rods. The porous media approach

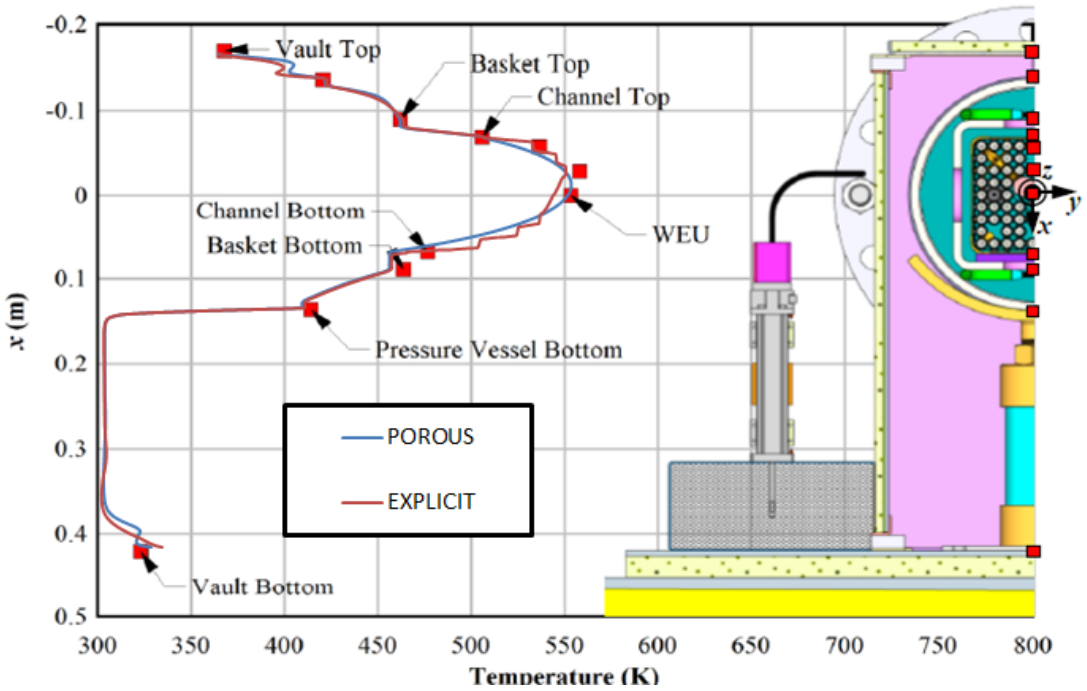

Figure 3-1 Experimental results for the vertical temperature profile for 2.50 kW, z = 1.219m, and helium at 100 kPa (red squares) with porous and explicit 2D results overlaid

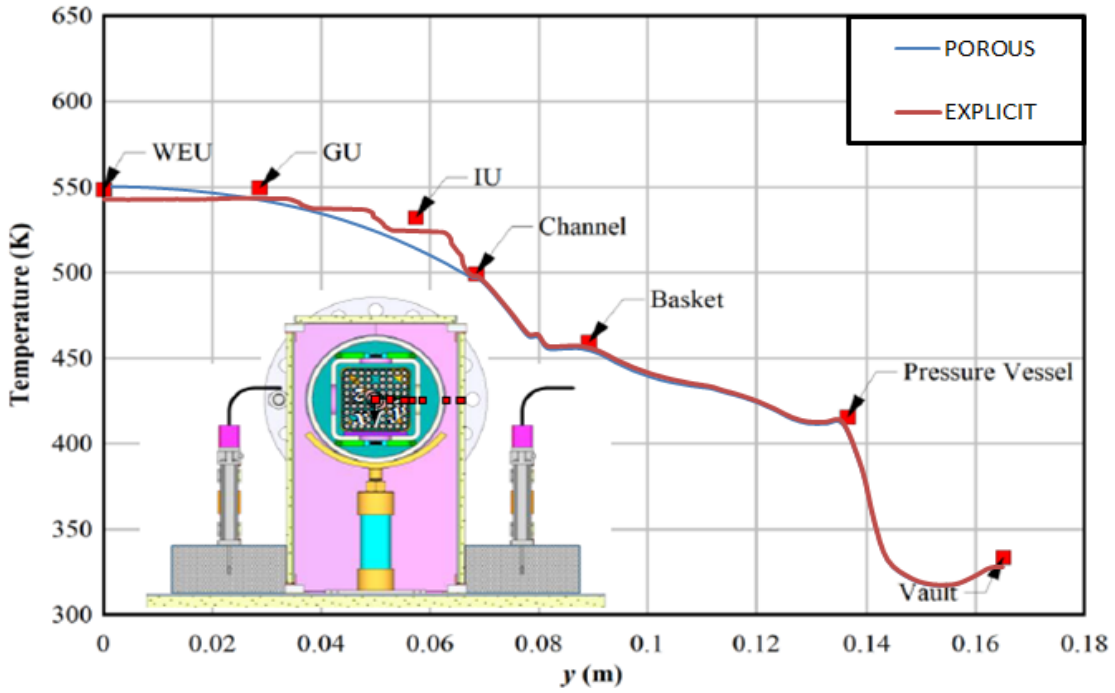

Figure 3-2 Experimental results for the horizontal temperature profile for 2.50 kW, z = 1.829m, and helium at 100 kPa (red squares) with porous and explicit 2D results overlaid

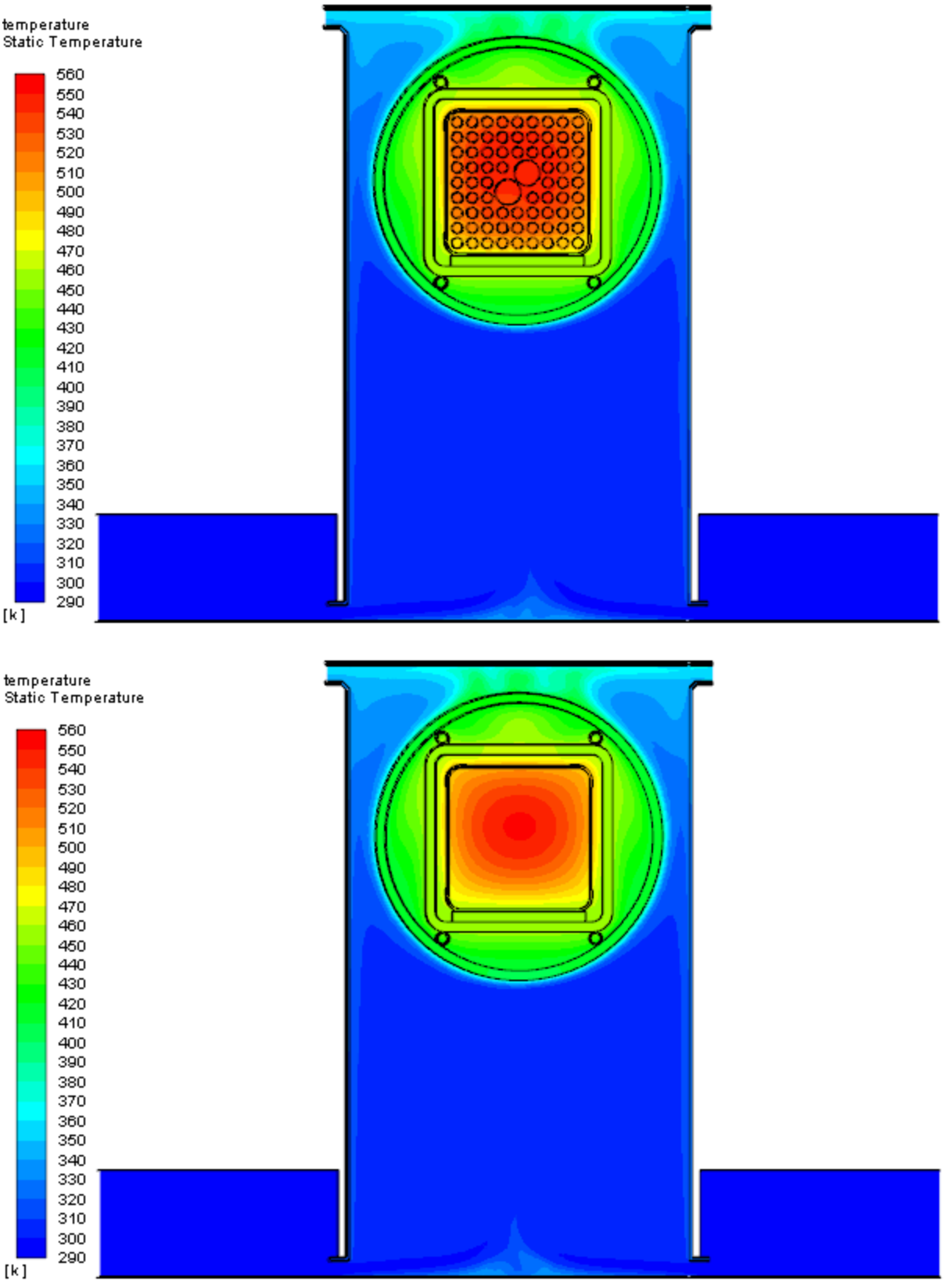

Figure 3-3 2D simulation of open case with helium (explicit above and porous below)

contains a smoother temperature profile, since the k_{eff} approach approximates the discrete fuel rods with a continuous function.

Another notable effect in the porous media approach, which is discernible in both the temperature profile plots in Figure 3-1 and Figure 3-2, as well as the temperature contours in Figure 3-3, is that it tends to concentrate the heat more in the center of the fuel bundle. In an actual fuel bundle, there is no heat generation in the very center, as that is the location of the water rods. Instead, the heat generation is around the perimeter of the fuel bundle, which elevates the temperature on the shoulders of the fuel bundle and gives a flatter temperature profile through the center. This leads to a slight underestimation in temperatures as shown in Figure 3-2 of pins such as in pin location (IU) with the porous media approach (i.e. pin (IU) TC is located in quadrant 3 in Figure 2-3).

Even with these small deviations between the two approaches, the porous media 2D CFD simulation results very closely match both the explicit 2D CFD simulation result and the experimental measurements. This is particularly true for the peak temperature values in the bundle, which are considered to be the most important values to match correctly for dry cask simulations. The porous media approach saves considerable time and effort in the simulation of casks, particularly with multiple fuel assemblies, and does not detract from the accuracy of the PCT prediction.

All the same conclusions may be drawn from the open case with air fill gas. Figure 3-4 and Figure 3-5 provide the vertical and horizontal temperature profile plots for the air case, with the temperature contour plots for the explicit and porous 2D cases shown in Figure 3-6.

Another observation to be drawn from the 2D CFD results in Figure 3-3 and Figure 3-6 is that the flow patterns within the vault and pressure vessel are indeed symmetric about the vertical axis. It is conceivable that the jets issuing from the inlet vents could become biased to one side of the enclosure, but this is not observed. The observation of symmetric flow patterns in the 2D simulation substantiates the use of a half-symmetry model in the full 3D simulation.

Table 3-1 compares the PCT and air mass flow rate for the helium explicit and porous 2D case.

Table 3-1 2D Porous and Explicit PCT and Mass Flow Results

Case	PCT (K)	Mass Flow (kg/s)
Helium—explicit	549.5	0.000102
Helium—porous	552.3	0.000103

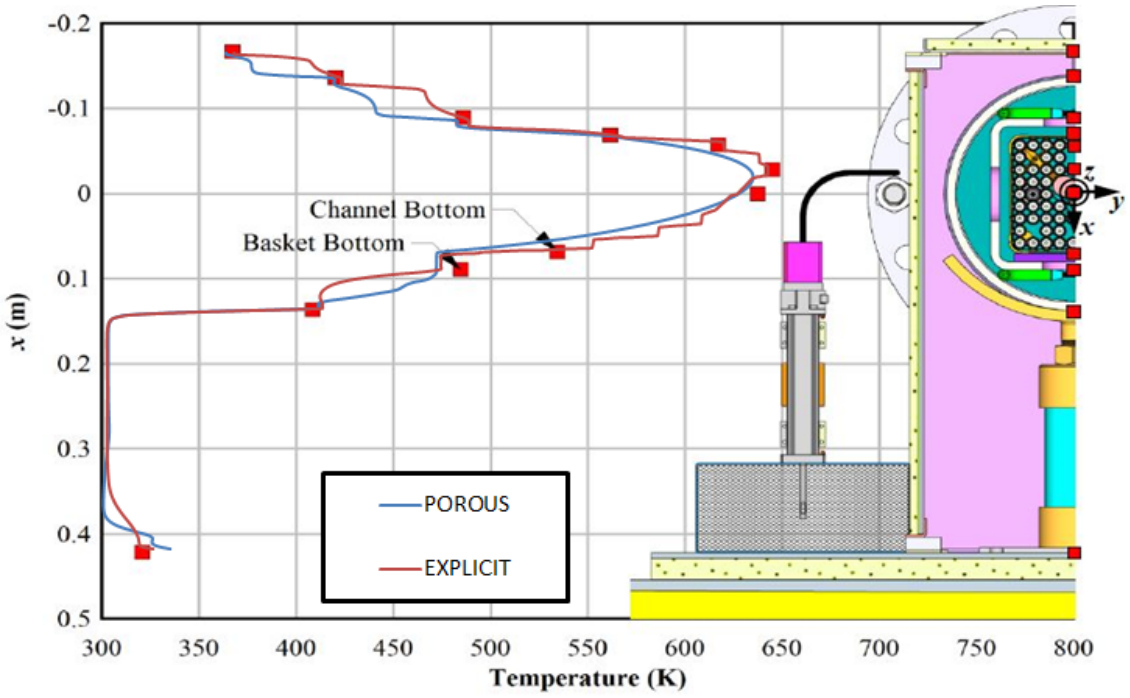

Figure 3-4 Experimental results for the vertical temperature profile for 2.50 kW, z = 1.219 m, and air at 100 kPa (red squares) with porous and explicit 2D results overlaid

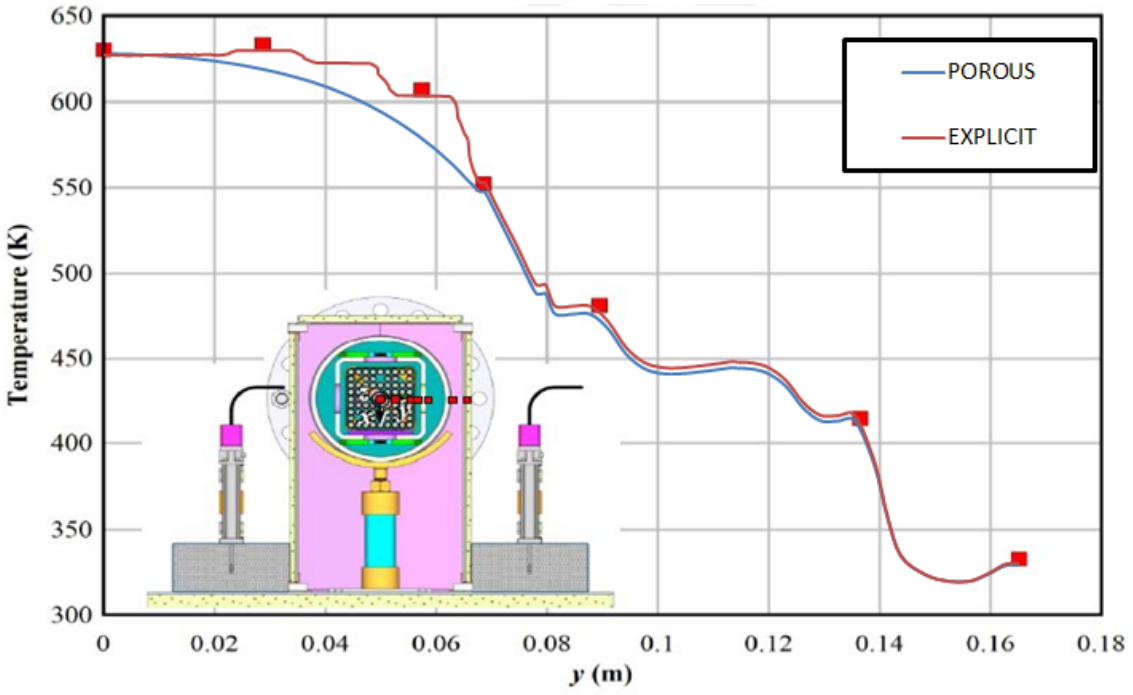

Figure 3-5 Experimental results for the horizontal temperature profile for 2.50 kW, z = 1.829 m, and air at 100 kPa (red squares) with porous and explicit 2D results overlaid

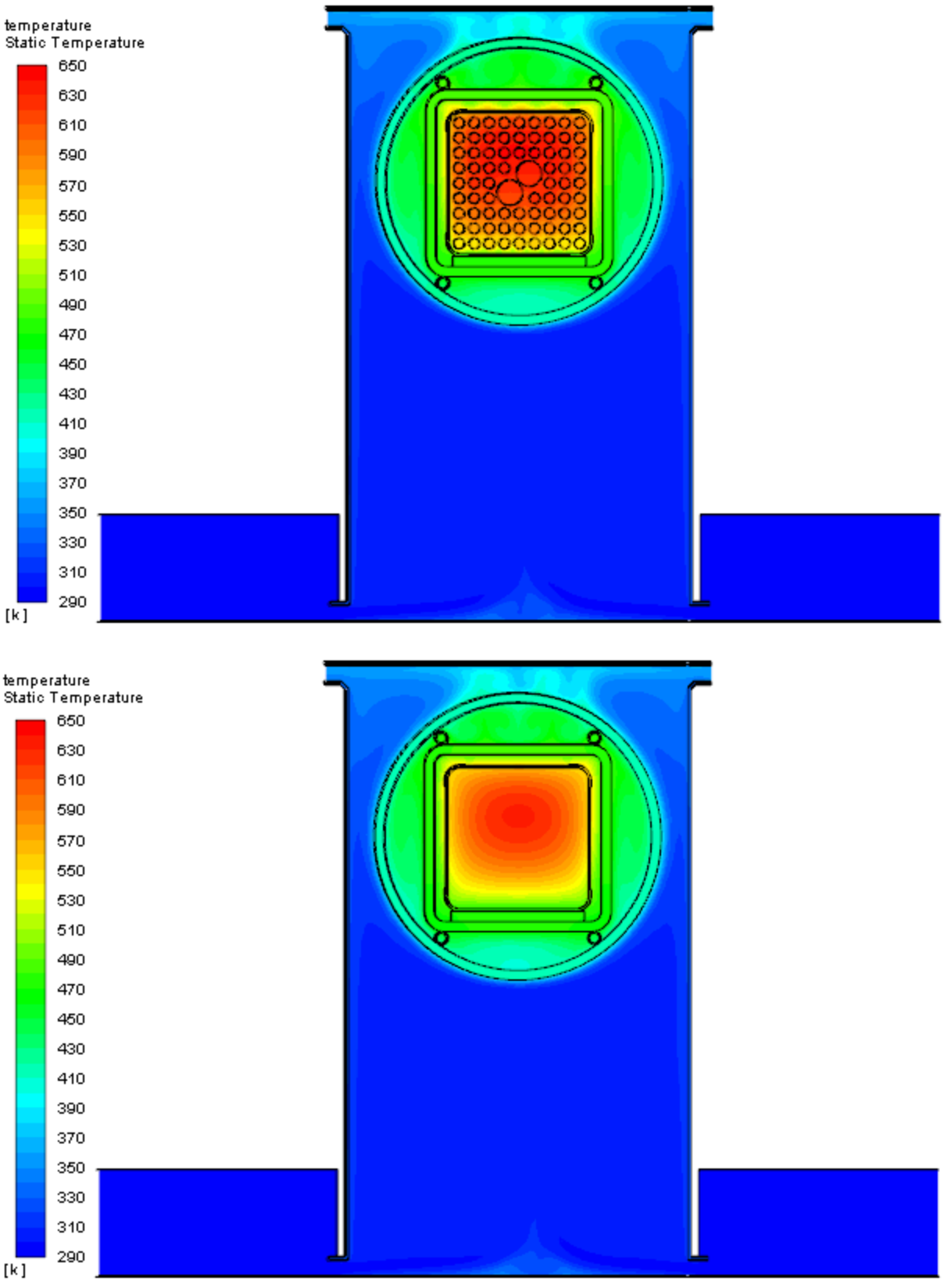

Figure 3-6 2D simulation of open case with air (explicit above and porous below)

3.2 Baseline Simulation Results

Using the porous media approach, heat is uniformly generated throughout the cross section of the channel box, and the channel box is broken into several sections along its axis representing areas where there is a full heater layout, partial heater layout, unheated sections, and changes in emissivity values. In the model, this heat is conducted through the porous media based on the local temperature-dependent k_{eff} value, which represents the combined radiation and conduction heat transfer in the actual fuel assembly. Additionally, the fill gas is allowed to flow because of natural convection within the porous media, but the effective hydraulic resistance due to the fuel rods, both in the axial and transverse directions, somewhat restricts the flow of the gas. Figure 3-7 presents the cross-sectional views of the temperature in the 3D simulation for the baseline helium case, and Figure 3-8 presents those for the baseline air case. Note the similarity to the 2D results in Figure 3-3 and Figure 3-6. In addition, Figure 3-11 shows an axial cross section view of the temperature along the symmetry plane for the baseline case with helium.

At high temperatures, heat transfer occurs primarily because of radiation, so the velocity within the fuel assembly due to convection is minimal. This is especially true with helium fill gas, where conduction is an order of magnitude greater than air, so velocity due to convection is limited further. The flow patterns inside the pressure vessel can be seen in Figure 3-9 for the baseline case with helium and Figure 3-10 for the baseline case with air. In the air case, there is more convection outside of the basket; however, both cases have very low velocity within the fuel assembly.

Heat generated within the fuel bundle is conducted through the metal of the channel box and is able to conduct, convect, or radiate through the fill gas to the painted steel basket. Heat may also pass through the bottom of the channel box through an aluminum bridge plate into the basket. There is a 0.9-mm deep recess in the bottom of the channel box that limits the contact area between the channel box and the bridge plate. Gas is also allowed to convect through the ends of the channel box, which is open at one end, and is partially restricted with a nozzle at the other end. However, this mode of heat transfer was found to cause very little convection and thus very little heat transfer.

From the basket, heat can again conduct, convect, or radiate through the fill gas to the painted steel pressure vessel, or it can conduct through the stabilizing tubes at the corners of the basket. It was assumed that the bottom stabilizer tubes are in contact with the pressure vessel and that a small gap exists between the top stabilizer tubes and the pressure vessel.

From the pressure vessel, heat is allowed to conduct, convect, or radiate to the air inside the vault and the vault enclosure, which is constructed of low-emissivity stainless steel. In this case, much more of the heat is transferred to the ambient air through convection, which can be seen in the higher velocity values outside the pressure vessel in Figure 3-9 for the baseline case with helium and Figure 3-10 for the baseline case with air.

The heated air creates a chimney effect within the vault, whereby the lower air density within the vault draws ambient air into the vault through the inlets, which are at a lower elevation, and expels hot air through the outlet vents, which are at the top of the vault. Heat is also expelled through the walls of the vault and through either end of the pressure vessel, which project out through the ends of the vault enclosure. Calculating the correct air mass flow rate requires achieving the correct heat balance, as well as setting the correct hydraulic resistance of gas flowing through the vault.

The flow through the inlet ducts is initially very uniform because of the inlet flow straighteners and the smooth contraction of the inlet nozzle. This aids flow measurement in a straight section of inlet duct before the airflow reaches the vault inlet vents. Once the airflow reaches the inlet vents, the flow inside the inlet duct quickly becomes nonuniform as it turns and accelerates through the vent, reducing the axial velocity within the inlet duct (Figure 3-12).

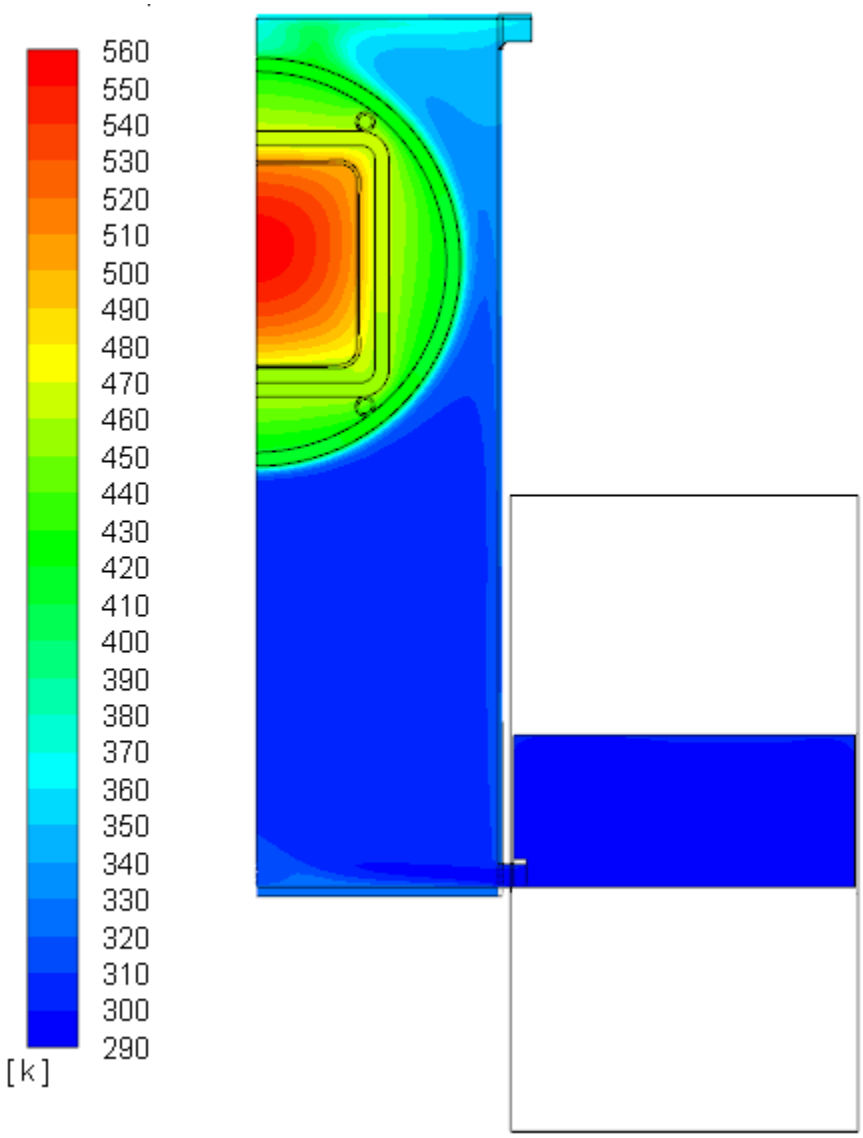

Figure 3-7 Temperature (K) in baseline 3D simulation of open case with helium at z = 1 m

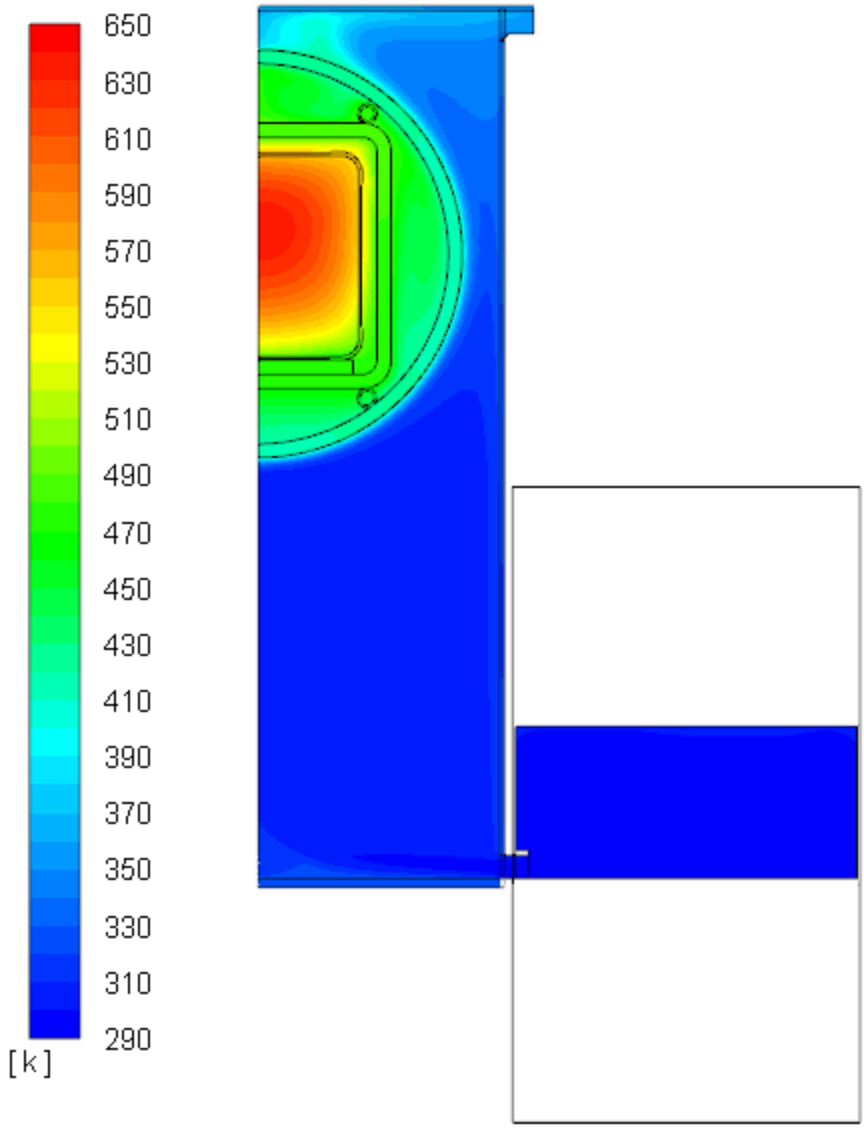

Figure 3-8 Temperature (K) in baseline 3D simulation of open case with air at z = 1 m

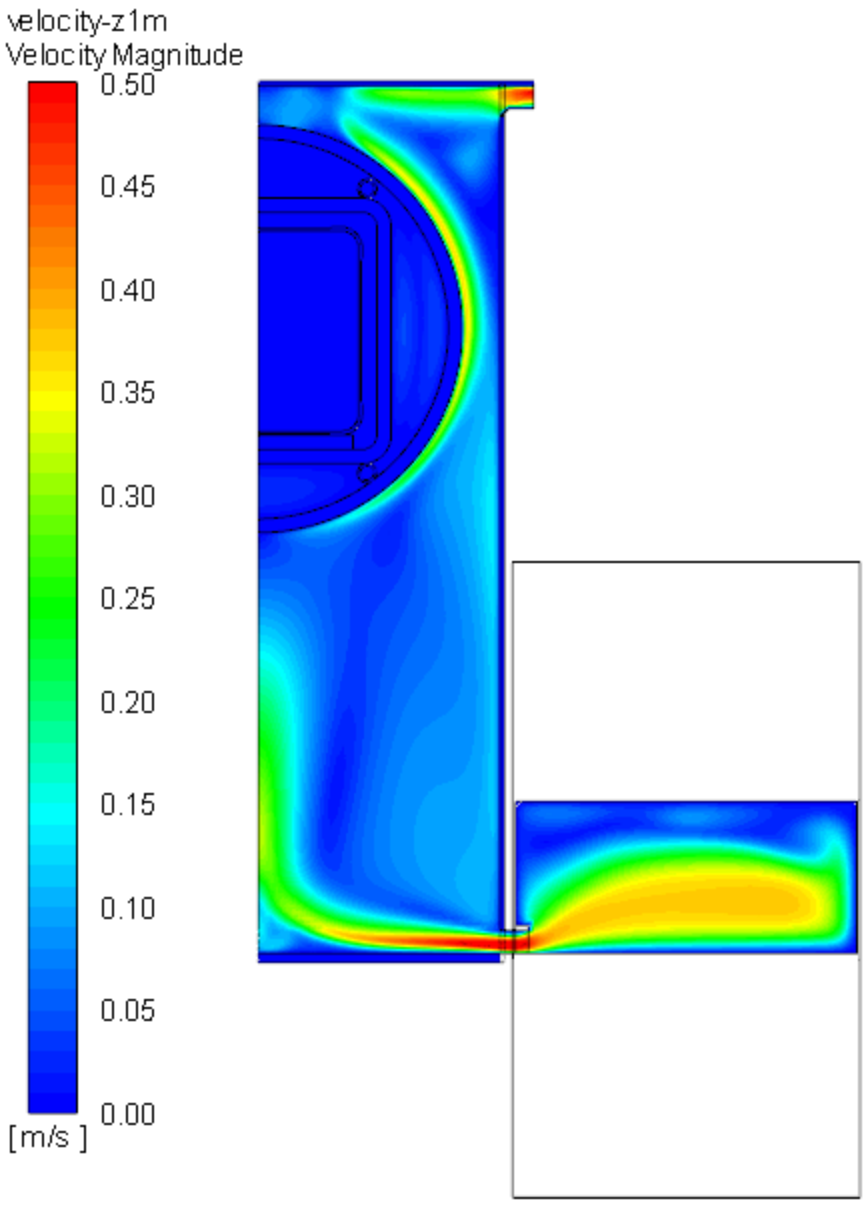

Figure 3-9 Velocity (m/s) in baseline 3D simulation of open case with helium at z = 1 m

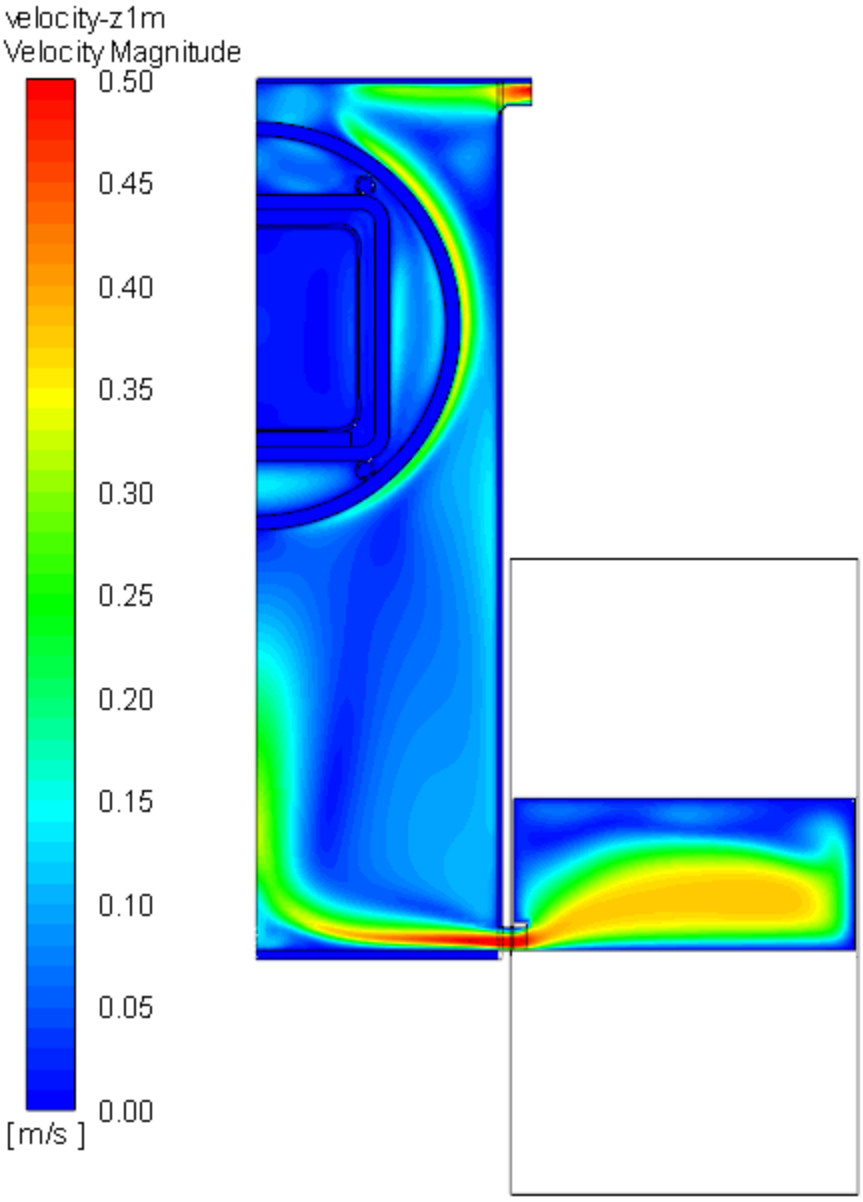

Figure 3-10 Velocity (m/s) in baseline 3D simulation of open case with air at z = 1 m

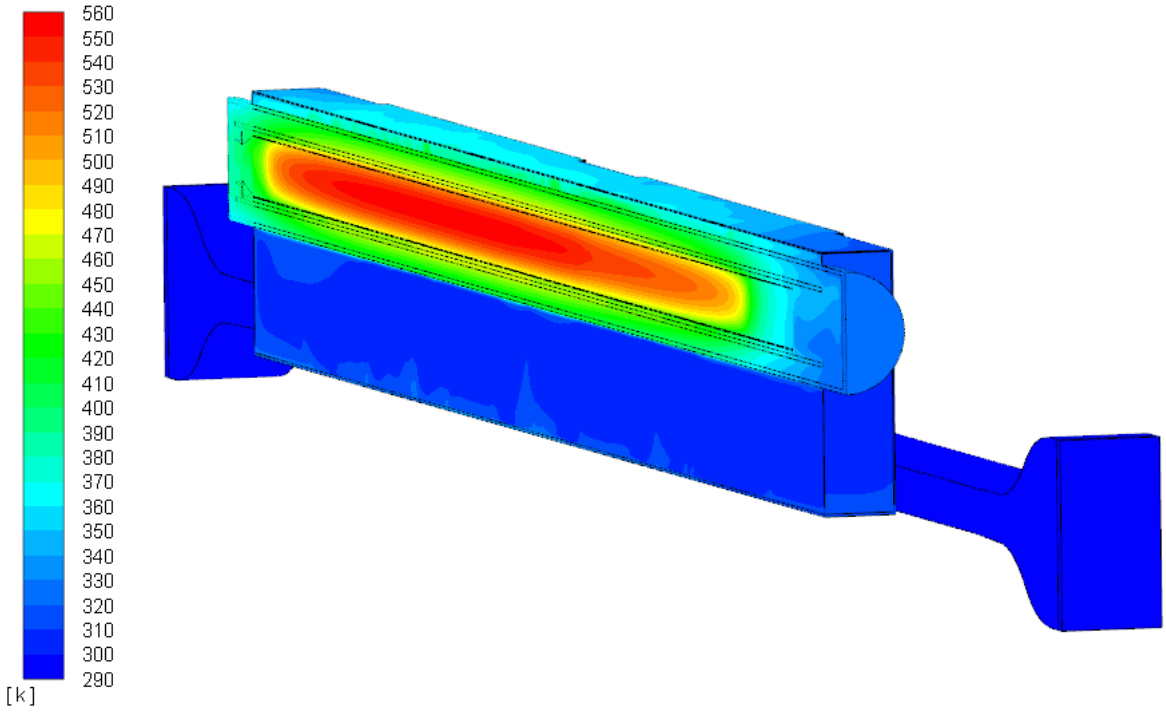

Figure 3-11 Temperature (K) in baseline 3D simulation of open case with helium on symmetry plane and walls of enclosure

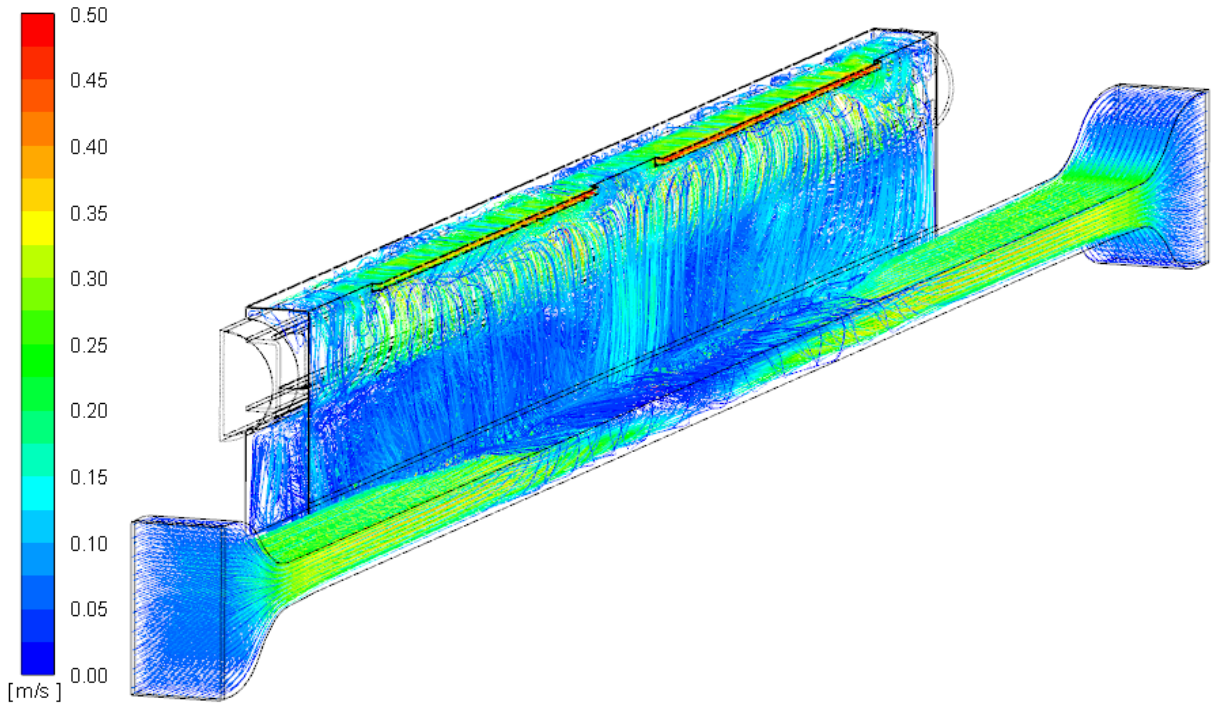

Figure 3-12 Pathlines of cooling air colored by velocity (m/s) in baseline 3D simulation of open case with helium

3.2.1 Validation Metrics

The metrics provided for simulation validation were total air mass flow rate, temperature in 21 separate locations, and the value and location of the PCT. The pin location WEU, EQ, ES, GU and IU are depicted in Figure 3-13. The following are the temperature measurements used for validation:

(1) axial measurement at WEU @ z = 0.610 m
(2) axial measurement at WEU @ z = 1.219 m (also a vertical profile measurement)
(3) axial measurement at WEU @ z = 1.829 m (also a horizontal profile measurement)
(4) axial measurement at WEU @ z = 2.438 m
(5) axial measurement at WEU @ z = 3.658 m
(6) vertical measurement at the top of the vault, z = 1.219 m
(7) vertical measurement at the top of the pressure vessel, z = 1.219 m
(8) vertical measurement at the top of the basket, z = 1.219 m
(9) vertical measurement at the top of the channel box, z = 1.219 m
(10) vertical measurement at fuel rod EQ, z = 1.219 m
(11) vertical measurement at fuel rod ES, z = 1.219 m
(12) vertical measurement at the bottom of the channel box, z = 1.219 m
(13) vertical measurement at the bottom of the basket, z = 1.219 m
(14) vertical measurement at the bottom of the pressure vessel, z = 1.219 m
(15) vertical measurement at the bottom of the vault, z = 1.219 m
(16) horizontal measurement at fuel rod GU, z = 1.829 m
(17) horizontal measurement at fuel rod IU, z = 1.829 m
(18) horizontal measurement at the channel box wall, z = 1.829 m
(19) horizontal measurement at the basket wall, z = 1.829 m
(20) horizontal measurement at the pressure vessel wall, z = 1.829 m
(21) horizontal measurement at the vault wall, z = 1.829 m

Figure 3-13 shows the heater pin naming convention, and Figure 3-14 shows the vertical and horizontal measurement locations.

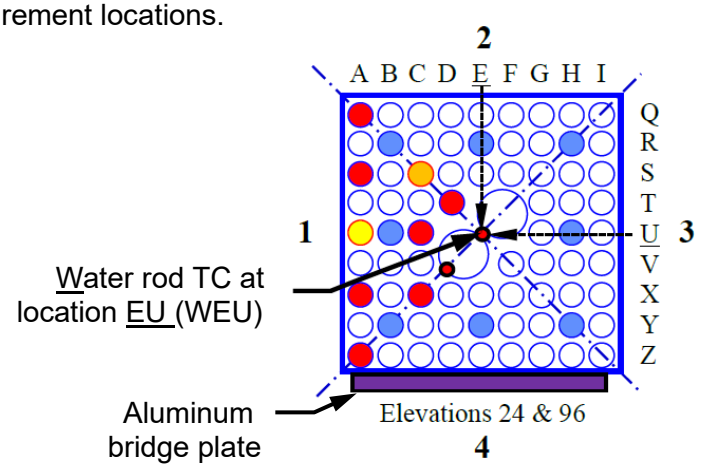

Figure 3-13 Fuel rod layout—axial measurements at water rod EU [3]

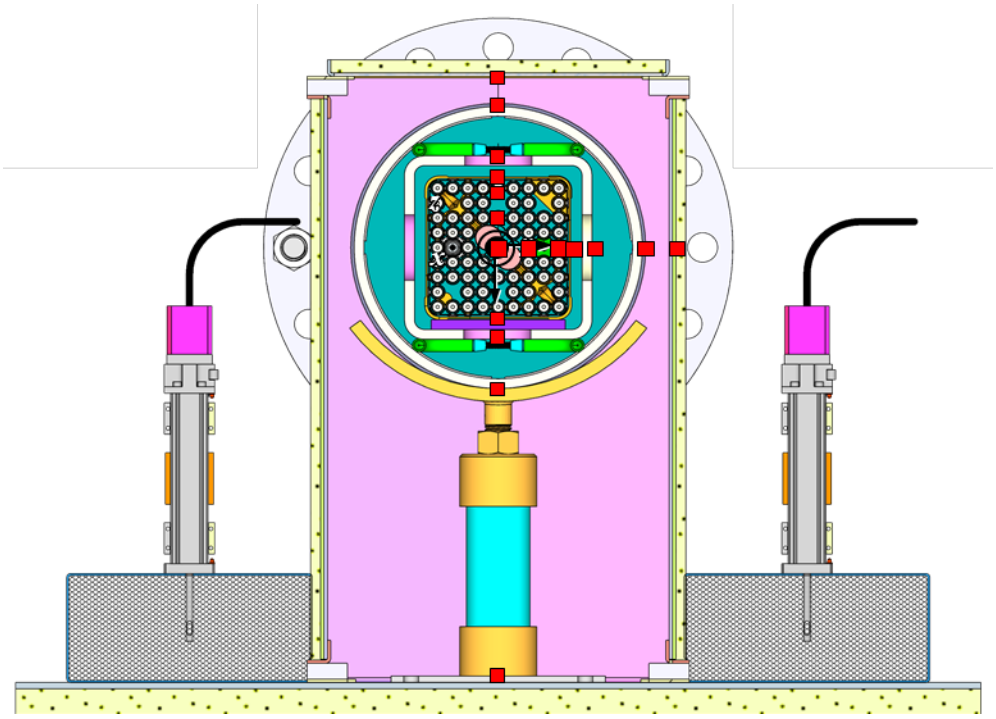

Figure 3-14 Vertical and horizontal measurement locations

3.3 Consistency Checks

The first step in validating the simulation and quantifying the uncertainty is to ensure that the simulation is internally consistent. Two consistency checks that are easy to demonstrate are mass conservation and energy conservation across the boundaries of the model.

Global mass conservation is checked by comparing the total mass inflow to the model with the total mass outflow. For a steady-state simulation, these values should be equal. Table 3-2 compares the mass inflow and outflow for the open case with helium. The error in the mass balance is 0.03 percent of the total mass flow, which is much smaller than other sources of uncertainty considered.

Table 3-2 Mass Balance Consistency Check

Model Boundary:	Units:	Mass Flow:
Inlet 1	(kg/s)	0.006618
Inlet 2	(kg/s)	0.006517
Outlet 1	(kg/s)	-0.007185
Outlet 2	(kg/s)	-0.005946
TOTAL	**(kg/s)**	**0.000004**

The total heat applied to the experiment for the open cases was measured to be 2,500 W. This was applied to the simulation as a volumetric heat source and escaped from the model boundaries through a combination of surface heat flux and heat advection through the outlet vents.

The full fuel section has a volume of 0.021512 m^3, and a heat generation source term of 39,692 W/m^3, for a total heat input of 853.8 W. The partial fuel section has a volume of 0.011186 m^3, and a heat generation source term of 35,401 W/m^3, for a total heat input of 396.0 W. This yields a total heat input to the simulation of 1,249.8 W for the half-symmetry model.

Table 3-3 reports the heat gain or loss through the inlet and outlet boundaries based on the mass flow and enthalpy of gas flowing through the model boundary. The enthalpy of air is reported relative to a reference temperature of 25 degrees C (77 degrees F). Since the ambient temperature of 297 K is colder than the reference temperature, a slight negative enthalpy is indicated at the model inlets.

The total imbalance in heat across the entire model is 2.1 W, or 0.2 percent of the total heat input. Again, this error is small compared to other sources of uncertainty in the simulation result. The heat and mass balances demonstrate model consistency and will not introduce significant additional uncertainty into the verification, validation, and uncertainty quantification (VVUQ) analysis.

Table 3-3 Energy Balance Consistency Check

Domain Location:	Units:	Heat:
Full Fuel Section	W	853.8
Partial Fuel Section	W	396.0
Inlet 1	W	-7.7
Inlet 2	W	-7.5
Outlet 1	W	-421.3
Outlet 2	W	-310.3
Vault Base	W	-22.7
Vault Sides	W	-227.7
Vault Top	W	-182.0
Exposed Pressure Vessel	W	-68.5
TOTAL	**W**	**2.1**

3.4 Verification, Validation, and Uncertainty Quantification

3.4.1 Overview

Uncertainty quantification was performed for the 10 cases analyzed using the techniques outlined in ASME V&V 20-2009 [5]. This document, which is the standard for verification and validation (V&V) and uncertainty quantification (UQ) for CFD and heat transfer applications, establishes steps to assess the accuracy of computational simulations. The accuracy of the method is obtained by the comparison between the experiment and the simulation of a local or global variable. From the validation process in V&V 20-2009, criteria for a CFD-grade experiment can be established [5]. A CFD-grade experiment should be able to validate a CFD model with a minimization of the validation uncertainty on some selected figures of merit variable. As PCT is used in NUREG-2215 [2] as a criterion to assess the safety of a dry cask, it is also used in this work as the figure of merit or the target variable to assess the validation uncertainty. In turn, the validation uncertainty can be used to qualify the experiment as CFD-grade for its intended purpose. As described in ASME V&V 20-2009 [5], Bestion et al., "Review of Uncertainty Methods for Computational Fluid Dynamics Application to Nuclear Reactor Thermal Hydraulics," issued in 2016 [12], Bestion et al., "Requirement for CFD-Grade Experiments for Nuclear Reactor Thermal-Hydraulics," issued in 2019 [13] and later in NUREG/CR-7260 [6], and NUREG-2238 [8], the minimization of the validation uncertainty of target variables such as PCT is a key factor and criteria for establishing a CFD-grade experiment. The following was extracted from references [5] [6] [8] [12] and [13]:

> The validation comparison error E in any validation process is defined as the difference between the solution denoted by S and the experimental data denoted by D:
>
> $$\mathrm{E} = \mathrm{S} - \mathrm{D}$$
>
> If T represents the true solution, then the error in the solution and experiment is:
>
> $$\delta_{\mathrm{S}} = \mathrm{S} - \mathrm{T}$$
>
> $$\delta_{\mathrm{D}} = \mathrm{D} - \mathrm{T}$$
>
> Then E can be written as:
>
> $$\mathrm{E} = (\mathrm{S} - \mathrm{T}) - (\mathrm{D} - \mathrm{T}) = \delta_{\mathrm{S}} - \delta_{\mathrm{D}}$$
>
> The simulation error δ_S consists of three categories including the modeling error δ_{model} due to physical modeling input, including approximations and assumptions; the numerical solution error δ_{num} stemming from the numerical algorithm and the discrete mesh used to solve the partial differential equations; and the input data errors δ_{input} resulting from the simulation input parameters including initial conditions, boundary conditions, and properties. E is thus the overall result of all the errors coming from the experimental data and the simulation:
>
> $$\mathrm{E} = \delta_{\mathrm{model}} + \delta_{\mathrm{input}} + \delta_{\mathrm{num}} - \delta_{\mathrm{D}}$$
>
> The unknown error δ_{model} produced by the modeling is isolated:

$$\delta_{\text{model}} = \text{E} - (\ \delta_{\text{input}} + \ \delta_{\text{num}} - \delta_{\text{D}})$$

The corresponding standard uncertainties for the input, numerical, and experimental errors are u_{input}, u_{num}, and u_D.

The validation standard deviation of the combination error $\delta_{\text{input}} + \ \delta_{\text{num}} - \delta_{\text{D}}$ is denoted as u_{val}, and if the three errors are mutually independent, then:

$$u_{val} = \sqrt{u_{input}^2 + u_{num}^2 + u_D^2}$$

$$\delta_{\text{model}} = \text{E} \pm u_{val}$$

If δ_{model} is also considered independent, then:

$$u_E = \sqrt{u_{model}^2 + u_{input}^2 + u_{num}^2 + u_D^2}$$

$$u_{model} = \sqrt{u_E^2 - u_{val}^2}$$

The ASME standard gives solutions to evaluate every term of the comparison error (E) and the validation uncertainty ($\mathbf{u_{val}}$). The sign and magnitude of the validation comparison error E are known once the validation comparison is made. The validation uncertainty can be estimated through the determination of the simulation uncertainty $u_{simulation}$ and the experimental uncertainty u_D. The simulation uncertainty consists of the numerical simulation uncertainty u_{num} and the input uncertainty u_{input}. However, there is no established method to estimate the physical modeling uncertainty u_{model}.

3.4.2 Modeling Uncertainty

The decision as to whether a certain parameter is to be included in the explicit calculation of simulation uncertainty or whether it should be included under the vaguer umbrella of modeling uncertainty is somewhat arbitrary. Numerical, experimental, and input uncertainties are discussed next. Modeling error and uncertainty are what remains after all these items have been rigorously quantified. It is the goal of the VVUQ analysis to quantify the modeling error and reduce it to the smallest possible value.

From these equations, the following criteria can be determined which are also shown in [5] [6] [8] [12] [13] :

- If $|\mathbf{E}| >> \mathbf{u_{val}}$, $\mathbf{u_{model}} \cong \mathbf{u_E}$. Then, $\mathbf{u_{val}}$ is relatively small, and the modeling error is larger than the validation uncertainty. In this case, the comparison between the code predictions and the experimental data can provide useful and precise information on the quality of the physical model. Consequently, the model has the possibility to be improved or calibrated using the data from the experiment in order to have less uncertainty in the result.

- If $|\mathbf{E}| < \mathbf{u_{val}}$, the larger validation uncertainty implies that the model accuracy cannot be improved if the combination δ_{input}, δ_{num}, and δ_{D} cannot be reduced. In this case, if the validation uncertainty is small enough to be useful—for example, if the validation uncertainty of PCT is smaller than the margin between the simulation PCT value and its limit—then this model is considered accurate for this application. On the other hand, if the validation uncertainty is larger than the margin, this kind of experiment will not be useful in improving the model.

- If $|\mathbf{E}| = \mathbf{u_{val}}$, the modeling error is within the noise level imposed by the input, numerical, and experimental uncertainties, and the possibility of model improvement is a challenge.

- If model uncertainty $\mathbf{u_{model}}$ is known or expected, sensitivity analyses of sensitive modeling parameters can be performed to investigate the impact that this model uncertainty can have on target variables such as PCT and $\mathbf{u_{val}}$.

    - If $\mathbf{u_{model}} < \mathbf{u_{val}}$, the experiment is not very informative.

    - **If** $\mathbf{u_{model}} > \mathbf{u_{val}}$, the experiment is capable of showing if the expected model uncertainty is reached.

3.4.3 CFD-Grade Experiment

A CFD-grade experiment is one that can be used to validate the physical model, which means that it provides a relatively low uncertainty of validation $\mathbf{u_{val}}$ and allows a good determination of the model uncertainty $\mathbf{u_{model}}$. Therefore, an experiment that minimizes both $\boldsymbol{\delta_{input}}$ and $\boldsymbol{\delta_{D}}$ also minimizes $\mathbf{u_{val}}$ and provides more information on the accuracy of the model. A CFD-grade experiment should provide the lowest values of δ_{input} and δ_{D} (i.e., low $\mathbf{u_{val}}$). In parallel, the CFD user or specialist should strive to minimize the numerical error $\mathbf{u_{num}}$ or at least follow well-established methods to quantify it correctly.

However, the capability of an experiment to provide information on the uncertainty of model parameters may not be the concern of a dry cask safety analysis. The final goal is often to compare a parameter of interest such as PCT to a safety criterion to assess if the dry cask is safe in the situation as designed. Very often, it is much more difficult to know all necessary boundary and initial conditions and flow-field variables in the region of interest with a low uncertainty or high confidence. As a result, $\mathbf{u_{input}}$ may be large. Such experiments should at least provide sufficient information to quantify the accuracy of CFD code predictions for the relevant parameters of interest in the safety analysis such as some local temperatures or PCT. In turn, this accuracy prediction can be used to assess whether a reliable conclusion for the safety case can be made. The experiment should target a predetermined code uncertainty for the selected target variable such as PCT or another variable. So, instead of providing data to allow quantifying the uncertainty of some specific model parameters, the goal is the prediction of the uncertainty in the target variable of interest. This uncertainty is the result of the propagation of various sources of uncertainty from $\boldsymbol{\delta_{input}}$, $\boldsymbol{\delta_{num}}$, and $\boldsymbol{\delta_{D}}$. As such, the minimization of these sources of errors remains the objective of the VVUQ process.

Another important requirement is the collaboration between the experiment designer and the code user from the start of the experimental project. The collaboration should target

the models used in the dry cask application as shown in NUREG-2152 [4]. Code users and safety analysts can then expose the goal of the experiment, in terms of model validation. Among these modeling goals that can be targeted and investigated are the type of turbulence model that governs the flow field, state laws for the fluid of interest, or porous media parameters if a porous media model is used. NUREG-2152 [4] and NUREG-2208 [17] contain a list of modeling challenges including boundary conditions for dry cask applications. In this important initial step, CFD code users can perform pre-calculations to help define the mockup in terms of geometrical design, range of flow variables, choice of boundary conditions, and scaling analyses. This collaboration can also be used to define the plan of the experiment. For these reasons, an exchange between experimentalists and code users should characterize a CFD-grade experiment from the beginning of its design to the end of the project.

The preliminary specification of fluid and solid volumes of interest and of inlet and outlet fluid surfaces is of prime importance in selecting where initial and boundary conditions must be known. A CFD-grade experiment should specify the boundary conditions, initial conditions, and model domain in a way that they can be used as simulation input data with the required accuracy.

A general requirement may be to define a priori acceptance criteria before designing an experiment. If the only objective is to validate a CFD code on a specific flow configuration, the acceptance criterion may be to minimize the validation uncertainty (i.e., experimental, numerical, and input uncertainties) in a specific target variable. In dry cask applications, examples may be the following:

- If the objective is to validate a CFD code for PCT, the acceptance criterion may be that the validation uncertainty related to this PCT should not exceed a given value.

- If the objective is to predict the canister wall heat transfer in a ventilated cask, the acceptance criterion may be that the validation uncertainty related to a predetermined temperature difference ΔT between the air inlet and outlet should not exceed a given value.

- If the objective is to predict the air mass flow rate in a ventilated cask, the acceptance criterion may be that the validation uncertainty related to a measured mass flow rate in the airflow passage should not exceed a given value.

In the last few years, dry cask applicants applied for licenses for cask design close to 50 kW or higher. The analyses accompanying these applications presented CFD thermal analysis cases with PCTs very close to the NUREG-2215 [2] allowable limit of 400 degrees C (752 degrees F), with margins as small as 10 degrees C (18°F). Thus, in this validation, the calculated validation uncertainty $\mathbf{u_{val}}$ will be compared to these margins to conclude whether the experiment used in this validation exercise can be classified as a CFD-grade experiment.

3.4.4 Numerical Uncertainty

Numerical uncertainty is made up of three major sources: computer round-off error, iterative convergence uncertainty, and discretization uncertainty. Discretization uncertainty can be spatial or temporal. However, this simulation is steady-state so temporal uncertainty is not of concern. Computer round-off error is extremely small compared to other sources.

3.4.4.1 Iterative Uncertainty

CFD engineers generally know that the models need to run until they are "converged." This is supposed to mean that the solution no longer varies with additional iterations. In reality, however, some solutions are better behaved than others. Some solutions converge very nicely, and the solution changes very little with each additional iteration, but some solutions are much "noisier" and can vary significantly within a range of values. This variation can be due to numerical instability in the solution or due to physically based unsteady flow patterns in a steady-state solution.

Once the solution reaches something resembling convergence, the output in question should be recorded for a large number of iterations to determine the range of values over which the output wanders. This range represents the iterative convergence uncertainty of a solution.

In this validation report, all simulation outputs were recorded for 1,000 iterations after the solution was considered to be converged for the baseline solution of both cases. The baseline value was taken as the average value over those 1,000 iterations, and the 95-percent confidence level was calculated as being within two standard deviations of the average value.

The iterative uncertainty was found to be a very small source of error for all temperature locations, with most locations having an iterative uncertainty of 0.1 K or less.

3.4.4.2 Discretization Uncertainty

The grid convergence index (GCI) proposed by Roache and outlined in ASME V&V 20-2009 [5] recommends that at least three grids should be used to determine the uncertainty of a solution with respect to the mesh. In this case, a coarse, medium, and fine mesh are used, and each level of refinement is accomplished by doubling the mesh resolution (Table 3-4).

For accurate convective heat transfer calculations—in this case, at the external surface of the pressure vessel—the y+ value for the mesh should be equal to or less than 1. If a y+ value of 1 is used for the fine mesh and is allowed to expand to greater values for coarser meshes, then the same boundary conditions are not truly being solved for each mesh resolution. On the other hand, if the coarse mesh has a y+ value of 1, and the mesh size is further reduced for the finer meshes, this significantly increases the size of the mesh required for the fine mesh case.

Table 3-4 Grid Convergence Index Mesh Sizes

GCI Mesh Size	Total Cells
Coarse	308,090
Medium	1,945,776
Fine	12,815,968

In this case, an inflation layer was applied to the surfaces where convective heat transfer was deemed important (external pressure vessel surface and internal vault walls) with a constant first cell mesh height for all cases and the same rate of cell inflation normal to the boundary surface. The inflation layer expanded to a bulk mesh size that doubled between the fine and medium mesh and doubled again between the medium and coarse mesh. Similarly, the mesh

size along the surface in each direction doubled between the fine and medium meshes, and again between the medium and coarse meshes. It is acknowledged that this does not provide a grid refinement ratio of 2 and that the mathematics for the GCI calculation do not strictly apply with this mesh approach; however, neither do they apply if the y+ value is significantly different from one mesh to another.

The grid refinement ratio, r, between the meshes in this meshing scheme is calculated as the ratio between cell counts of successive meshes to the one-third power. With this estimation, the grid refinement ratio is nearly constant between the two meshes at a value of 1.86, which is the value used in the subsequent analysis.

The GCI, which is the 95-percent confidence level uncertainty in the solution as a result of the mesh, can be calculated for the finest of three meshes as follows:

$$GCI_{fine} = \frac{F_s * |\varphi_2 - \varphi_1|}{r^p - 1}$$

where ϕ is the solution result, and 1, 2, and 3 represent the fine, medium, and coarse meshes respectively. F_s is an empirically derived factor of safety, which is 1.25 for an asymptotically converging set of three or more meshes. For a constant grid refinement ratio, the order of convergence, p, can be calculated as follows:

$$p = \frac{\ln\left(\frac{\varphi_3 - \varphi_2}{\varphi_2 - \varphi_1}\right)}{\ln(r)}$$

If only two meshes are used to calculate the GCI, an order of convergence of 1 is used, along with a factor of safety of 3.0 to account for the larger uncertainty associated with using fewer mesh resolution levels.

To achieve a meaningful GCI, ASME V&V 20-2009 highly recommends using a constant grid refinement ratio, geometrically similar cells in each refinement level, and structured cells where possible. It is allowable to use a grid refinement ratio of less than 2 (but preferably greater than 1.3); however; in this case, there were several thin solids sections that were meshed only one cell across in the coarse mesh. This mesh topology dictated that a doubling of the mesh was the smallest grid refinement ratio that could be used.

The GCI was calculated at every location where an experimental temperature measurement was recorded, as well as for the total mass flow rate. Most of these model outputs did not demonstrate asymptotic convergence with the three meshes used, particularly in areas of strong temperature gradients. ASME V&V 20-2009 suggests that four or more mesh resolutions should be used to convincingly demonstrate asymptotic response in difficult problems; however; the computational resources necessary to perform another doubling of mesh resolution were prohibitive. Since most predictions did not obey asymptotic convergence, the GCI was calculated from solutions from just two mesh resolutions: the medium mesh and the fine mesh.

Even though the larger factor of safety of 3.0 was used in the GCI analysis, the uncertainty due to spatial discretization for the PCT and air mass flow rate are still relatively low as shown in Table 3-5 and Table 3-6. The GCI for the PCT in the helium and air cases are 3.6 K and 3.7 K

respectively, whereas the GCI for air mass flow rate in the helium and air cases are 0.0003 and 0.0002 kg/s respectively. In all cases, these values are smaller than both the experimental and input uncertainty values.

In instances where temperature measurements are located on a steep temperature gradient (for example, measurement WEU 5, which is located at the end of the cold end of the partial heater section), changes in mesh resolution have a significant impact on where the measurement sits relative to the temperature gradient. In those cases, the GCI for those locations is much greater than it is for the PCT, which inherently exists at a location where the temperature gradient is zero.

Table 3-5 PCT and Mass Flow Rate GCI Values for Open Case with Helium

GCI 2.5kW, 100 kPa Helium Open Case	PCT	Mass Flow Rate
Refinement Ratio, r	1.86	1.86
Factor of Safety, F_s	3.0	3.0
Coarse Mesh	559.6 K	0.0273 kg/s
Medium Mesh	558.7 K	0.0264 kg/s
Fine Mesh	557.6 K	0.0263 kg/s
Order of Convergence, p	1	1
GCI (fine–medium)	3.6 K	0.0003 kg/s

Table 3-6 PCT and Mass Flow Rate GCI Values for Open Case with Air

GCI 2.5 kW, 100 kPa Air Open Case	PCT	Mass Flow Rate
Refinement Ratio, r	1.86	1.86
Factor of Safety, F_s	3.0	3.0
Coarse Mesh	640.4 K	0.0274 kg/s
Medium Mesh	640.4 K	0.0264 kg/s
Fine Mesh	639.4 K	0.0263 kg/s
Order of Convergence, p	1	1
GCI (fine–medium)	3.7 K	0.0002 kg/s

3.4.4.3 Overall Numerical Uncertainty

Table 3-7 presents the overall numerical uncertainty from all sources for the open case with helium fill gas, and Table 3-8 shows the uncertainty for the open case with air fill gas. When computing the total numerical uncertainty, it is not sufficient to use the root mean square (RMS) addition of iterative convergence error and discretization error, because the two errors are correlated [5]. Instead they must be combined using simple addition.

The overall numerical uncertainty for the PCT and mass flow rate is low relative to other sources of uncertainty, particularly input uncertainty. However, in locations of steep temperature gradients, the spatial discretization uncertainty can be significantly higher and can be a leading cause of simulation uncertainty.

Table 3-7 Overall Numerical Uncertainty for Open Case with Helium

Overall Numerical Uncertainty	PCT	Mass Flow Rate
Computer Round-off	±0.0 K	±0.0000 kg/s
Iterative Convergence	±0.0 K	±0.0000 kg/s
Spatial Discretization	±3.6 K	±0.0003 kg/s
Total Numerical Uncertainty:	**±3.6 K**	**±0.0003 kg/s**

Table 3-8 Overall Numerical Uncertainty for Open Case with Air

Overall Numerical Uncertainty	PCT	Mass Flow Rate
Computer Round-off	0.0 K	0.0000 kg/s
Iterative Convergence	0.1 K	0.0000 kg/s
Spatial Discretization	3.7 K	0.0002 kg/s
Total Numerical Uncertainty:	**3.8 K**	**0.0002 kg/s**

3.4.5 Input Uncertainty

3.4.5.1 Input Uncertainty Method

The input uncertainty method used was the finite difference method (also variously called sensitivity coefficient method, perturbation method, mean value method, and possibly others). This is a local approach to determining the input uncertainty, whereby an independent input variable (e.g., total decay heat) is changed by a small amount, and the effect that this variable has on the solution is recorded. If the uncertainty of the input is known, then the resulting uncertainty of the solution due to the uncertainty of the input can be calculated using the following equation:

$$u_{input}{}^2 = \sum_{i=1}^{n} \left(\frac{\partial S}{\partial X_i} u_{X_i} \right)^2$$

where:

u_{input} = total input uncertainty
S = simulation result
u_{X_i} = corresponding standard uncertainty in input parameter X_i
X_i = input parameter
n = number of inputs in the sensitivity study

$\partial S/\partial X_i$ = sensitivity coefficient

Each input variable was perturbed both up and down by its uncertainty value, so two separate cases were run for each input variable in addition to the baseline case. In the case of the 0.9-mm gap between the channel box and the aluminum bridge plate, this gap was removed, and there was no corresponding sensitivity case to increasing the gap size.

This method works only in the local neighborhood around the baseline solution, and only as long as the solution is fairly linear with respect to the inputs in that neighborhood. There are more complex global methods of determining uncertainty (Monte Carlo, Latin Hypercube, and others), but they typically require more knowledge of the probability distribution of the input variables than is generally available, and with a large number of input variables, they require hundreds or perhaps thousands of cases to achieve statistical significance.

3.4.5.2 Input Uncertainty Results

The input uncertainty was calculated for eight different simulation inputs that were deemed to be the largest contributors to the total simulation uncertainty:

- heating power
- external HTC
- inlet straightener hydraulic resistance
- fuel hydraulic resistance
- orientation angle relative to vertical
- filled 0.9-mm gap between the channel box and aluminum bridge plate
- ambient temperature
- emissivity values

For the filled 0.9-mm gap in the channel box that provides extra thermal resistance in heat traveling into the aluminum bridge plate, this was a binary sensitivity study as to whether the gap was present, as in the baseline simulation, or there was no gap. For all other cases, the inputs were perturbed both higher and lower by the amount of the uncertainty in the input.

For the heat input and the ambient temperature, the uncertainties in the input values were provided with the boundary conditions for each case. For many of the other inputs, measurement uncertainty was not provided, and in some cases, the input values themselves were not provided. When simulation inputs are not provided, the modeler must make a calculation or educated guess to obtain the input value, which introduces uncertainty into the simulation. In these cases, a conservative but reasonable estimate of the uncertainty in these input values was assumed.

When ambient temperatures were perturbed higher and lower, the ambient density was also modified accordingly. This ensures that an artificially high or low mass flow rate would not be induced through the vault via the constant pressure inlet and outlet boundaries. Changes in barometric pressure would also have this effect, but sensitivity testing demonstrated that the range of natural variation in barometric pressure at the test location had a negligible effect on the air mass flow rate and temperatures within the dry cask simulator (DCS) compared to the other inputs that were evaluated.

The external heat transfer correlations that were calculated based on Nusselt number correlations using the wall temperature and geometric configuration of the vault were assumed to be accurate to within ±33 percent. All external HTC values were perturbed up and down together. The straightener hydraulic resistance, provided as a simulation input, was assumed to have an uncertainty of ±30 percent. The hydraulic resistance of the fuel bundle, an input to the porous media properties in the simulation, was assumed to have an uncertainty of ±50 percent.

The orientation angle of the DCS installation relative to vertical was assumed to be ±1 degree with respect to the z-axis, which amounts to an elevation difference of 70 mm (3 inches) over a length of 4 meters (m) (157.4 inches). In the open tests, the results were found to be quite insensitive to changes in orientation of 1 degree, so these sensitivity tests were not included in the eight blind cases.

Table 2-1 lists the emissivity values used for all materials in the input sensitivity study. All values were measured with the same type of instrument. Since the same instrument was used to measure the emissivity values, the uncertainties in the emissivity measurements were considered to be correlated with each other. When evaluating the uncertainty due to emissivity values, all emissivity values were perturbed higher and lower together, resulting in a colder and hotter condition within the DCS respectively.

The uncertainties due to each of these eight inputs as shown in Table 3-9 and Table 3-10 were presumed to be independent of each other, so the total input uncertainty was calculated using RMS summation. The dominant input uncertainty for temperature measurements in all cases was found to be the uncertainty in emissivity.

Uncertainty in emissivity values was the largest source of input uncertainty for the PCT value (and most other temperature measurements) by an order of magnitude. The effect of emissivity uncertainty with air fill gas was more than double the effect with helium fill gas. This is because the thermal conductivity of helium is much greater than that of air, so a significant portion of the heat transfer is accomplished via conduction, whereas with air, nearly all of the heat transfer is accomplished via radiation.

The largest source of input uncertainty for the air mass flow rate is the uncertainty in the straightener hydraulic resistance, followed by the uncertainty in ambient temperature. Neither of these contributes a very large uncertainty, so the total input uncertainty in air mass flow rate remains low.

Table 3-9 Input Uncertainty for Open Case with Helium

Input Variable:	PCT	Mass Flow Rate
Heating Power	+1.1 K / -1.1 K	+0.0001 / -0.0001 kg/s
External HTC	+0.3 K / -0.3 K	+0.0002 / -0.0002 kg/s
Straightener Hydraulic Resistance	+0.5 K / -0.5 K	+0.0010 / -0.0009 kg/s
Fuel Hydraulic Resistance	+0.0 K / -0.0 K	+0.0000 / -0.0000 kg/s
Orientation Angle (gravity)	+0.0 K / -0.0 K	+0.0001 / -0.0001 kg/s
Channel Box 0.9-mm Gap	-1.3 K	+0.0000 kg/s
Ambient Temperature	+1.7 K / -1.8 K	+0.0004 / -0.0004 kg/s
Emissivity	+7.8 K / -11.7 K	+0.0001 / -0.0001 kg/s
Total Input Uncertainty	**+8.1 K / -11.9 K**	**+0.0011 / -0.0010 kg/s**

Table 3-10 Input Uncertainty for Open Case with Air

Input Variable:	PCT	Mass Flow Rate
Heating Power	+1.0 K / -1.1 K	+0.0000 / -0.0001 kg/s
External HTC	+0.2 K / -0.2 K	+0.0002 / -0.0002 kg/s
Straightener Hydraulic Resistance	+0.3 K / -0.4 K	+0.0009 / -0.0009 kg/s
Fuel Hydraulic Resistance	+0.6 K / -2.4 K	+0.0000 / -0.0000 kg/s
Orientation Angle (gravity)	+0.0 K / -0.1 K	+0.0001 / -0.0001 kg/s
Channel Box 0.9-mm Gap	-2.6 K	+0.0000 kg/s
Ambient Temperature	+1.2 K / -1.3 K	+0.0003 / -0.0004 kg/s
Emissivity	+18.5 K / -28.3 K	+0.0001 / -0.0001 kg/s
Total Input Uncertainty	**+18.5 K / -28.6 K**	**+0.0010 / -0.0010 kg/s**

3.4.5.3 Correlated versus Uncorrelated Input Variables

With so many inputs for CFD models of practical interest, there must be an approach to make the input uncertainty analysis tractable. The resources required to run two additional cases for every simulation input are immense. One way to reduce the number of simulations required is to eliminate the inputs that the solution is insensitive to; however; this still leaves many inputs.

Another approach is to group similar inputs into the same category and perturb them all together. This approach was taken with the external HTC values and the emissivity values.

Although these values may in fact be independent of each other, perturbing them all together is a more conservative approach and is similar to analyzing them as though they are in fact correlated.

The largest input uncertainty in predicting PCT was found to be the uncertainty in emissivity values. In this case, the emissivity values of Inconel, Zircaloy, painted carbon steel, the vault stainless steel, the aluminum bridge plate, and the insulation were all perturbed higher and lower together. It can be argued that the uncertainty in these measurements is correlated because they were all measured with the same instruments under the same conditions; however, it may be beneficial to know which material contributed the most to the overall uncertainty in PCT (emissivity did not substantially affect the air mass flow rate).

To investigate this further, a separate input sensitivity study was conducted for the emissivity values of the different materials for the two open cases, with the results documented in Table 3-11 and Table 3-12. The emissivity uncertainties in Zircaloy, Inconel, and the painted steel resulted in the largest share of uncertainty, which is consistent with these being by far the hottest components with the highest share of heat transfer occurring via radiation. The uncertainty in emissivity of stainless steel and insulation, which are at much lower temperatures, adds very little to the overall uncertainty of the simulation.

If the emissivity uncertainty values for each material were in fact uncorrelated, the overall uncertainty due to emissivity values would be significantly lower than if they were correlated—roughly half in the case of the open helium case.

It is noteworthy that when the separate uncertainties are treated as correlated and the individual components are summed to reach the total emissivity uncertainty, the result is very similar to the case in which all emissivity values are perturbed together. This indicates that the heat must travel sequentially from the Inconel to the Zircaloy to the painted steel and that the majority of the heat transfer is via radiation.

Table 3-11 Emissivity Uncertainty for Open Case with Helium

Material:	PCT
Inconel	+2.3 K / -1.8 K
Zircaloy (all together)	+1.5 K / -5.4 K
Painted Carbon Steel	+3.9 K / -3.6 K
Vault Stainless Steel (all together)	+0.4 K / -0.4 K
Aluminum Bridge Plate	+0.0 K / -0.0 K
Insulation	+0.1 K / -0.1 K
Total Emissivity Uncertainty (Uncorrelated)	**+4.8 K / -6.7 K**
Total Emissivity Uncertainty (Correlated)	**+8.2 K / -11.3 K**
Uncertainty When All Emissivity Perturbed at Once	**+7.8 K / -11.7 K**

Table 3-12 Emissivity Uncertainty for Open Case with Air

Material:	PCT
Inconel	+4.4 K / -15.4 K
Zircaloy (all together)	+8.6 K / -6.8 K
Painted Carbon Steel	+5.5 K / -4.8 K
Vault Stainless Steel (all together)	+0.3 K / -0.3 K
Aluminum Bridge Plate	+0.0 K / -0.1 K
Insulation	+0.0 K / -0.1 K
Total Emissivity Uncertainty (Uncorrelated)	**+11.1 K / -17.6 K**
Total Emissivity Uncertainty (Correlated)	**+18.8 K / -27.5 K**
Uncertainty When All Emissivity Perturbed at Once	**+18.5 K / -28.3 K**

3.4.6 Experimental Uncertainty

SNL provided the experimental uncertainty for all measurements for the open cases, along with the measured values. The uncertainty in all temperature measurements was reported to be 1 percent of the absolute temperature. For the helium case, this means the PCT of 559 K has an uncertainty of ±5.6 K. Similarly, the PCT of 647 K measured in the air case has an uncertainty of ±6.5 K.

The uncertainty in total air mass flow rate for the two open cases was reported to be 0.0004 kg/s [3] [9]. This value was used in the UQ; however, there is reason to believe that this is an underestimate of the actual measurement uncertainty. The uncertainty of the hot wire anemometer is reported to be ±0.025 m/s for the ambient temperatures encountered [3] [9]. With a total inlet duct area of 0.0934 m^2, this uncertainty in velocity equates to an uncertainty in total flow of 0.00234 m^3/s, or 0.00233 kg/s. This uncertainty is more than 5 times the reported uncertainty. The discrepancy arises from the treatment of the individual hotwire measurements as uncorrelated; however, if hotwire consistently reads in error (either consistently higher or consistently lower than the actual value), the error of the individual measurements over the cross section of the duct will not be uncorrelated.

3.4.7 Validation Uncertainty Quantification

The total validation uncertainty is a combination of the numerical uncertainty, the input uncertainty, and the experimental uncertainty, presented in Table 3-13 for the open helium case and Table 3-14 for the open air case. These calculations of overall validation uncertainty were repeated for the air mass flow rate, as well as for all locations corresponding to the 21 temperature measurements in the experiment.

Table 3-13 Total Validation Uncertainty for Open Case with Helium

Total Validation Uncertainty	PCT	Mass Flow Rate
Total Numerical Uncertainty	+3.6 K / -3.6 K	+0.0003 / -0.0003 kg/s
Total Input Uncertainty	+8.1 K / -11.9 K	+0.0011 / -0.0010 kg/s
Total Experimental Uncertainty	+5.6 K / -5.6 K	+0.0004 / -0.0004 kg/s
Total Validation Uncertainty	**+10.5 K / -13.7 K**	**+0.0012 / -0.0011 kg/s**

Table 3-14 Total Validation Uncertainty for Open Case with Air

Total Validation Uncertainty	PCT	Mass Flow Rate
Total Numerical Uncertainty	+3.8 K / -3.8 K	+0.0002 / -0.0002 kg/s
Total Input Uncertainty	+18.5 K / -28.6 K	+0.0010 / -0.0010 kg/s
Total Experimental Uncertainty	+6.5 K / -6.5 K	+0.0004 / -0.0004 kg/s
Total Validation Uncertainty	**+20.0 K / -29.5 K**	**+0.0011 / -0.0011 kg/s**

3.5 Comparison with Experimental Data

Once the uncertainty in the simulation has been calculated, the simulation result can be compared with the measured experimental data to see how well the model performed. When validating a CFD model, it is helpful to have many data points for comparisons so that any model deficiencies can be more easily identified. If only a few global variables are used for validation (e.g., PCT and air mass flow rate), it may be difficult to determine the root cause of any modeling errors. It is also easier for offsetting errors to go unnoticed.

In this case, there are temperature measurements spread throughout the model domain, which are very helpful for finding model inputs that do not match reality. All simulation outputs are compared against the experimentally measured values in Table 3-15 for the open helium case and Table 3-16 for the open air case. For ease of reference, a column on the right has been included to indicate whether the test result lies within the CFD model uncertainty band. If the measurement is marked with a green “YES,” the measurement falls within the model uncertainty band, and the simulation is considered valid at that point. If the measurement is marked with a red “NO,” the experimentally measured value falls outside of the validation uncertainty. The positive and negative uncertainty intervals for all points were calculated as described in Section 3.4 of this document.

For each case, there are also three plots showing the axial, vertical, and horizontal temperature profiles within the cask as shown in Figure 3-15, Figure 3-16 and Figure 3-17 respectively for the open helium case, and in Figure 3-18, Figure 3-19 and Figure 3-20 respectively for the open air case. CFD results are plotted with a continuous orange line showing all CFD values along the axis in question. At the location of each experimental measurement, error bars are included, which represent the total validation uncertainty at each point. Experimentally measured values are shown with blue diamonds and do not include error bars. The validation uncertainty already includes experimental uncertainty, so if the experimentally measured value

falls within the CFD uncertainty band, the solution is validated at that point. If the experimental data fall outside the uncertainty band, the solution is not validated.

The PCT in the CFD simulation was found by querying the model for the highest temperature within the simulation and its location. Since this was a symmetry model with uniform porous media within the channel box, the highest temperature was always on the centerline of the fuel assembly (y = 0). The uncertainty in PCT location was determined by evaluating at what distance the temperature decreased from the PCT by the value of the experimental uncertainty. In other words, the uncertainty band in the z direction is the distance from the simulation's PCT location in the positive and negative direction that the PCT falls by 5.6 K (in the case of the open case with helium) from 558.6 K to 553.0 K. In this case, that distance is 0.679 m in the positive z direction and 0.939 m in the negative z direction. This process is repeated for each principal axis and for each test case.

The axial temperature gradient is very shallow, so this approach results in a very broad uncertainty band. The transverse uncertainty bands, where temperature gradients are much higher, cover a span of only a few fuel rods.

Table 3-15 Open Test Results for 2.5-kW, 100-kPa, Helium

Parameter	Test Result	CFD Result	Positive Uncert.	Negative Uncert.	Compare Error, E	Valid ?
Airflow Rate (kg/s)	0.0283	0.0263	0.0012	-0.0011	0.0021	NO
PCT Location						
X value (m)		-0.008	0.042	-0.032		
Y value (m)		0.000	0.039	-0.039		
Z value (m)	1.22	1.677	0.679	-0.939	-0.457	YES
PCT Value (K)	558.6	557.6	10.5	-13.7	0.9	YES
WEU (x = 0, y = 0)						
z = 0.610 m	555	550.4	10.5	-13.5	4.1	YES
z = 1.219 m	553	556.2	10.5	-13.6	-2.9	YES
z = 1.829 m	548	556.5	10.6	-13.8	-8.2	YES
z = 2.438 m	537	545.1	12.6	-15.2	-8.3	YES
z = 3.658 m	466	474.9	13.4	-14.6	-8.8	YES
Vertical (y = 0 m, z = 1.219 m)						
x = -0.169 m (K)	368	369.4	5.5	-7.2	-1.7	YES
x = -0.137 m (K)	421	424.7	6.0	-6.2	-4.1	YES
x = -0.090 m (K)	462	466.5	7.5	-7.5	-4.6	YES
x = -0.068 m (K)	506	510.4	8.9	-9.1	-4.6	YES
x = -0.057 m (K)	536	525.7	10.9	-11.8	10.7	YES
x = -0.029 m (K)	558	552.4	10.4	-13.1	5.6	YES
x = 0.000 m (K)	553	556.2	10.5	-13.6	-2.9	YES
x = 0.068 m (K)	477	468.8	13.0	-15.3	8.0	YES
x = 0.090 m (K)	464	460.0	14.2	-14.1	3.5	YES
x = 0.137 m (K)	414	415.6	9.7	-9.5	-1.4	YES
x = 0.421 m (K)	323	329.8	6.6	-6.6	-6.8	NO
Horizontal (x = 0 m, z = 1.829 m)						
y = 0.000 m (K)	548	556.5	10.6	-13.8	-8.2	YES
y = 0.029 m (K)	550	547.6	14.2	-16.2	1.9	YES
y = 0.057 m (K)	532	519.6	13.0	-13.8	12.6	YES
y = 0.068 m (K)	499	503.8	9.6	-9.7	-4.5	YES
y = 0.089 m (K)	459	463.5	8.2	-8.1	-4.2	YES
y = 0.137 m (K)	416	419.3	6.5	-6.5	-3.6	YES
y = 0.165 m (K)	334	332.8	5.6	-5.6	0.8	YES

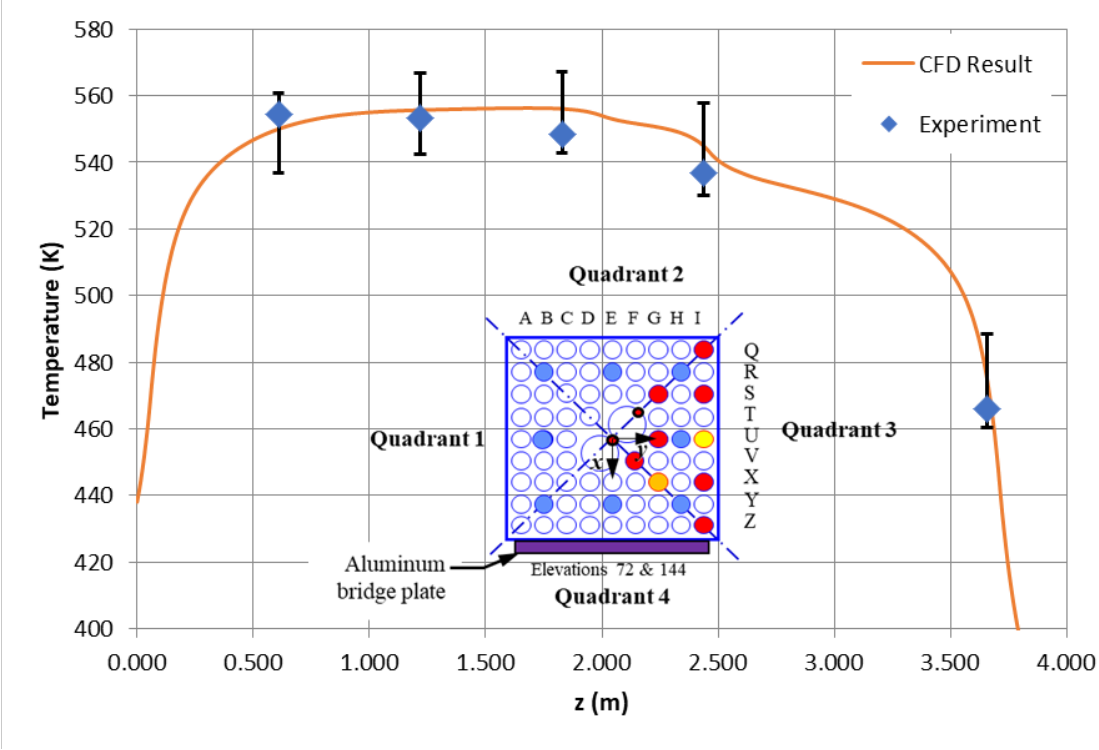

Figure 3-15 Axial temperature profile for the 2.5-kW, 100-kPa, helium test (open)

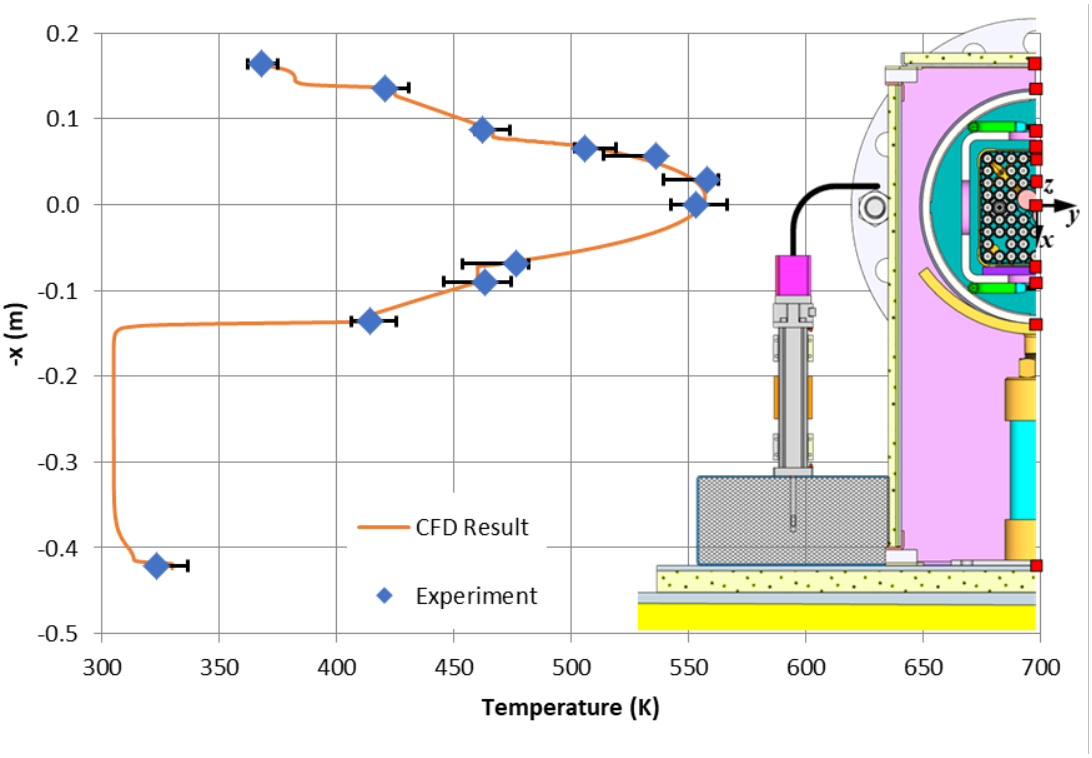

Figure 3-16 Vertical temperature profile for the 2.5-kW, 100-kPa, helium test (open)

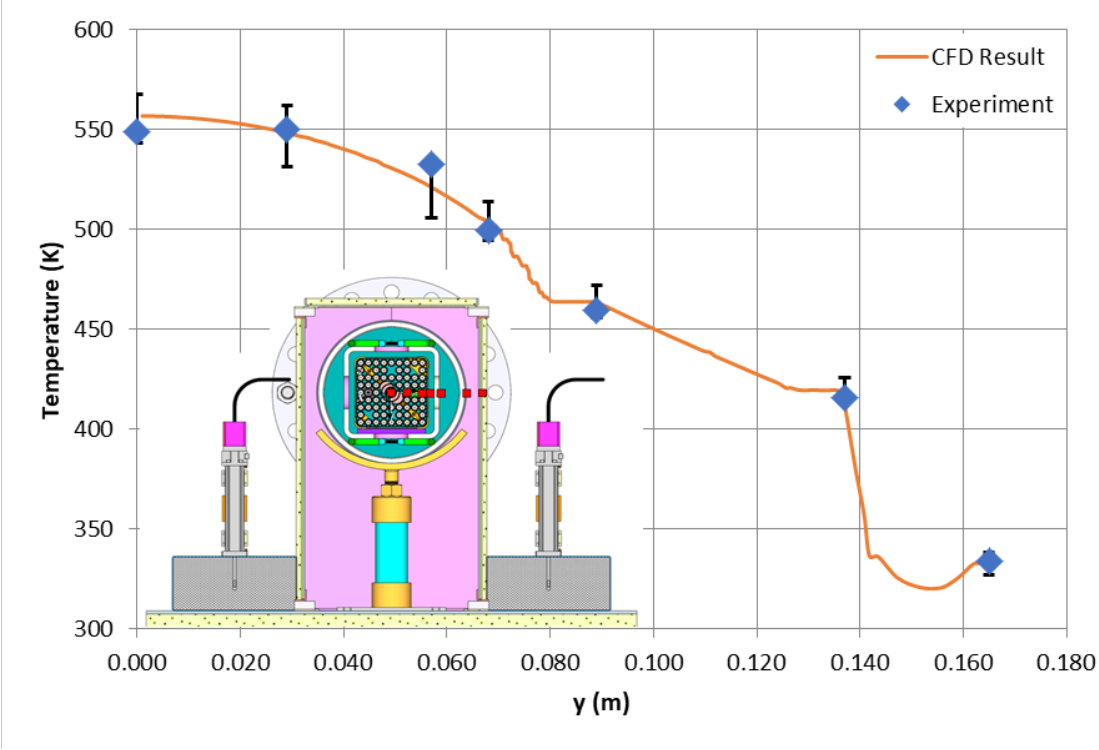

Figure 3-17 Horizontal temperature profile for the 2.5-kW, 100-kPa, helium test (open)

Table 3-16 Open Test Results for 2.5-kW, 100-kPa, Air

Parameter	Test Result	CFD Result	Positive Uncert.	Negative Uncert.	Compare Error, E	Valid?
Airflow Rate (kg/s)	0.0277	0.0263	0.0011	-0.0011	0.0014	NO
PCT Location						
X value (m)		-0.017	0.035	-0.034		
Y value (m)		0.000	0.037	-0.037		
Z value (m)	0.61	1.557	0.465	-0.986	-0.947	YES
PCT Value (K)	647.0	639.4	20.0	-29.5	7.6	YES
WEU (x = 0, y = 0)						
z = 0.610 m (K)	645	628.3	19.3	-28.8	16.3	YES
z = 1.219 m (K)	637	634.4	19.5	-29.0	3.0	YES
z = 1.829 m (K)	630	633.7	19.4	-28.9	-3.5	YES
z = 2.438 m (K)	615	613.7	22.6	-30.2	1.0	YES
z = 3.658 m (K)	527	513.6	26.9	-29.2	13.9	YES
Vertical (y = 0 m, z = 1.219 m)						
x = -0.169 m (K)	367	368.3	6.3	-6.3	-1.1	YES
x = -0.137 m (K)	420	423.8	6.7	-6.9	-3.7	YES
x = -0.090 m (K)	486	486.1	8.9	-9.2	-0.3	YES
x = -0.068 m (K)	562	568.1	17.1	-17.3	-6.6	YES
x = -0.057 m (K)	617	595.5	21.2	-24.8	21.4	NO
x = -0.029 m (K)	645	635.7	20.2	-29.3	9.0	YES
x = 0.000 m (K)	637	634.4	19.5	-29.0	3.0	YES
x = 0.068 m (K)	534	497.2	18.6	-29.4	37.0	NO
x = 0.090 m (K)	484	473.3	16.2	-15.9	11.2	YES
x = 0.137 m (K)	408	416.2	8.8	-8.4	-7.9	YES
x = 0.421 m (K)	321	330.1	6.1	-6.4	-9.1	NO
Horizontal (x = 0 m, z = 1.829 m)						
y = 0.000 m (K)	630	633.7	19.4	-28.9	-3.5	YES
y = 0.029 m (K)	634	622.0	22.8	-29.8	11.8	YES
y = 0.057 m (K)	607	579.3	21.2	-24.0	27.7	NO
y = 0.068 m (K)	552	550.8	15.6	-15.5	1.3	YES
y = 0.089 m (K)	481	479.9	9.0	-8.9	1.3	YES
y = 0.137 m (K)	414	418.7	6.8	-6.9	-4.3	YES
y = 0.165 m (K)	333	332.6	5.7	-5.8	0.0	YES

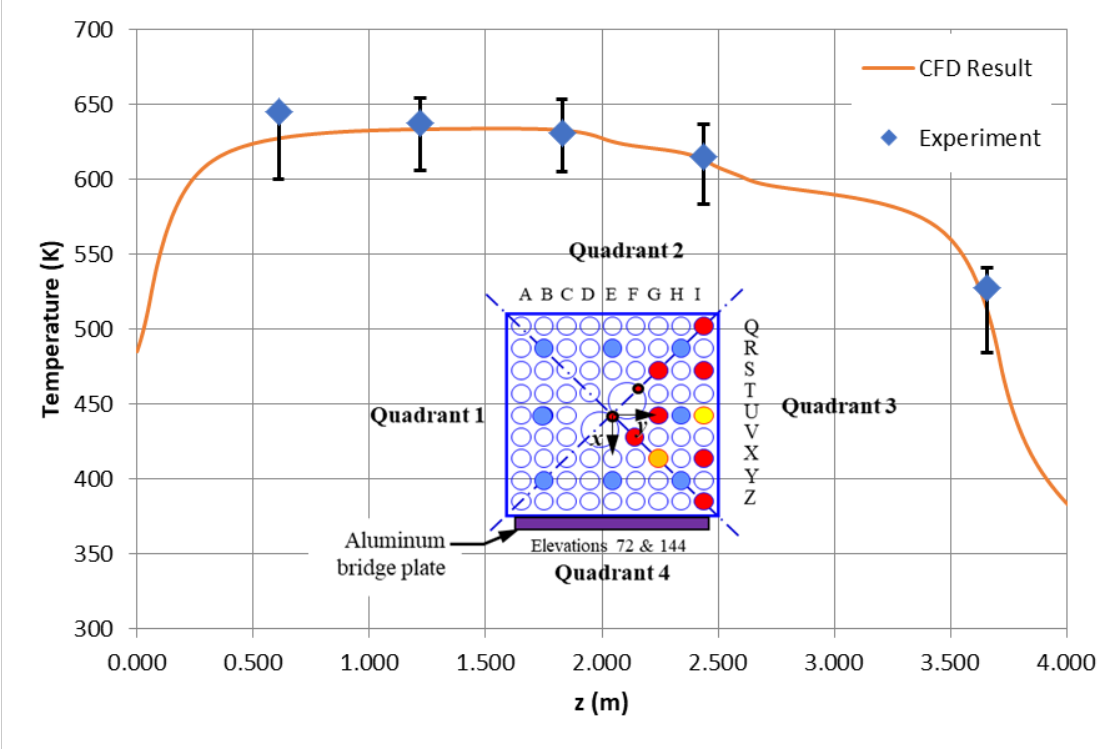

Figure 3-18 Axial temperature profile for the 2.5-kW, 100-kPa, air test (open)

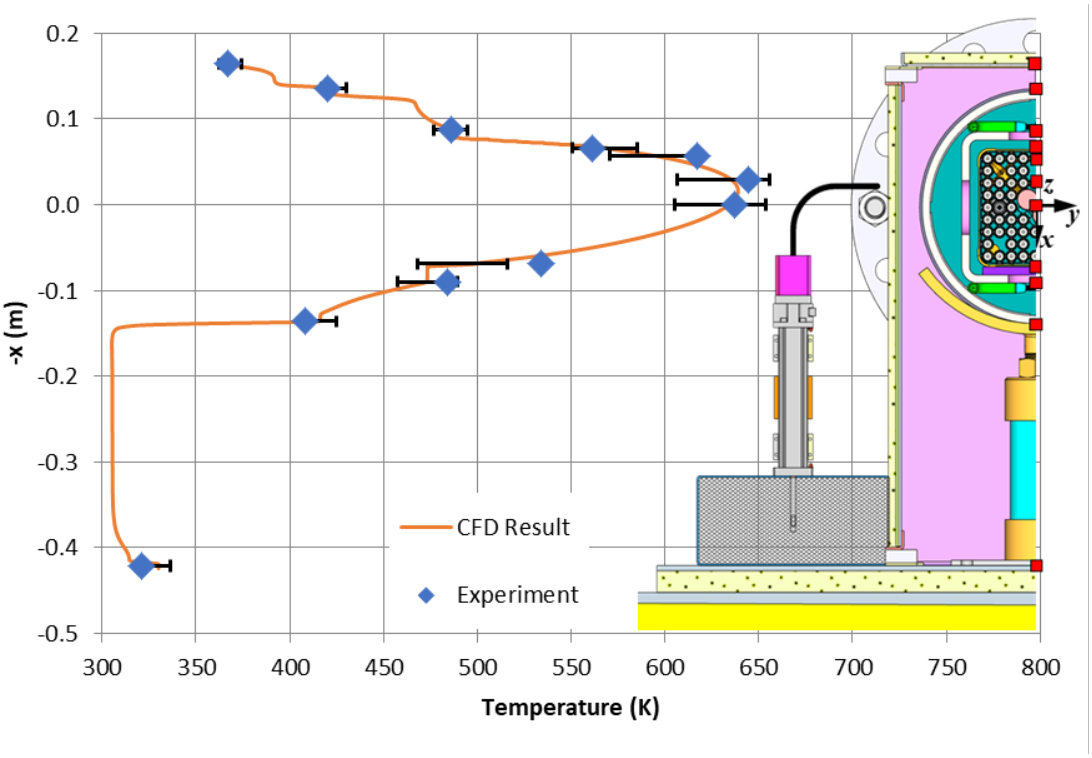

Figure 3-19 Vertical temperature profile for the 2.5-kW, 100-kPa, air test (open)

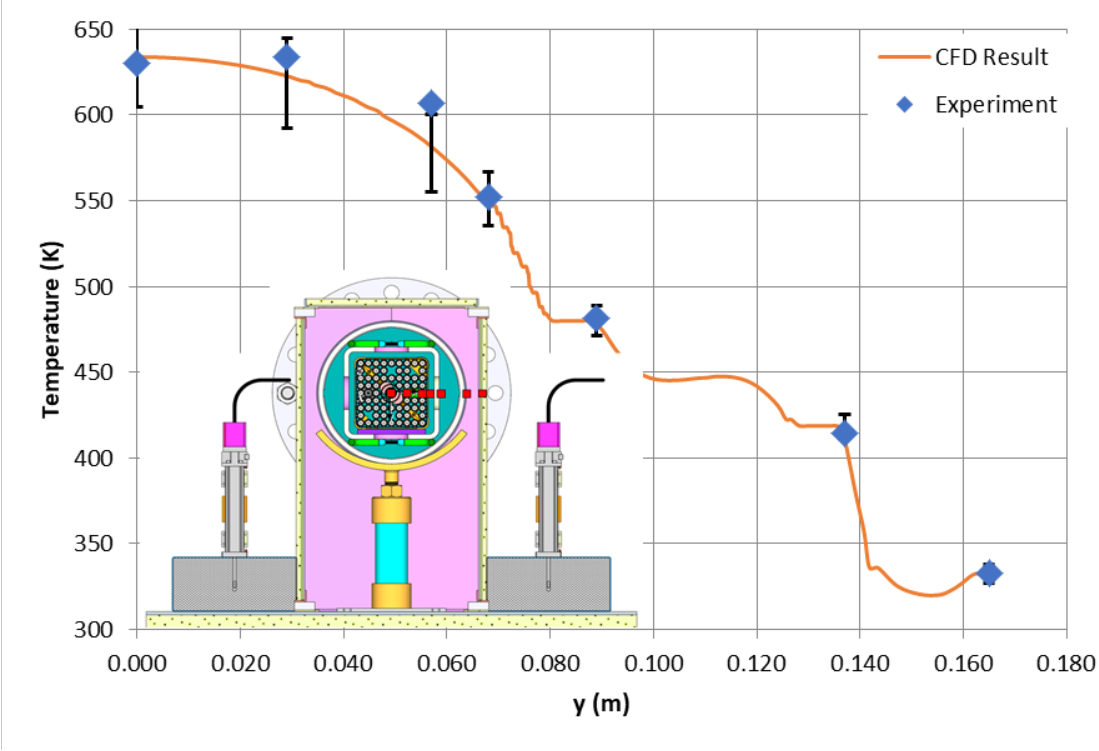

Figure 3-20 Horizontal temperature profile for the 2.5-kW, 100-kPa, air test (open)

4 PREDICTIVE RESULTS

After the model was validated with the two open test cases, modelers were asked to predict the same output values for eight blind cases. The modelers were provided the input values measured during each experimental test run (ambient temperature, input power, fill gas used, and the vessel pressure) along with measurement uncertainty. The modelers were then asked to provide the air mass flow rate and temperature at the same 21 locations as were presented for the open cases and the value and location of the PCT.

The eight blind simulations were run with the same boundary conditions as the two open cases, with the exception of the experimentally measured input values given to the modelers.

The numerical and input uncertainty were calculated the same way as for the two open cases, except the sensitivity of the HDCS to a 1-degree tilt relative to gravity was not included in the sensitivity analysis, as this was found to be of little consequence for the two open cases.

Input sensitivity runs were not completed for three cases: 1,000-W air at 100 kPa, 1,000-W helium at 100 kPa, and 500-W helium at 800 kPa. Instead, the overall input uncertainty values were interpolated from neighboring conditions for the two 1,000-W conditions. For the 500-W helium at 800 kPa, the input uncertainty was assumed to be the same as for the 500-W helium at 100 kPa condition on the basis that the 5,000-W helium, 800-kPa condition had a lower input uncertainty than the 5,000-W helium, 100-kPa condition.

For experimental uncertainty, since the measured values were not known when this analysis was conducted, the experimental uncertainty was based on the CFD simulation results instead. Temperature uncertainty was taken to be 1 percent of the computed temperature in kelvin, and mass flow rate uncertainty was taken as 1.5 percent of the computed mass flow rate.

Tables and plots for all the cases that were evaluated are shown in Appendix A , including both open and blind cases. The data presented here are the same blind data that were submitted to SNL before the experimental results were provided to the modelers. Table 4-1 and Figure 4-1 present the comparison between experimental and predicted values of airflow rate for all cases. Table 4-2 and Figure 4-2 present the comparison between experimental and predicted values of PCT. Appendix A contains tables and plots with all the detailed information comparing experimental and predicted values for each of the 10 cases investigated.

Air mass flow rates are underpredicted by the CFD model in all cases and are within the simulation uncertainty band in 4 of the 10 cases. The simulation uncertainty for air mass flow rate is relatively small—between 4 and 8 percent for all cases—so predicted values are still relatively close to experimental measurements even if they are not covered by the simulation uncertainty. The error in mass flow rate is proportionately smaller at higher heat flux values.

The PCT values were well predicted by the simulation, with the experimentally measured value within the simulation uncertainty of the calculated result for 9 of the 10 cases. The PCT comparison error is negative for the three 5-kW heat flux cases (CFD overpredicts temperature) but within the validation uncertainty as shown in Table 4-2, and comparison error is positive for the rest of the cases (CFD underpredicts temperature) but within the validation uncertainty except for one case as shown in Table 4-2. The temperature uncertainty is much greater for cases with air fill gas than for those with helium, primarily because of the emissivity input uncertainty. These trends are true for all temperature measurements, not just the PCT.

Overall, of the 260 measurements including temperature, air mass flow rate, and PCT and PCT location used for validation in both the open and blind tests (26 in each of 10 tests), 204, or 79 percent, were found to match experimental data within the simulation uncertainty band. The rest of the predictions were not too far from the validation uncertainty. Of the 260 measurements, 30 (11 percent of the data) were within 1 percent of the validation uncertainty band, 16 predictions (6.2 percent of the data) were within 2 percent of the corresponding validation uncertainty, and 6 more predictions (2.3 percent of the data) were within 3 percent of the corresponding validation uncertainty.

Temperature measurement locations that tended to predict more poorly include the following:

- The vault floor was consistently colder in the simulation than in the experiment, with 5 of the 10 cases falling within the simulation uncertainty band. This is likely due to the resulting higher heat flux imposed at the floor of the vault.
- The WEU measurement at axial location z = 0.610 m consistently predicted colder than experimental measurements with 6 of the 10 cases falling within the simulation uncertainty band. This is mainly due to the porous media model smearing of the temperature field.
- The bottom of the channel box was consistently colder in the simulation than in the experiment, with 6 of the 10 cases falling within the simulation uncertainty band. This suggests that there was more thermal resistance between the channel box, the bridge plate, and the basket than was included in the CFD model.
- The horizontal temperature measurement at the pin location IU was consistently colder in the simulation than in the experiment, with 6 of the 10 cases falling within the simulation uncertainty band. This was shown in the 2D comparison of porous modeling with explicit modeling of the fuel assembly internals. With the porous media approach, the heat generation is spread uniformly throughout the fuel bundle cross section, whereas in reality, the water rods occupy the center of the fuel bundle and the heating occurs mostly around the periphery of the assembly. Although the PCT is well predicted, porous media tend to underpredict the temperature at the “shoulders” of the fuel bundle.

Temperature locations that tended to best predict experimental results within the simulation uncertainty band include the following:

- PCT, as discussed previously.
- The WEU measurements at axial locations of z = 1.829 m, 2.438 m, and 3.658 m all had 9 of the 10 cases falling within the simulation uncertainty band.
- The top and side of the vault both had 10 of the 10 cases falling within the uncertainty band, indicating that the external HTC and insulation thermal resistance were well predicted at those locations.
- The basket bottom was well predicted with 10 of the 10 cases falling within the uncertainty band. This is somewhat unexpected considering that the neighboring measurement point at the bottom of the channel box predicted poorly.

The remaining temperature measurement locations all predicted within the simulation uncertainty band for 8 of the 10 cases.

Besides the very localized effect of closing the 0.9-mm gap between the channel box and the aluminum bridge plate, two factors dominated the overall uncertainty in local temperature measurements. The first is the uncertainty in emissivity values, particularly within the pressure vessel where temperatures are elevated. The second is the spatial discretization uncertainty, or GCI, which was a factor in areas of high temperature gradients that were more sensitive to grid refinement.

The uncertainty in the location of PCT was determined for the axial, vertical, and horizontal directions; however, only the axial location of the PCT was provided with the experimental results. The uncertainty in PCT location in each direction was established by determining the distance in each of the six cardinal directions (+x, -x, +y, -y, +z, -z) that was required for the temperature to decrease from the PCT by a given amount, ΔT. The ΔT value used to determine the uncertainty in PCT location was the experimental uncertainty in the PCT value, or 1 percent of the absolute temperature measurement. The uncertainty could just as easily have been the simulation uncertainty of the PCT for each case, which would give a larger uncertainty in PCT location.

Because of the sharper gradients in the vertical and horizontal directions, the uncertainty in PCT location was relatively small—generally around 40 mm in each direction. However, in the axial direction, the uncertainty in PCT location is much greater because of the shallow gradient in temperature along the length of the fuel assembly. The CFD model in all cases predicted the location of the PCT to be at a greater z coordinate than was measured in the experiment; however, in all cases the experimental value was within the simulation uncertainty of the calculated value. Table 4-3 and Figure 4-3 provide the results for axial location of PCT measurement.

Given the large uncertainty in axial PCT location, this parameter is not particularly useful in validating the model. Using temperature measurements at specific locations along the length of the fuel assembly to validate the simulation is easier for the modeler and provides more meaningful data. However, this does highlight one trend in the experiment data that the simulation did not accurately capture. In the high-heat experiments with air fill gas, the peak temperature moved closer to the nozzle end of the fuel assembly. The CFD simulation did not show this trend, and the modelers do not have a ready explanation for why this occurred in the experiment. In Appendix A , the plots of axial temperature profile for each case show this trend.

Table 4-1 Air Mass Flow Rate Prediction (kg/s)

Test Description	Test Result	CFD Result	Positive Uncert.	Negative Uncert.	Compare Error, E	Valid?
0.5 kW, 100 kPa, Helium—BLIND	0.0165	0.0137	0.0013	0.0012	0.0027	NO
1.0 kW, 100 kPa, Helium—BLIND	0.0195	0.0181	0.0012	-0.0011	0.0014	NO
2.5 kW, 100 kPa, Helium—OPEN	0.0283	0.0263	0.0012	-0.0011	0.0021	NO
5.0 kW, 100 kPa, Helium—BLIND	0.0354	0.0346	0.0018	-0.0019	0.0008	YES
0.5 kW, 800 kPa, Helium—BLIND	0.0157	0.0135	0.0011	-0.0010	0.0022	NO
5.0 kW, 800 kPa, Helium—BLIND	0.0338	0.0337	0.0022	-0.0021	0.0002	YES
0.5 kW, 100 kPa, Air—BLIND	0.0141	0.0136	0.0011	-0.0010	0.0004	YES
1.0 kW, 100 kPa, Air—BLIND	0.0194	0.0183	0.0011	-0.0011	0.0011	YES
2.5 kW, 100 kPa, Air—OPEN	0.0277	0.0263	0.0011	-0.0011	0.0014	NO
5.0 kW, 100 kPa, Air—BLIND	0.0359	0.0339	0.0015	-0.0014	0.0020	NO

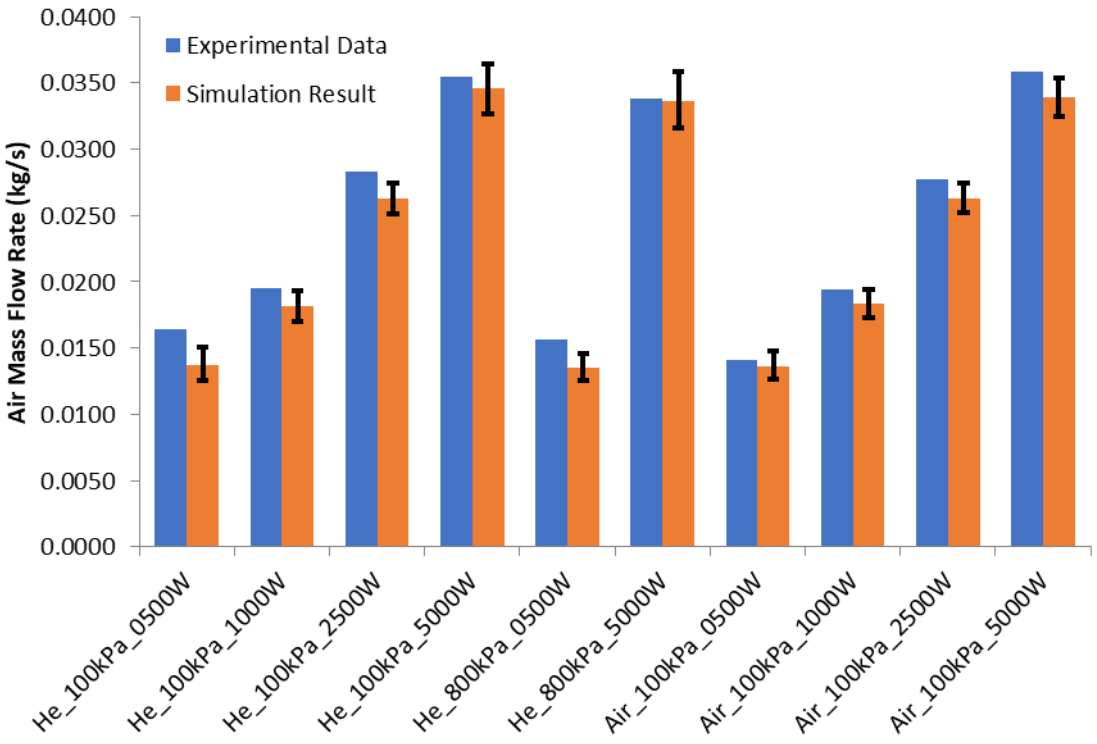

Figure 4-1 Air mass flow rate predictions (kg/s)

Table 4-2 PCT Prediction (K)

Test Description	Test Result	CFD Result	Positive Uncert.	Negative Uncert.	Compare Error, E	Valid?
0.5 kW, 100 kPa, Helium—BLIND	373.3	371.3	5.5	6.0	2.1	YES
1.0 kW, 100 kPa, Helium—BLIND	433.0	431.6	6.7	-7.8	1.4	YES
2.5 kW, 100 kPa, Helium—OPEN	558.6	557.6	10.5	-13.7	0.9	YES
5.0 kW, 100 kPa, Helium—BLIND	694.0	699.8	16.0	-21.7	-5.8	YES
0.5 kW, 800 kPa, Helium—BLIND	367.7	363.4	5.1	-5.6	4.3	YES
5.0 kW, 800 kPa, Helium—BLIND	677.1	683.4	10.9	-17.6	-6.3	YES
0.5 kW, 100 kPa, Air—BLIND	426.6	414.9	8.2	-11.2	11.7	NO
1.0 kW, 100 kPa, Air—BLIND	501.4	491.1	11.1	-15.8	10.2	YES
2.5 kW, 100 kPa, Air—OPEN	647.0	639.4	20.0	-29.5	7.6	YES
5.0 kW, 100 kPa, Air—BLIND	781.9	787.5	28.3	-39.9	-5.6	YES

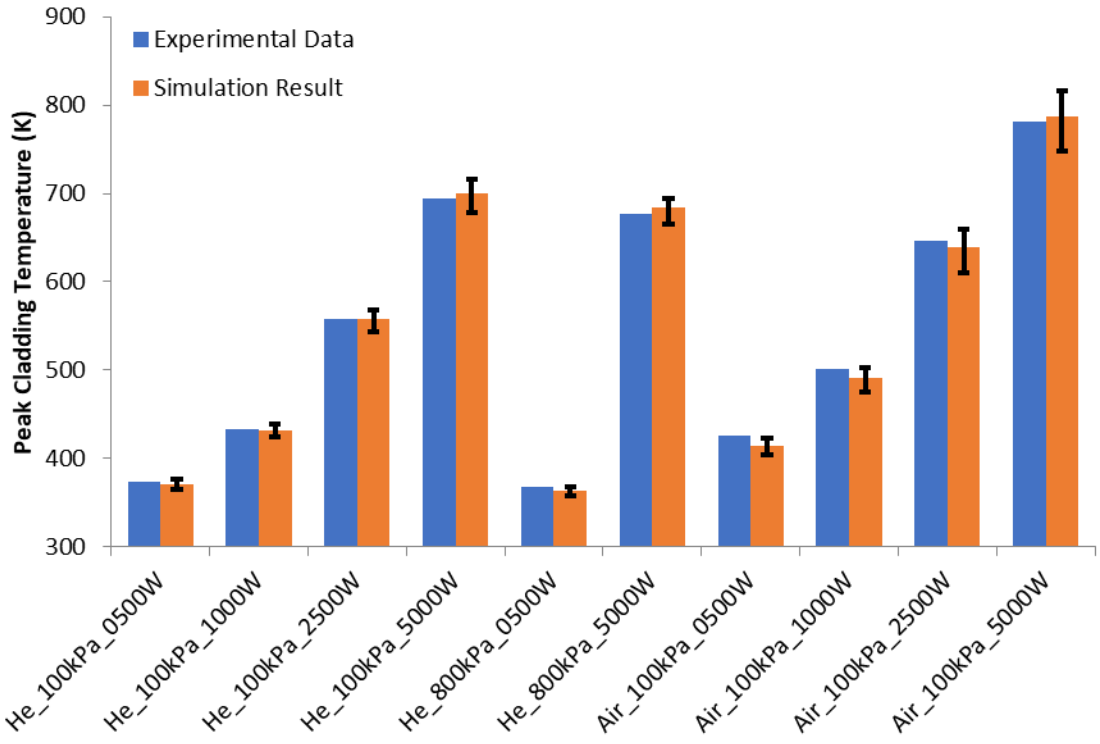

Figure 4-2 PCT prediction (K)

Table 4-3 PCT Location Prediction (m)

Test Description	Test Result	CFD Result	Positive Uncert.	Negative Uncert.	Compare Error, E	Valid?
0.5 kW, 100 kPa, Helium—BLIND	1.220	1.669	0.780	-1.121	-0.449	YES
1.0 kW, 100 kPa, Helium—BLIND	1.220	1.669	0.702	-1.057	-0.449	YES
2.5 kW, 100 kPa, Helium—OPEN	1.220	1.677	0.679	-0.939	-0.457	YES
5.0 kW, 100 kPa, Helium—BLIND	1.220	1.677	0.434	-1.097	-0.457	YES
0.5 kW, 800 kPa, Helium—BLIND	1.220	1.549	0.850	-0.939	-0.329	YES
5.0 kW, 800 kPa, Helium—BLIND	1.220	1.565	0.495	-0.821	-0.345	YES
0.5 kW, 100 kPa, Air—BLIND	1.220	1.517	0.625	-0.915	-0.297	YES
1.0 kW, 100 kPa, Air—BLIND	1.220	1.517	0.541	-0.900	-0.297	YES
2.5 kW, 100 kPa, Air—OPEN	0.610	1.557	0.465	-0.986	-0.947	YES
5.0 kW, 100 kPa, Air—BLIND	0.610	1.589	0.427	-1.065	-0.979	YES

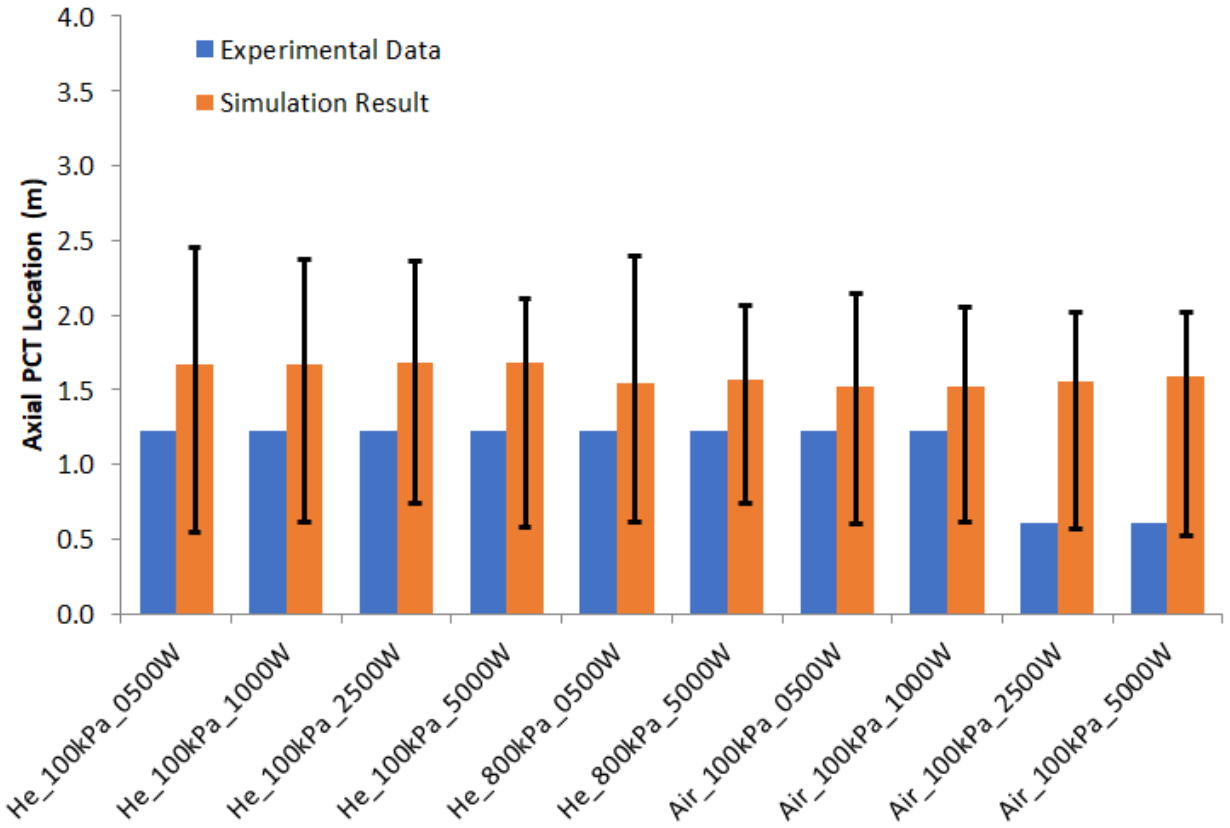

Figure 4-3 PCT location prediction (m)

5 DISCUSSION

The results presented for the two open cases and eight blind cases are the same results that were presented to SNL before the blind test results were made available to the modelers. Based on the experimental results, another round of model validation could be undertaken to further improve the models, but this was not the purpose of this benchmarking exercise or of this document.

Overall, the CFD model does a good job of matching the experimental results within the simulation uncertainty, with 79 percent of the temperature, air mass flow rate, PCT, and PCT location measurements falling within the simulation uncertainty of the predicted values. The rest of the predictions were within 3 percent of the error between CFD predictions and experimental data.

The input data provided to the modelers by SNL were very thorough and included all the values required for the CFD model inputs, along with their associated uncertainty. The largest source of temperature uncertainty in this simulation was the uncertainty in emissivity values. The emissivity measurements that were taken at discrete locations on the Zircaloy channel box, Inconel heater rod cladding, and painted steel basket and pressure vessel indicated significant variation in emissivity across the surfaces of these components. Since most of the heat transfer within the pressure vessel is via radiation—especially with air as the fill gas—the simulations are sensitive to this uncertainty in emissivity. For the baseline (2.5-kW) helium case, the total uncertainty in PCT was +10/-14 K, with +8/-12 K due to emissivity uncertainty. For the baseline (2.5-kW) air case, the total uncertainty in PCT was +20/-30 K, with +19/-28 K due to emissivity uncertainty. Based on these values, it is not possible to validate the simulation to within the 10–20 K temperature margin that many applicants usually have in their CFD predictions. Even if the PCT is within the simulation uncertainty band, the uncertainty in emissivity masks any other modeling errors that may exist, which could contribute to errors as large as the margin that applicants are seeking. Based on these results, these experiments cannot be called CFD-grade for this explicit purpose. Given the care that went into conducting this experiment, this underscores the difficulty in ensuring accurate model predictions of DCSS installations that are within 10–20 degrees C (18–36 degrees F) of their PCT limits.

The variations in emissivity values are likely caused by the extended use of many of these components over several years. These components were operating in an oxidizing environment (air) at elevated temperatures, which alters the surface finish of the components and changes the emissivity. This is important to note for actual DCSS installations if the emissivity of high-temperature components is expected to change over time. For new DCSS installations in a nonoxidative environment, the emissivity of the cask surfaces will likely be more consistent across the area of each component, and the emissivity is less likely to change over time, reducing the uncertainty of emissivity values for the installation. After several years in a reactor and spent fuel pool, the fuel assemblies can be expected to be fully oxidized, which also reduces the uncertainty in their surface emissivity values.

As in previous DCSS analyses using the porous media approach to simplify modeling of the fuel bundle [4] [6] [8] [17], the porous media approach was found to accurately predict the PCT within the uncertainty of the simulation. These further builds confidence in the ability of a correctly applied porous media model to accurately simulate DCSS installations. With this confidence in the best estimate model that includes the most likely scenario supplemented by UQ, the use of conservative boundary conditions and conservative geometric assumptions, or

both, should result in conservative predictions. Although it is necessary in an application to be thorough in describing and demonstrating that the model inputs are conservative, applicants prefer the conservative model as it is a simple and straightforward modeling approach as opposed to completing an extensive UQ of the input parameters as shown here. Applicants will still need to demonstrate that spatial discretization uncertainty is sufficiently low, but this is generally a small portion of the overall UQ at the PCT location where temperature gradients are inherently low.

In contrast to the PCT results, the mass flow rate prediction did not fall within the simulation uncertainty band of the experimental data. Although the CFD predictions are fairly close to the experimental data, with less than an 8-percent deviation in all but the lowest heat flux cases, the simulation uncertainty band is smaller in most cases. The uncertainty in experimental air mass flow rate measurements may be higher than reported with the experimental results [9]. The reported mass flow uncertainty is based on an assumption that the error in velocity measurements across the inlet duct used to calculate total flow rate is uncorrelated. However, if there is a systematic error in the velocity measurement, the errors in the measurements cannot be considered independent of each other, and the error in mass flow rate would be more than 5 times the reported value, as discussed in Section 3.4.6 of this document. If this larger experimental uncertainty value of 0.00233 kg/s is used in the uncertainty analysis, all CFD simulation results would fall within the uncertainty bounds of the experimentally measured values. Considering how close the simulation temperature measurements are to the experimental values, and the coupled nature of heat rejection and air mass flow rate, it seems as though both should match the experimental data equally well or equally poorly.

The many temperature measurements throughout the cask provide a great deal of information for model validation. In places where the simulation was within uncertainty bands for most or all the test conditions, the model boundary conditions can be considered to be well chosen. Locations where the simulation did not match experimental measurements within the simulation uncertainty are areas that can be studied to improve the quality of the simulation and reduce modeling error. Mass flow rate was measured only at the inlet to the HDCS, so there is less information available to determine the cause of the modeling error in mass flow rate. With natural convection, the temperature and mass flow rate are interdependent, so some information is available, but air temperature measurements taken at the outlet vents would have aided in validating the mass and energy balance in the vault.

Three different modeling groups participated in the numerical validation and benchmarking exercise, including the NRC, Pacific Northwest National Laboratory, and Empresa Nacional del Uranio, S.A., S.M.E. [9]. The SNL validation synthesis report [9] states the following about the models that were used to validate the HDCS cases as presented in this report: “Based on the combined RMS error results, NRC model offered the best overall fit to the experimental data.” The report also adds that “NRC was the only institution that accompanied the base case model with uncertainty quantification.” The report also states the following:

> The NRC submission was an extensive effort that captures the effect of introducing simulation uncertainty bounds in the comparison of model results to experimental data. The method, which is derived from the ASME verification and validation approach [ASME V&V 20-2009] [5] is explored in the validation uncertainty section in Chapter 3 of the synthesis report [9], which shows how the uncertainty quantification can be used to provide a better measure of model prediction accuracies. Overall, this model validation method takes both measurement and simulation uncertainties into account and serves as an example of how the model validation uncertainty quantification can be further

explored. By definition, NRC thermal model is considered validated if the combined RMS error normalized by the validation uncertainty is less than 1, and this was shown to be the case.

6 CONCLUSIONS

A CFD validation of data collected using a horizontal dry cask system (HDCS) followed guidelines from NUREG-2152 [4] and ASME V&V 20-2009 [5]. The HDCS, a test apparatus simulating the fuel compartment of a dry cask, was constructed and operated to produce first-of-a-kind, high-fidelity transient and steady-state thermal-hydraulic datasets suitable for CFD model validation. The experiment tested configurations for the horizontal storage cask systems and validated the CFD models successfully. Ten unique datasets were collected and analyzed for these efforts using both helium and air as a fill gas. This report covers all the measured data, with appropriate limitations, to validate the thermal model that the NRC uses for dry cask applications.

The dry cask CFD modeling technique using porous media to simulate the fuel assembly internals was validated with experimental data in two open cases and then benchmarked against yet more experimental data in eight blind cases. The CFD predictions were found to match experimental data within the simulation uncertainty for the majority of the comparison metrics used and, in particular, for the PCT value, which was accurately predicted for 9 of the 10 cases evaluated. This report, along with NUREG-2238, "Validation of a Computational Fluid Dynamics Method Using Vertical Dry Cask Simulator Data," issued June 2020 [8], and NUREG/CR-7260, "CFD Validation of Vertical Dry Cask Storage System," issued May 2019 [6], demonstrate how to implement ASME V&V 20-2009 [5] to quantify the uncertainty of a DCSS CFD model.

The PCT validation uncertainty in helium cases varied between 6 to 20 degrees C (11 to 36 degrees F) for decay heat varying between 0.5 to 5 kW respectively. In the air fill cases, the PCT validation uncertainty varied between 8 to 40 degrees C (14 to 72 degrees F) for decay heat between 0.5 to 5 kW respectively. The high values for validation uncertainty in all the validated cases in this report are primarily due to the uncertainty in the emissivity of the components used in this experiment. These values are significantly smaller than those obtained in the CFD validation of the TN32 cask documented in NUREG/CR-7260 [6]. However, applicants' PCT predictions are generally within a margin of 10–20 degrees C (18–36 degrees F), especially for cask designs with a high heat load. For this reason, a thermal model with a validation uncertainty of 6–40 degrees C (11–72 degrees F) as obtained in this report using the best estimate analysis (i.e., the most likely scenario supplemented by a complete UQ analysis as shown in this report) will not be useful to justify predictions with a margin of 10–20 degrees C (18–36 degrees F). Conversely, if a thermal model with conservative input parameters was used, UQ for input parameters is not necessary. Only numerical uncertainty consisting of discretization errors (i.e., GCI), round-off errors, and iteration errors is required. In this validation exercise, the PCT numerical uncertainty varied from 0.4–4.1 degrees C (1–7 degrees F) for the helium fill gas cases and from 1.3–4.9 degrees C (2–9 degrees F) for the air fill gas cases. Consequently, thermal models that have conservative input parameters (as usually used by applicants following CFD modeling guidelines as documented in NUREG-2152 [4]) would generally be deemed acceptable with adequately demonstrated thermal margins.

There is some discrepancy in the temperature profile between the porous media modeling approach and the experimental data; however, this is to be expected and is acceptable as porous media smear the temperature field because of the assumptions used to simplify the geometry (i.e., fuel rod and grid spacers are not represented) and the use of the porous model to represent the missing geometry (i.e., the use of an equivalent frictional, inertial resistance, porosity, and effective thermal conductivity to model the missing geometry). The CFD model in

this validation generally under-predicted air mass flow rate but was still close to the measured value. The validation synthesis report [9] states, “Based on the combined RMS error results, NRC model offered the best overall fit to the experimental data.”

It is demonstrated that the porous media approach is an accurate method (i.e., has the right physical models) to predict the PCT value, given accurate simulation inputs. This enables applicants to take a conservative approach in demonstrating the thermal compliance of their cask by using conservative boundary conditions and geometric assumptions, while using an accurate modeling process as documented in NUREG-2152 [4]. There will always be numerical uncertainty in any simulation, and it should be demonstrated that the numerical uncertainty is less than the margin. However, the use of conservative input values makes the need for the rigorous input sensitivity (UQ for input parameters) demonstrated here unnecessary.

When the cask is designed for higher decay heat, the PCT values are getting close to the limit, and the obtained margin is questionable, the method presented in this report to evaluate the UQ can be used to show certainty and confidence in the obtained margins. The method presented here, when used properly, will inform the applicant and thermal reviewer about the confidence and the certainty of the margin for any cask design. Often, the cask applicant uses the worst-case scenario to perform dry cask thermal analyses, especially when there are enough margins from the allowable PCT limit. The worst-case scenario model should be based on proven conservative input values using a phenomena identification and ranking table (PIRT). The right PIRT should include all the possible input variables and modeling settings with possible uncertainties. As such, the worst-case scenario model will consist of input choices that will impact the dry cask thermal performance negatively (i.e., each input variable will lead to a higher PCT). The modeling uncertainty for this type of thermal model should include only numerical uncertainties. In this case, the safety margins would generally be acceptable if it is demonstrated that it adequately covers the numerical uncertainty and any other additional unknown modeling uncertainties given that the thermal model for the worst case scenario followed CFD best practice guidelines as documented in NUREG-2152 [4].

The discussions and conclusion section of the Electric Power Research Institute (EPRI) DOE cask demonstration report validation exercise [7] indicated that “CFD dry cask thermal models are generally conservative.” However, the NRC cask demonstration CFD analysis as documented in NUREG/CR-7260 [6] showed that the EPRI report statement is acceptable only when conservative analysis is used. NUREG/CR-7260 [6] showed that if a best estimate model (i.e., most likely or base case scenario supplemented by UQ as done in the report) was used, detailed reasons for the PCT and temperature field over-predictions can be explained. In that thermal model round robin, involving the DOE cask demonstration project [6] [7], geometrical uncertainties (i.e., gaps) were the main reasons for temperature prediction deviations as explained in detail by NUREG/CR-7260 [6]. NUREG/CR-7260 showed a PCT validation uncertainty of 62 degrees C (112 degrees F) for the DOE cask demonstration exercise. This unusually high validation uncertainty was mainly caused by the uncertainty in knowledge of the fluid gaps in the cask geometry. The validation exercise contained in this report, NUREG-2238 [8], NUREG/CR-7260 [6], and the SNL validation synthesis reports [9] [10] showed that the CFD thermal model as described in this report using CFD best practice guidelines as documented in NUEREG-2152 [4] resulted in PCT predictions that agreed very favorably with the experimental data within the calculated validation uncertainty.

7 REFERENCES

[1] U.S. NRC, Title 10 of the *Code of Federal Regulations* (10 CFR) Part 72, "Licensing requirements for the independent storage of spent fuel nuclear fuel, high level radioactive waste, and reactor-related greater than Class C waste," U.S. Nuclear Regulatory Commission, Washington, DC.

[2] U.S. NRC, NUREG-2215, "Standard Review Plan for Spent Fuel Dry Storage Systems and Facilities," U.S. Nuclear Regulatory Comission, Washighton, DC, April 2020.

[3] E. Lindgren, S. G. Durbin, R. J. Pulido and A. Salazar, "Update on the Thermal Hydraulic Investigations of a Horizontal Dry Cask Simulator," SAND2019-11688 R, Sandia National Laboratories, Albuquerque, NM, September 2019.

[4] U.S. NRC, NUREG-2152, "Computational Fluid Dynamics Best Practice Guidelines for Dry Cask Applications," U.S. Nuclear Regulatory Commision, Washington, DC, March 2013.

[5] ASME, V&V 20-2009, "Standard for Verification and Validation in Computational Fluid Dynamics and Heat Transfer," ASME, New York, NY, 2009.

[6] U.S. NRC, NUREG/CR-7260, "CFD Validation of Vertical Dry Cask Storage System," Office of Nuclear Reagulatory Research, U.S. Nuclear Regulatory Commission, Washington, DC, May 2019.

[7] EPRI 3002013124, "High-Burrnup Used Fuel Dry Storage System Thermal Modeling Benchmark," Electric Power Research Institute, Palo Alto, Ca, Apil 2020.

[8] U.S. NRC, NUREG-2238, "Validation of a Computational Fluid Dynamics Method Using Vertical Dry Cask Simulator Data," Office of Nuclear Regulatory Research, U.S. Nuclear Regulatory Commission, Washighton, DC, June 2020.

[9] R. Pulido, R. Fasano, E. Lindgren and S. Durbin, "Blind Modeling Validation Exercises Using the Horizontal Dry Cask Simulator," SAND2020-10344 R, Sandia National Laboratories, Albuquerque, NM, September 2020.

[10] R. Pulido, E. Lindgren and S. Durbin, "Modeling Validation Exercises Using the Dry Cask Simulator," SAND2019-6079R, Sandia National Laboratories, Alburqueque, NM, May 2019.

[11] EPRI 3003018441, "Phenomena Indentification and Ranking Table (PIRT) for Thermal Modeling," Electric Power Research Institute, Palo Alto, CA, June 2020.

[12] D. Bestion et al., "Review of Uncertainty Methods for Computational Fluid Dynamics Application to Nuclear Reactor Thermal Hydraulics," Organisation for Economic Co-operation and Development, Nuclear Energy Agency, Committee on the Safety of Nuclear Installations, Working Group on Analysis and Management of Accidents, CFD Working Group, Paris, France, 2016.

[13] D. Bestion et al., "Requirement for CFD-Grade Experiments for Nuclear Reactor Thermal-Hydraulics," Organisation for Economic Co-operation and Development, Nuclear Energy Agency, Committee on the Safety of Nuclear Installations, Working Group on Analysis and Management of Accidents, CFD group, Paris, France, 2019.

[14] U.S. NRC, Regualtory Guide 1.203, "Transient and Accident Analysis Methods," U.S. Nuclear Regulatory Commision, Washington, DC, 2005.

[15] U.S. NRC, NUREG-0800, "Standard Review Plan for the Review of Safety Analysis Reports for Nuclear Power Plants: LWR Edition," Office of Nuclear Regulatory Research, U.S. Nuclear Regulatory Commission, Washington, DC, March 2017.

[16] E. Lindgren and S. Durbin, "Materials and Dimensional Reference Handbook for the Boiling Water Reactor Dry Cask Simulator," SAND2017-13058R, Sandia National Laboratories, Albequerque, NM, November 2017.

[17] U.S. NRC, NUREG-2208, "Validation of Computational Fluid Dynamics Methods Using Prototypic Light Water Reactor Spent Fuel Assembly Thermal-Hydraulic Data," Office of Nuclear Regulatory Research, U.S. Nuclear Regulatory Commission, Washighton, DC, March 2017.

[18] TRW Environmental Safety Systems, Inc., "Spent Nuclear Fuel Effective Thermal Conductivity Report," Las Vegas, NV, July 1996.

APPENDIX A
DETAILED RESULTS FROM ALL CASES

The following tables contain comparisons of computational fluid dynamics (CFD) results with the experimentally measured values for all measurements submitted to Sandia National Laboratories for all 10 conditions evaluated. Each measurement includes the simulation uncertainty and whether the CFD result accurately predicts the experimental measurement within the simulation uncertainty.

Additionally, plots of the temperature profiles along the axial, vertical, and horizontal directions are included for each test case. Experimentally measured values are shown as blue diamonds, and CFD predicted values are shown as continuous orange curves along the axis in question. Error bars are provided at each experimental measurement location to denote the simulation uncertainty at each location. The experimental uncertainty is contained within the simulation uncertainty, so there are no separate error bars for the experimental uncertainty.

Table A-1 Blind Test Results for 0.5-kW, 100-kPa, Helium

Parameter	Test Result	CFD Result	Positive Uncert.	Negative Uncert.	Compare Error, E	Valid?
Airflow Rate (kg/s)	0.0165	0.0137	0.0013	0.0012	0.0027	NO
PCT Location						
X value (m)		-0.010	0.043	0.042		
Y value (m)		0.000	0.075	0.075		
Z value (m)	1.22	1.669	0.780	1.121	-0.449	YES
PCT Value (K)	373.3	371.3	5.5	6.0	2.1	YES
WEU (x = 0, y = 0)						
z = 0.610 m (K)	371	367.7	5.6	6.3	3.0	YES
z = 1.219 m (K)	371	370.5	5.6	6.1	0.8	YES
z = 1.829 m (K)	370	370.8	5.6	6.0	-0.9	YES
z = 2.438 m (K)	366	367.0	6.1	6.4	-1.2	YES
z = 3.658 m (K)	343	343.3	6.1	6.3	-0.6	YES
Vertical (y = 0 m, z = 1.219 m)						
x = -0.169 m (K)	315	312.8	3.9	5.0	2.1	YES
x = -0.137 m (K)	332	331.3	4.9	5.0	0.9	YES
x = -0.090 m (K)	344	342.9	4.7	4.9	1.1	YES
x = -0.068 m (K)	358	356.2	5.0	5.2	1.5	YES
x = -0.057 m (K)	366	361.0	5.8	6.1	5.3	YES
x = -0.029 m (K)	373	369.5	5.5	6.0	3.8	YES
x = 0.000 m (K)	371	370.5	5.6	6.1	0.8	YES
x = 0.068 m (K)	348	343.5	6.1	6.5	4.1	YES
x = 0.090 m (K)	344	341.3	6.2	6.4	3.1	YES
x = 0.137 m (K)	330	330.0	5.4	5.5	0.5	YES
x = 0.421 m (K)	303	303.1	4.5	4.5	-0.3	YES
Horizontal (x=0 m, z = 1.829 m)						
y = 0.000 m (K)	370	370.8	5.6	6.0	-0.9	YES
y = 0.029 m (K)	370	367.9	6.6	6.9	2.5	YES
y = 0.057 m (K)	365	358.9	6.2	6.4	5.8	YES
y = 0.068 m (K)	355	354.1	5.3	5.4	1.3	YES
y = 0.089 m (K)	344	342.4	5.1	5.2	1.2	YES
y = 0.137 m (K)	331	330.7	4.8	4.8	0.6	YES
y = 0.165 m (K)	306	304.0	4.6	4.5	2.0	YES

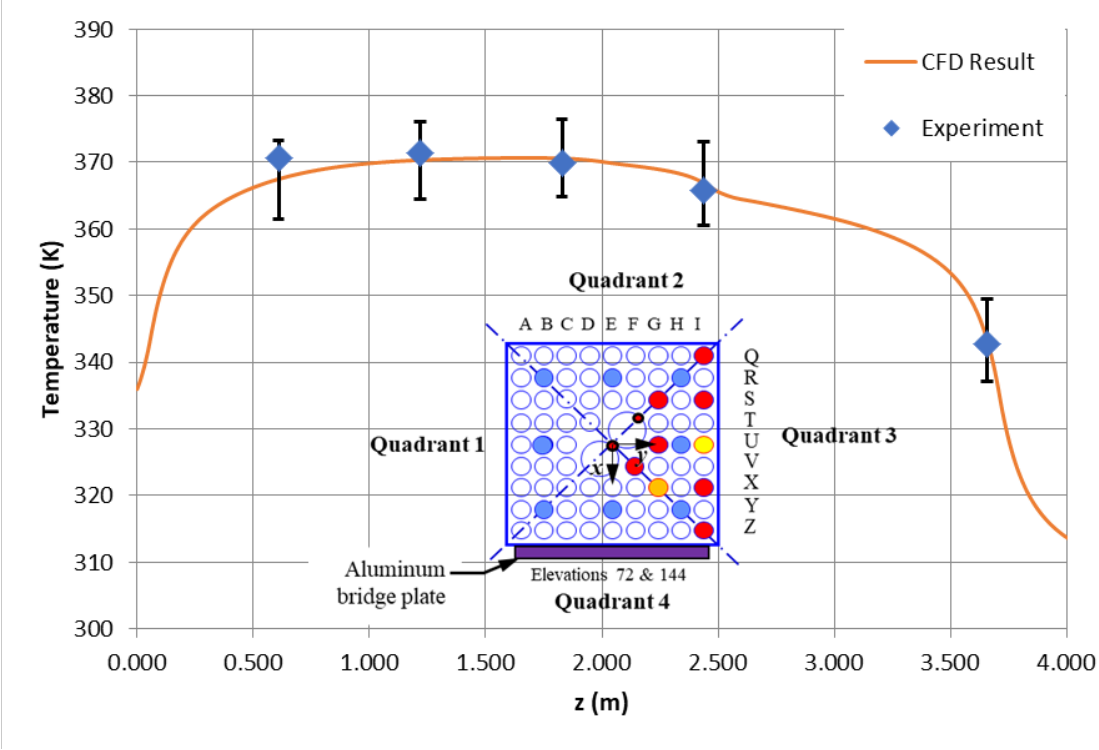

Figure A-1 Axial temperature profile for the 0.5-kW, 100-kPa, helium test (blind)

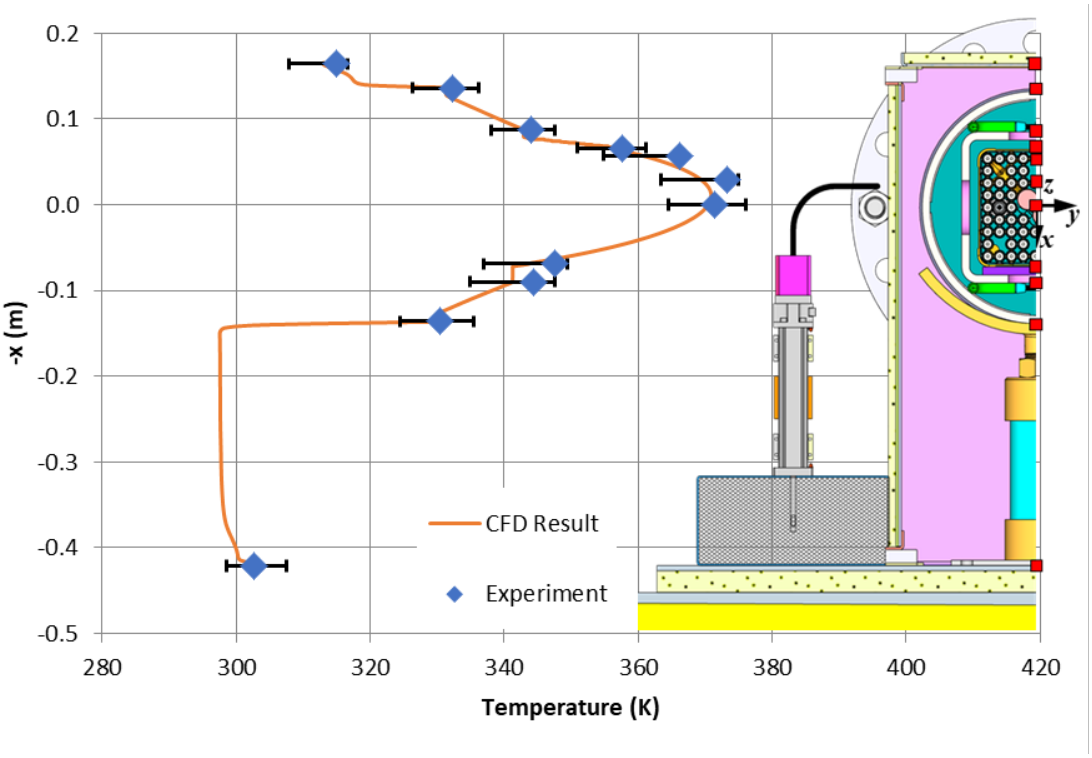

Figure A-2 Vertical temperature profile for the 0.5-kW, 100-kPa, helium test (blind)

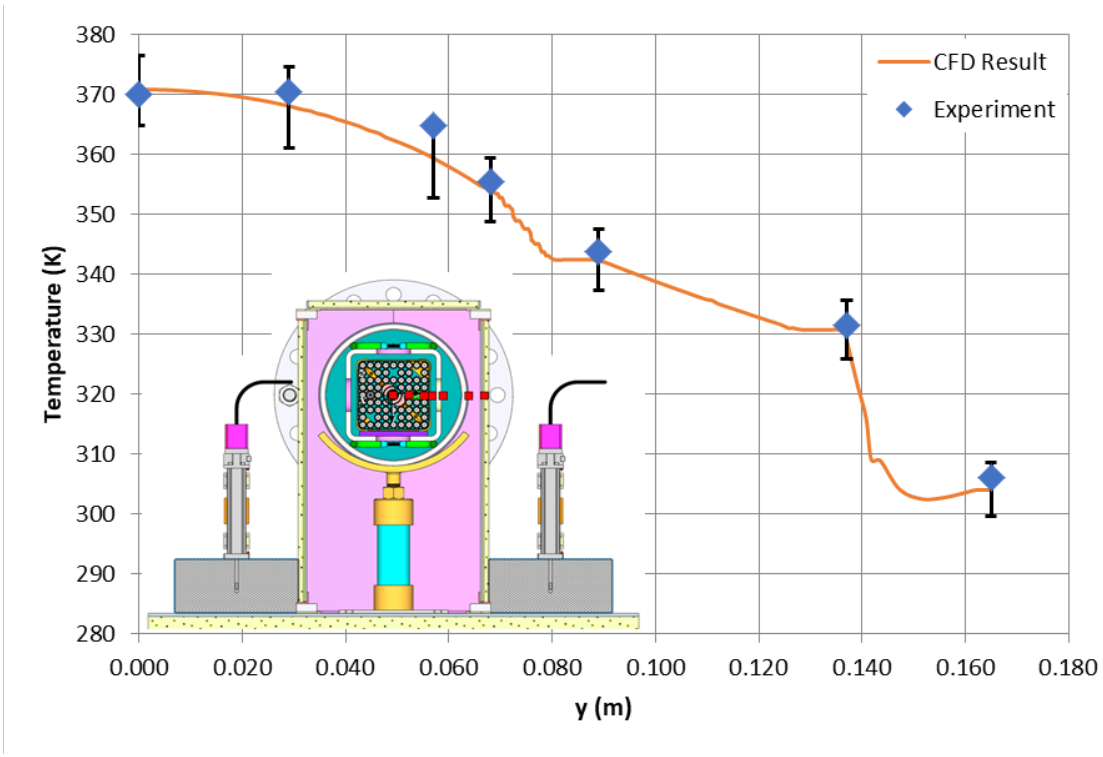

Figure A-3 Horizontal temperature profile for the 0.5-kW, 100-kPa, helium test (blind)

Table A-2 Blind Test Results for 1.0-kW, 100-kPa, Helium

Parameter	Test Result	CFD Result	Positive Uncert.	Negative Uncert.	Compare Error, E	Valid?
Airflow Rate (kg/s)	0.0195	0.0181	0.0012	-0.0011	0.0014	NO
PCT Location						
X value (m)		-0.010	0.039	-0.038		
Y value (m)		0.000	0.075	-0.075		
Z value (m)	1.22	1.669	0.702	-1.057	-0.449	YES
PCT Value (K)	433.0	431.6	6.7	-7.8	1.4	YES
WEU (x = 0, y = 0)						
z = 0.610 m (K)	429	426.4	6.5	-7.8	3.0	YES
z = 1.219 m (K)	430	430.6	6.7	-7.8	-0.4	YES
z = 1.829 m (K)	427	430.8	6.9	-7.9	-3.5	YES
z = 2.438 m (K)	421	424.5	7.5	-8.4	-3.6	YES
z = 3.658 m (K)	381	384.7	7.5	-8.0	-3.4	YES
Vertical (y = 0 m, z = 1.219 m)						
x = -0.169 m (K)	331	329.9	6.3	-7.2	1.3	YES
x = -0.137 m (K)	359	361.4	4.9	-5.1	-2.2	YES
x = -0.090 m (K)	381	382.2	5.4	-5.5	-1.7	YES
x = -0.068 m (K)	404	405.5	5.9	-6.1	-1.6	YES
x = -0.057 m (K)	420	413.9	6.9	-7.4	6.1	YES
x = -0.029 m (K)	433	428.7	6.6	-7.6	4.3	YES
x = 0.000 m (K)	430	430.6	6.7	-7.8	-0.4	YES
x = 0.068 m (K)	387	383.1	7.5	-8.4	4.2	YES
x = 0.090 m (K)	381	379.1	7.9	-8.0	2.3	YES
x = 0.137 m (K)	356	358.3	5.7	-5.7	-2.1	YES
x = 0.421 m (K)	309	312.7	4.8	-4.8	-3.5	YES
Horizontal (x = 0 m, z = 1.829 m)						
y = 0.000 m (K)	427	430.8	6.9	-7.9	-3.5	YES
y = 0.029 m (K)	429	425.8	8.7	-9.4	2.9	YES
y = 0.057 m (K)	419	410.3	8.0	-8.3	9.1	NO
y = 0.068 m (K)	401	401.8	6.3	-6.5	-0.6	YES
y = 0.089 m (K)	380	380.9	5.8	-5.9	-1.4	YES
y = 0.137 m (K)	358	359.5	5.1	-5.1	-2.0	YES
y = 0.165 m (K)	315	314.0	4.7	-4.6	1.2	YES

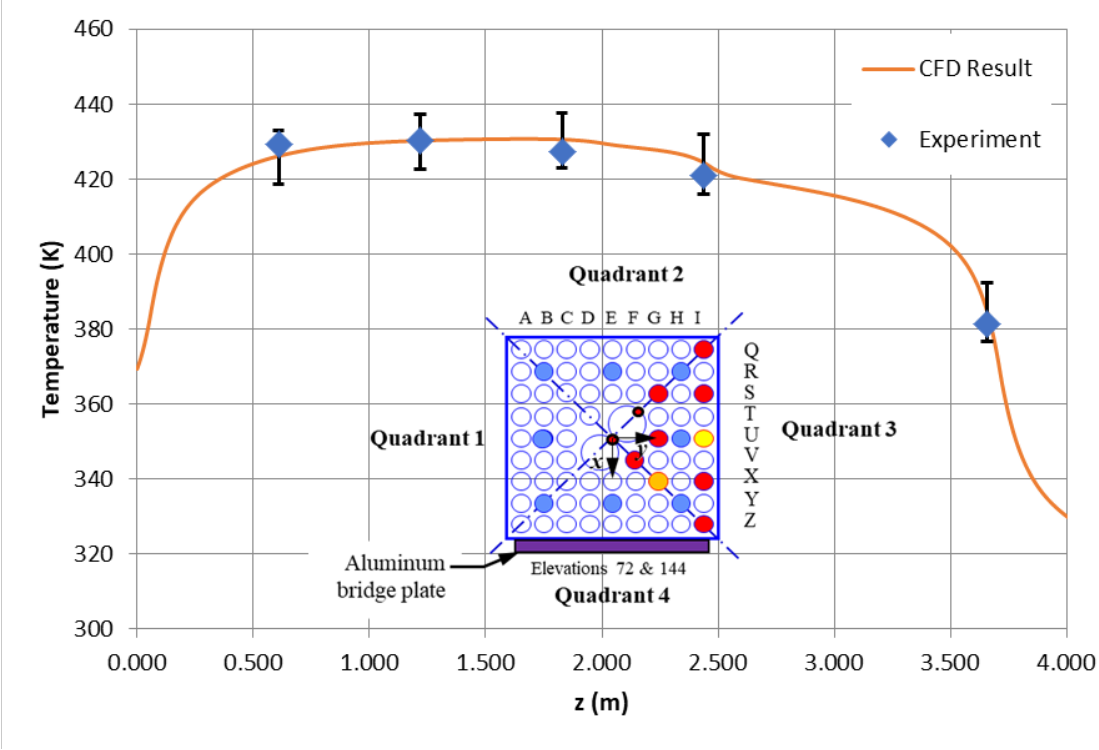

Figure A-4 Axial temperature profile for the 1.0-kW, 100-kPa, helium test (blind)

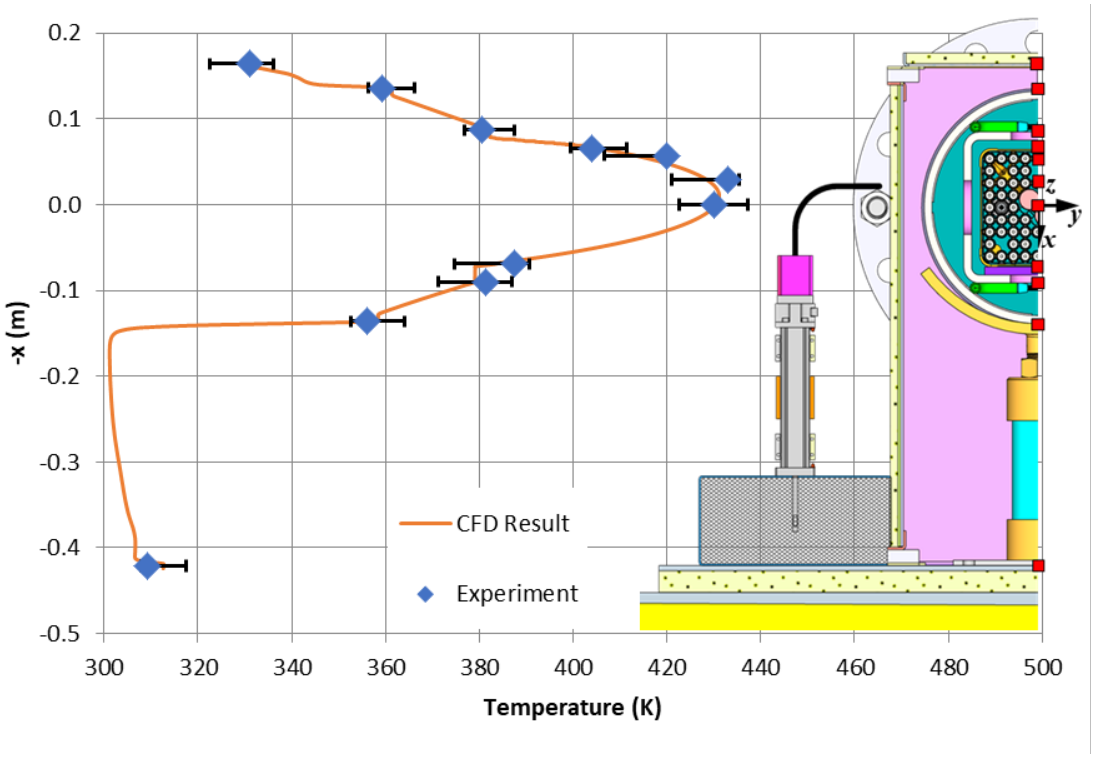

Figure A-5 Vertical temperature profile for the 1.0-kW, 100-kPa, helium test (blind)

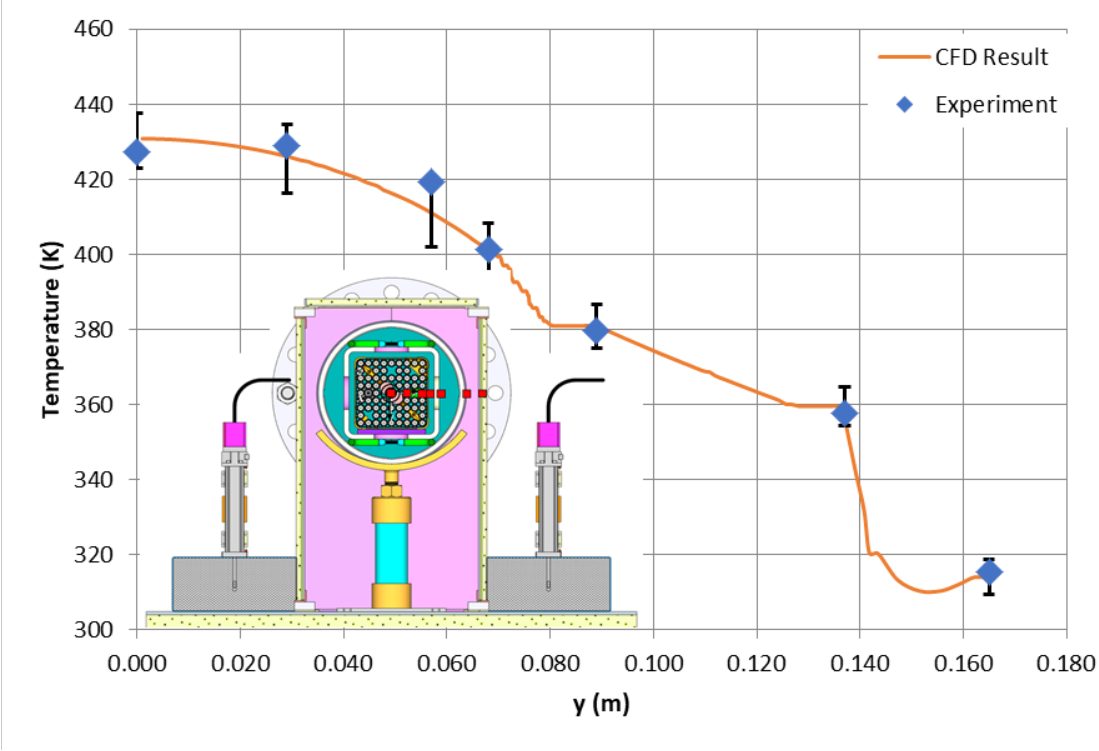

Figure A-6 Horizontal temperature profile for the 1.0-kW, 100-kPa, helium test (blind)

Table A-3 Open Test Results for 2.5-kW, 100-kPa, Helium

Parameter	Test Result	CFD Result	Positive Uncert.	Negative Uncert.	Compare Error, E	Valid?
Airflow Rate (kg/s)	0.0283	0.0263	0.0012	-0.0011	0.0021	NO
PCT Location						
X value (m)		-0.008	0.042	-0.032		
Y value (m)		0.000	0.039	-0.039		
Z value (m)	1.22	1.677	0.679	-0.939	-0.457	YES
PCT Value (K)	558.6	557.6	10.5	-13.7	0.9	YES
WEU (x = 0, y = 0)						
z = 0.610 m (K)	555	550.4	10.5	-13.5	4.1	YES
z = 1.219 m (K)	553	556.2	10.5	-13.6	-2.9	YES
z = 1.829 m (K)	548	556.5	10.6	-13.8	-8.2	YES
z = 2.438 m (K)	537	545.1	12.6	-15.2	-8.3	YES
z = 3.658 m (K)	466	474.9	13.4	-14.6	-8.8	YES
Vertical (y = 0 m, z = 1.219 m)						
x = -0.169 m (K)	368	369.4	5.5	-7.2	-1.7	YES
x = -0.137 m (K)	421	424.7	6.0	-6.2	-4.1	YES
x = -0.090 m (K)	462	466.5	7.5	-7.5	-4.6	YES
x = -0.068 m (K)	506	510.4	8.9	-9.1	-4.6	YES
x = -0.057 m (K)	536	525.7	10.9	-11.8	10.7	YES
x = -0.029 m (K)	558	552.4	10.4	-13.1	5.6	YES
x = 0.000 m (K)	553	556.2	10.5	-13.6	-2.9	YES
x = 0.068 m (K)	477	468.8	13.0	-15.3	8.0	YES
x = 0.090 m (K)	464	460.0	14.2	-14.1	3.5	YES
x = 0.137 m (K)	414	415.6	9.7	-9.5	-1.4	YES
x = 0.421 m (K)	323	329.8	6.6	-6.6	-6.8	NO
Horizontal (x = 0 m, z = 1.829 m)						
y = 0.000 m (K)	548	556.5	10.6	-13.8	-8.2	YES
y = 0.029 m (K)	550	547.6	14.2	-16.2	1.9	YES
y = 0.057 m (K)	532	519.6	13.0	-13.8	12.6	YES
y = 0.068 m (K)	499	503.8	9.6	-9.7	-4.5	YES
y = 0.089 m (K)	459	463.5	8.2	-8.1	-4.2	YES
y = 0.137 m (K)	416	419.3	6.5	-6.5	-3.6	YES
y = 0.165 m (K)	334	332.8	5.6	-5.6	0.8	YES

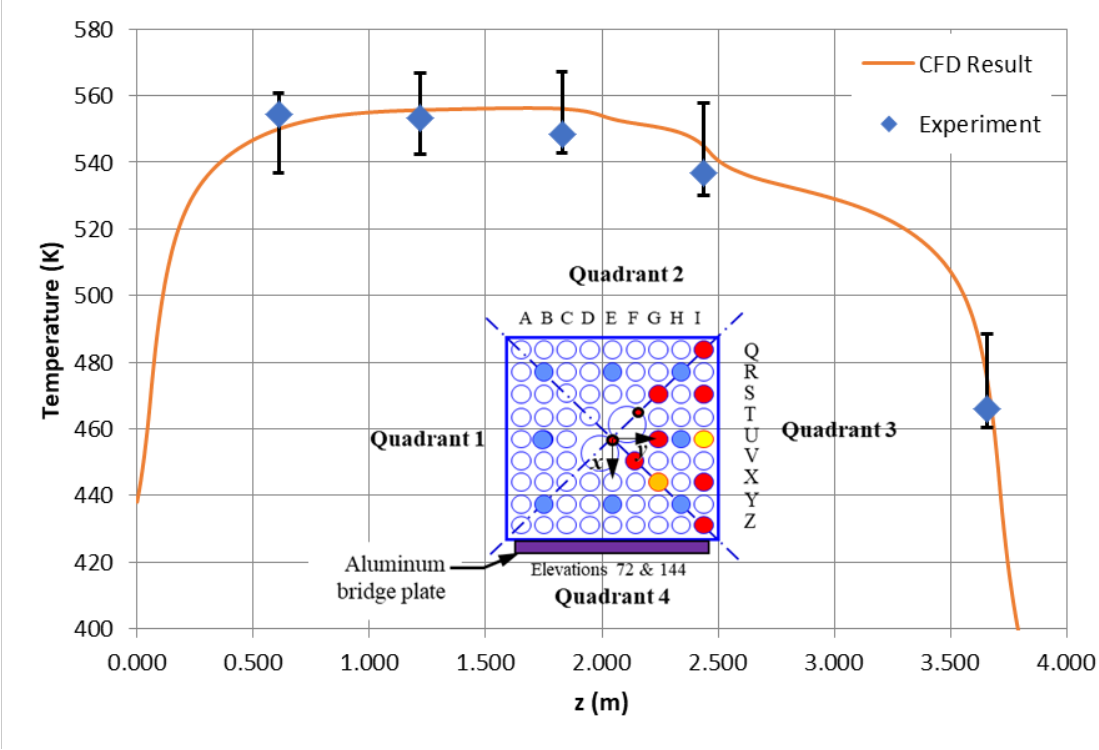

Figure A-7 Axial temperature profile for the 2.5-kW, 100-kPa, helium test (open)

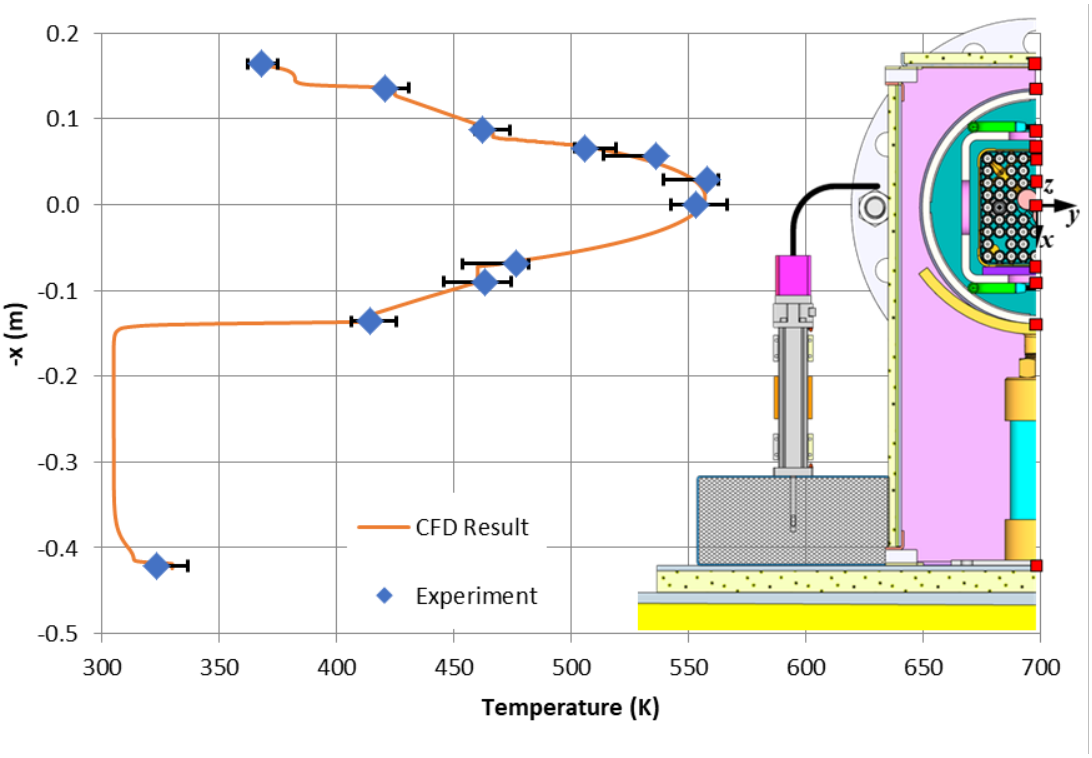

Figure A-8 Vertical temperature profile for the 2.5-kW, 100-kPa, helium test (open)

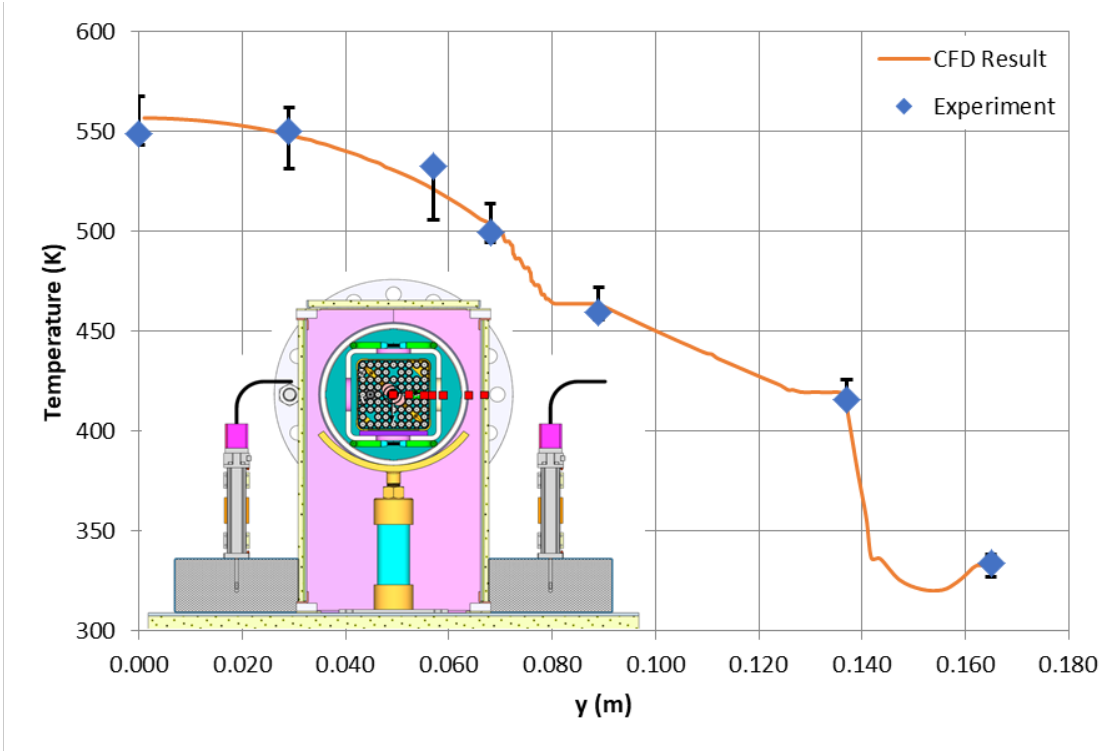

Figure A-9 Horizontal temperature profile for the 2.5-kW, 100-kPa, helium test (open)

Table A-4 Blind Test Results for 5.0-kW, 100-kPa, Helium

Parameter	Test Result	CFD Result	Positive Uncert.	Negative Uncert.	Compare Error, E	Valid?
Airflow Rate (kg/s)	0.0354	0.0346	0.0018	-0.0019	0.0008	YES
PCT Location						
X value (m)		-0.008	0.036	-0.035		
Y value (m)		0.000	0.037	-0.037		
Z value (m)	1.22	1.677	0.434	-1.097	-0.457	YES
PCT Value (K)	694.0	699.8	16.0	-21.7	-5.8	YES
WEU (x = 0, y = 0)						
z = 0.610 m (K)	690	692.2	15.9	-21.4	-2.5	YES
z = 1.219 m (K)	684	698.2	16.3	-21.7	-13.9	YES
z = 1.829 m (K)	678	698.5	15.5	-21.5	-20.8	YES
z = 2.438 (K)	665	681.4	17.7	-22.9	-16.8	YES
z = 3.658 m (K)	572	583.5	19.8	-22.4	-11.6	YES
Vertical (y = 0 m, z = 1.219 m)						
x = -0.169 m (K)	416	425.0	15.6	-14.8	-8.9	YES
x = -0.137 m (K)	492	506.2	9.4	-8.8	-14.4	NO
x = -0.090 m (K)	555	569.0	12.1	-11.5	-14.4	NO
x = -0.068 m (K)	618	632.4	14.2	-13.8	-14.1	NO
x = -0.057 m (K)	663	654.3	16.4	-17.6	8.3	YES
x = -0.029 m (K)	693	692.3	16.2	-20.7	0.7	YES
x = 0.000 m (K)	684	698.2	16.3	-21.7	-13.9	YES
x = 0.068 m (K)	577	573.5	20.5	-23.9	3.5	YES
x = 0.090 m (K)	555	558.3	22.8	-22.3	-3.0	YES
x = 0.137 m (K)	479	486.5	13.8	-13.4	-7.4	YES
x = 0.421 m (K)	340	357.5	12.4	-12.4	-17.6	NO
Horizontal (x = 0 m, z = 1.829 m)						
y = 0.000 m (K)	678	698.5	15.5	-21.5	-20.8	YES
y = 0.029 m (K)	677	685.9	19.1	-23.3	-9.1	YES
y = 0.057 m (K)	651	645.9	17.3	-18.8	5.5	YES
y = 0.068 m (K)	607	623.1	13.6	-13.7	-16.2	NO
y = 0.089 m (K)	549	563.1	10.5	-10.4	-14.1	NO
y = 0.137 m (K)	482	493.0	7.5	-7.7	-10.8	NO
y = 0.165 m (K)	361	362.3	5.5	-6.0	-1.6	YES

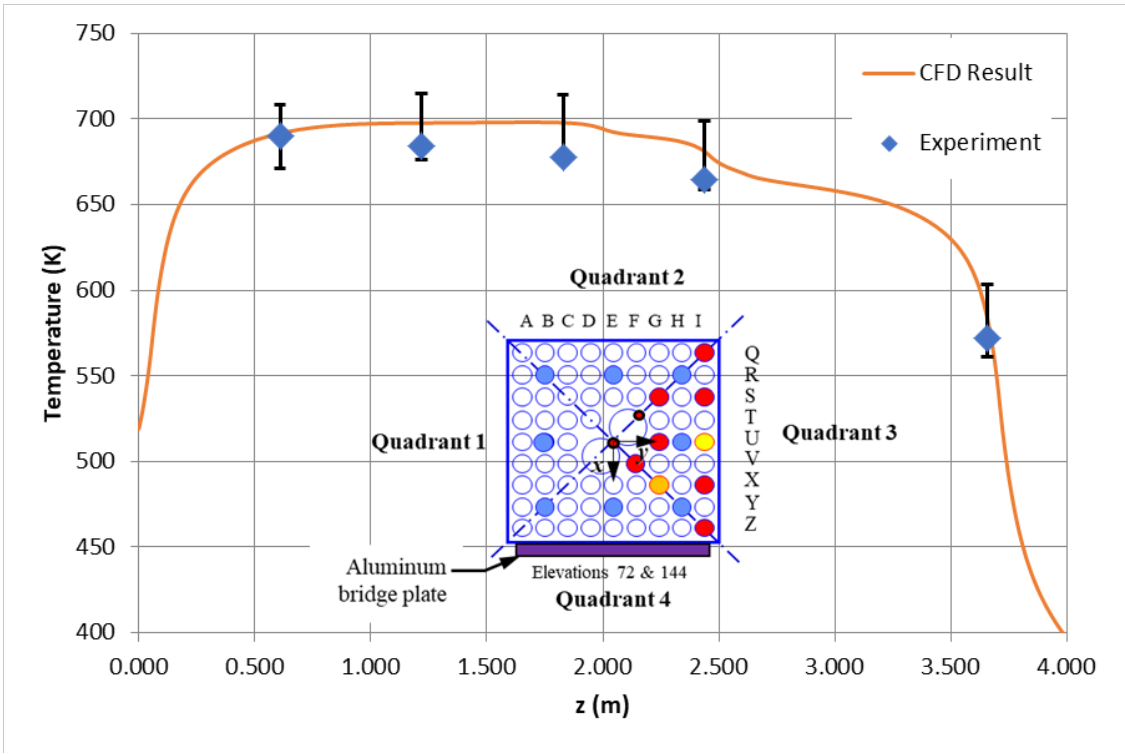

Figure A-10 Axial temperature profile for the 5.0-kW, 100-kPa, helium test (blind)

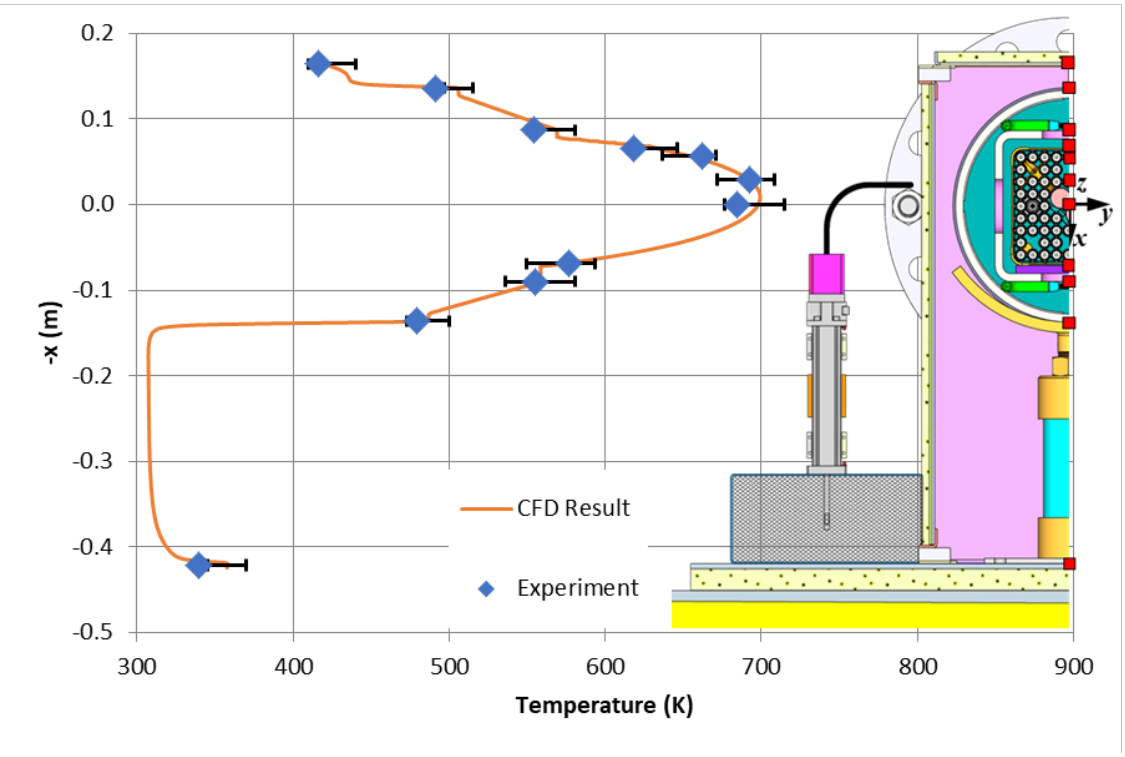

Figure A-11 Vertical temperature profile for the 5.0-kW, 100-kPa, helium test (blind)

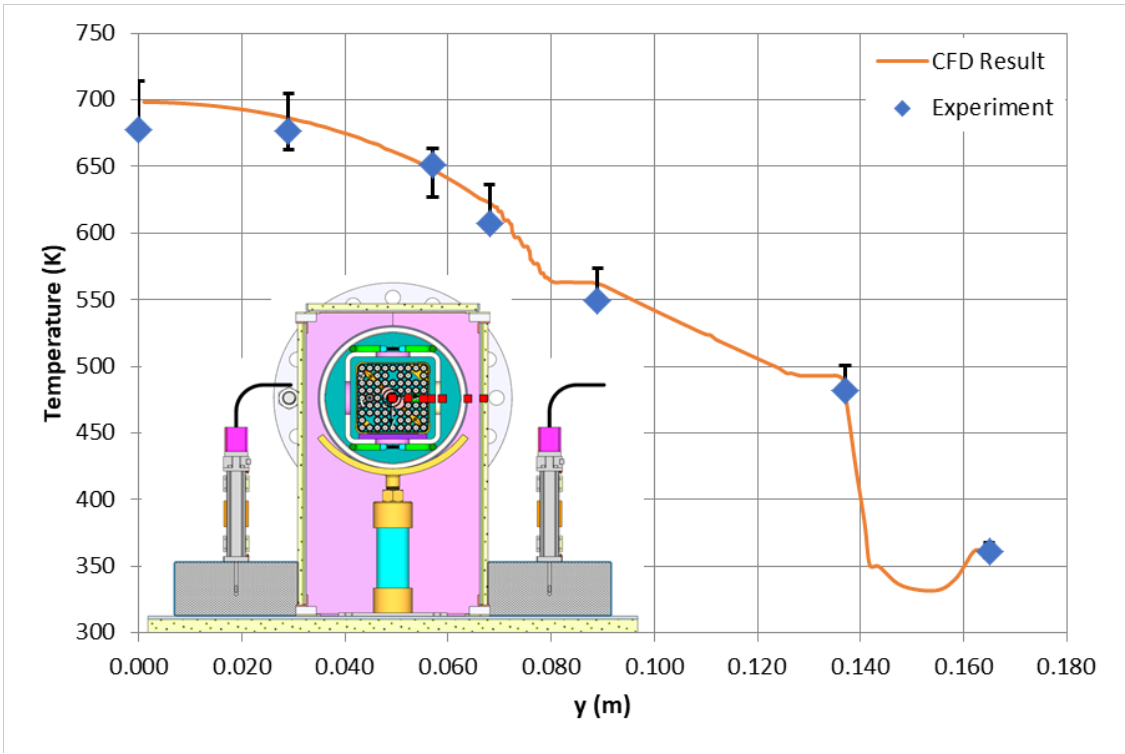

Figure A-12 Horizontal temperature profile for the 5.0-kW, 100-kPa, helium test (blind)

Table A-5 Blind Test Results for 0.5-kW, 800-kPa, Helium

Parameter	Test Result	CFD Result	Positive Uncert.	Negative Uncert.	Compare Error, E	Valid?
Airflow Rate (kg/s)	0.0157	0.0135	0.0011	-0.0010	0.0022	NO
PCT Location						
X value (m)		-0.037	0.043	-0.035		
Y value (m)		0.000	0.065	-0.065		
Z value (m)	1.22	1.549	0.850	-0.939	-0.329	YES
PCT Value (K)	367.7	363.4	5.1	-5.6	4.3	YES
WEU (x = 0, y = 0)						
z = 0.610 m (K)	365	355.1	4.9	-5.6	9.4	NO
z = 1.219 m (K)	364	358.7	5.0	-5.6	5.4	NO
z = 1.829 m (K)	363	358.7	5.0	-5.5	4.4	YES
z = 2.438 m (K)	360	354.7	5.1	-5.5	5.0	YES
z = 3.658 m (K)	335	332.9	5.0	-5.3	2.4	YES
Vertical (y = 0 m, z = 1.219 m)						
x = -0.169 m (K)	314	312.7	4.1	-5.2	1.2	YES
x = -0.137 m (K)	330	331.8	4.5	-4.7	-1.4	YES
x = -0.090 m (K)	339	340.3	4.6	-4.8	-1.1	YES
x = -0.068 m (K)	354	354.9	4.8	-5.1	-1.1	YES
x = -0.057 m (K)	362	359.5	5.0	-5.3	2.9	YES
x = -0.029 m (K)	368	362.6	5.1	-5.6	5.1	NO
x = 0.000 m (K)	364	358.7	5.0	-5.6	5.4	NO
x = 0.068 m (K)	341	338.7	4.7	-5.3	1.9	YES
x = 0.090 m (K)	338	337.2	4.8	-5.0	0.6	YES
x = 0.137 m (K)	326	327.6	4.7	-4.8	-1.3	YES
x = 0.421 m (K)	302	302.6	4.4	-4.4	-1.0	YES
Horizontal (x = 0 m, z = 1.829 m)						
y = 0.000 m (K)	363	358.7	5.0	-5.5	4.4	YES
y = 0.029 m (K)	364	358.3	5.0	-5.4	5.6	NO
y = 0.057 m (K)	358	354.7	5.0	-5.2	3.7	YES
y = 0.068 m (K)	350	350.5	4.8	-5.0	-1.0	YES
y = 0.089 m (K)	338	338.7	4.6	-4.7	-0.5	YES
y = 0.137 m (K)	330	329.7	4.6	-4.6	-0.1	YES
y = 0.165 m (K)	305	303.8	4.5	-4.4	1.3	YES

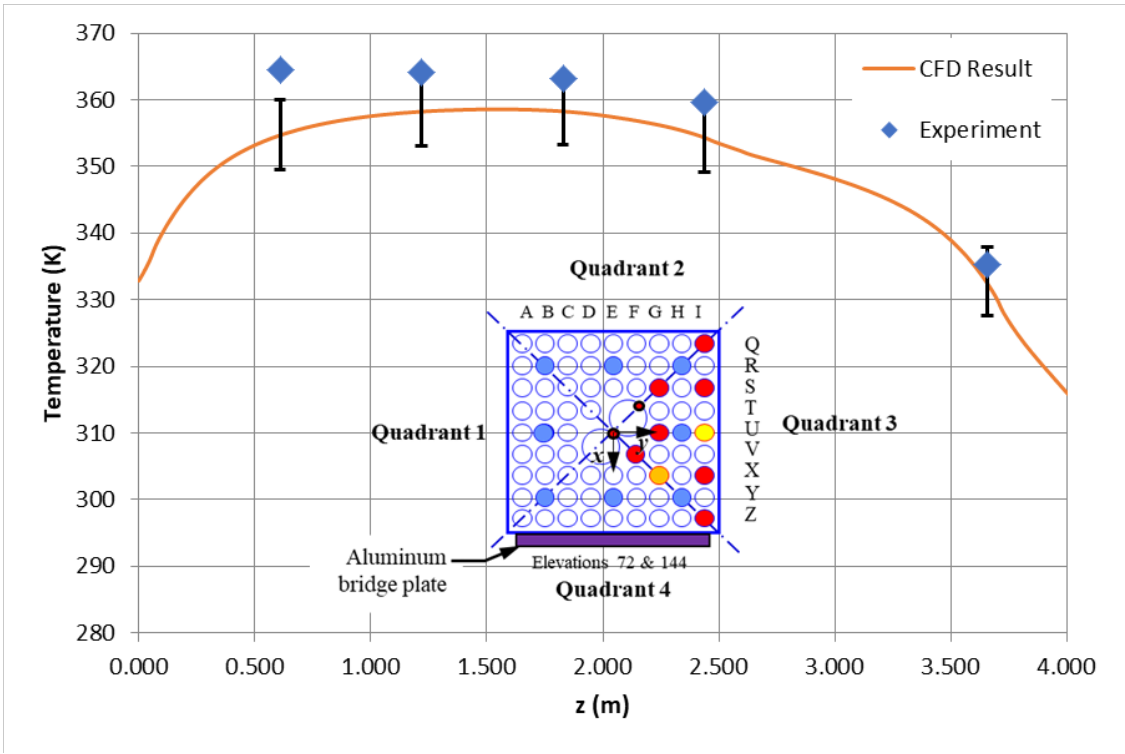

Figure A-13 Axial temperature profile for the 0.5-kW, 800-kPa, helium test (blind)

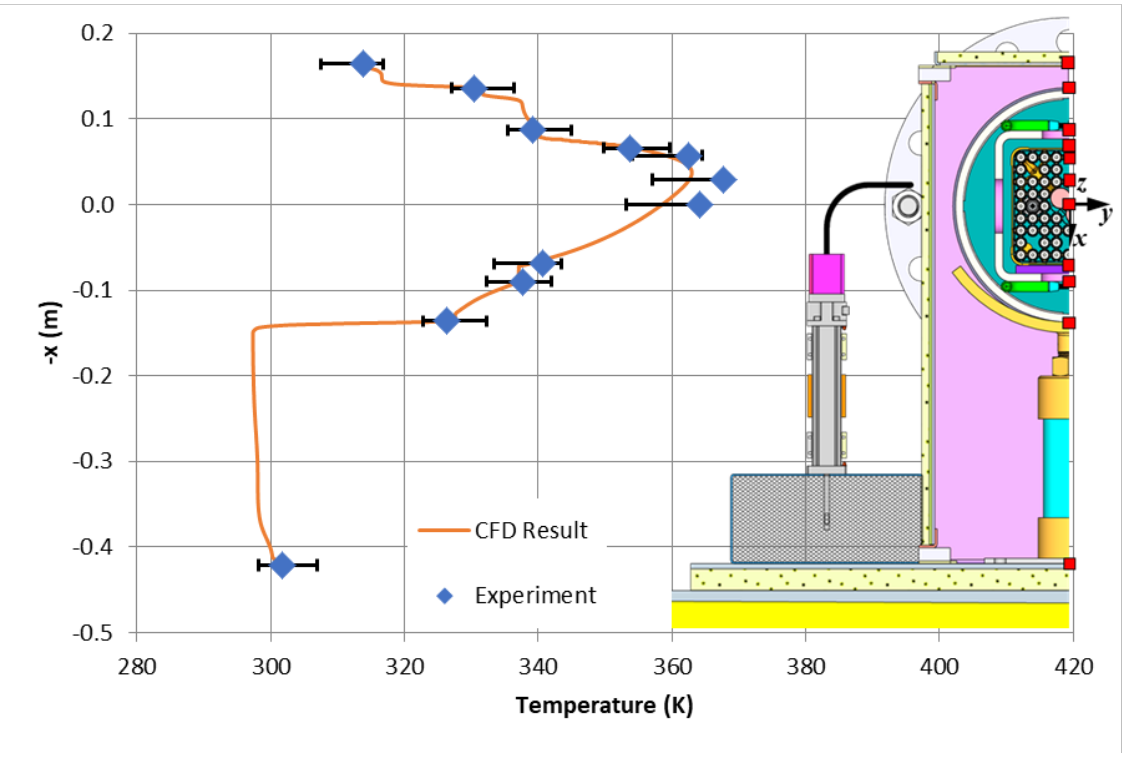

Figure A-14 Vertical temperature profile for the 0.5-kW, 800-kPa, helium test (blind)

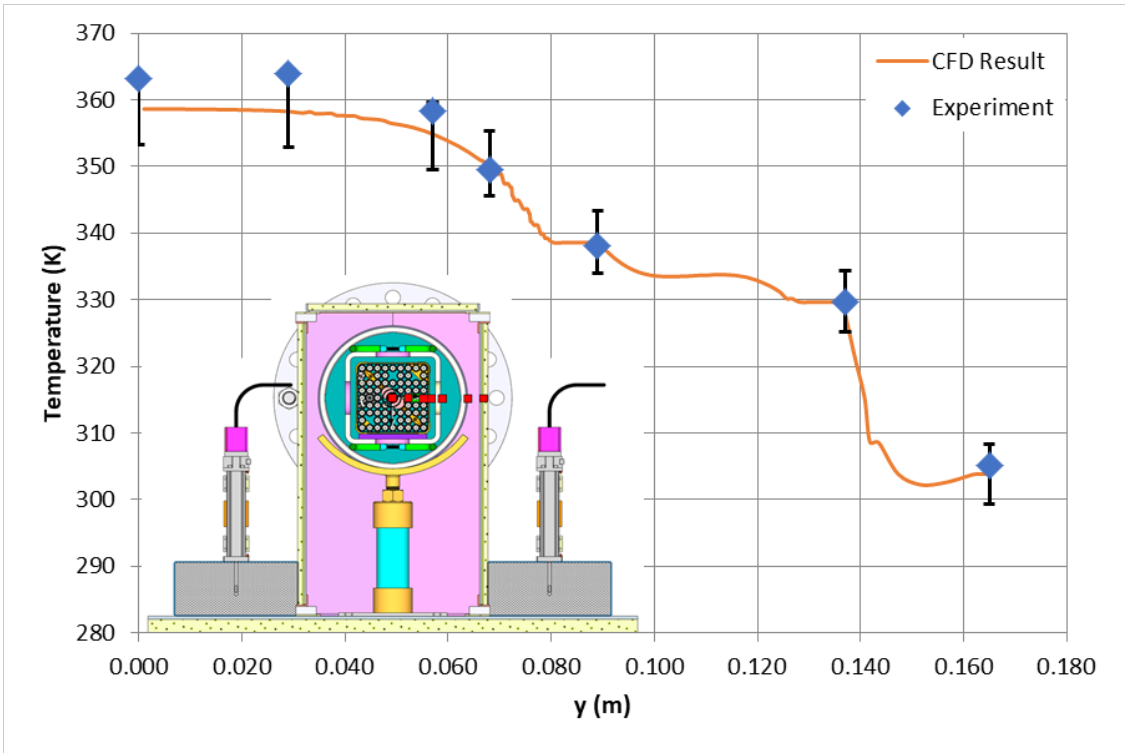

Figure A-15 Horizontal temperature profile for the 0.5-kW, 800-kPa, helium test (blind)

Table A-6 Blind Test Results for 5.0-kW, 800-kPa, Helium

Parameter	Test Result	CFD Result	Positive Uncert.	Negative Uncert.	Compare Error, E	Valid?
Airflow Rate (kg/s)	0.0338	0.0337	0.0022	-0.0021	0.0002	YES
PCT Location						
X value (m)		-0.027	0.035	-0.033		
Y value (m)		0.000	0.042	-0.042		
Z value (m)	1.22	1.565	0.495	-0.821	-0.345	YES
PCT Value (K)	677.1	683.4	10.9	-17.6	-6.3	YES
WEU (x = 0, y = 0)						
z = 0.610 m (K)	670	658.0	11.7	-18.6	12.4	NO
z = 1.219 m (K)	665	671.1	11.3	-18.0	-6.1	YES
z = 1.829 m (K)	660	670.9	10.9	-17.9	-11.0	YES
z = 2.438 m (K)	646	649.2	13.4	-18.9	-2.7	YES
z = 3.658 m (K)	533	522.4	15.4	-15.8	10.2	YES
Vertical (y = 0 m, z = 1.219 m)						
x = -0.169 m (K)	412	422.4	14.5	-13.6	-10.6	YES
x = -0.137 m (K)	486	507.9	10.3	-10.3	-21.9	NO
x = -0.090 m (K)	537	558.6	6.8	-7.8	-21.9	NO
x = -0.068 m (K)	604	629.4	9.7	-12.0	-25.3	NO
x = -0.057 m (K)	650	653.0	13.8	-17.2	-3.3	YES
x = -0.029 m (K)	677	682.4	11.0	-17.8	-5.3	YES
x = 0.000 m (K)	665	671.1	11.3	-18.0	-6.1	YES
x = 0.068 m (K)	551	550.2	14.0	-17.7	1.2	YES
x = 0.090 m (K)	530	537.9	16.1	-16.2	-8.2	YES
x = 0.137 m (K)	459	473.1	9.8	-9.9	-13.9	NO
x = 0.421 m (K)	333	350.9	10.9	-10.9	-17.5	NO
Horizontal (x = 0 m, z = 1.829 m)						
y = 0.000 m (K)	660	670.9	10.9	-17.9	-11.0	YES
y = 0.029 m (K)	660	663.6	11.9	-17.2	-3.5	YES
y = 0.057 m (K)	635	632.4	11.2	-13.8	2.4	YES
y = 0.068 m (K)	589	609.7	8.4	-9.9	-20.5	NO
y = 0.089 m (K)	529	546.2	6.2	-7.0	-17.3	NO
y = 0.137 m (K)	476	488.6	5.0	-5.2	-12.4	NO
y = 0.165 m (K)	354	358.1	5.6	-6.1	-3.8	YES

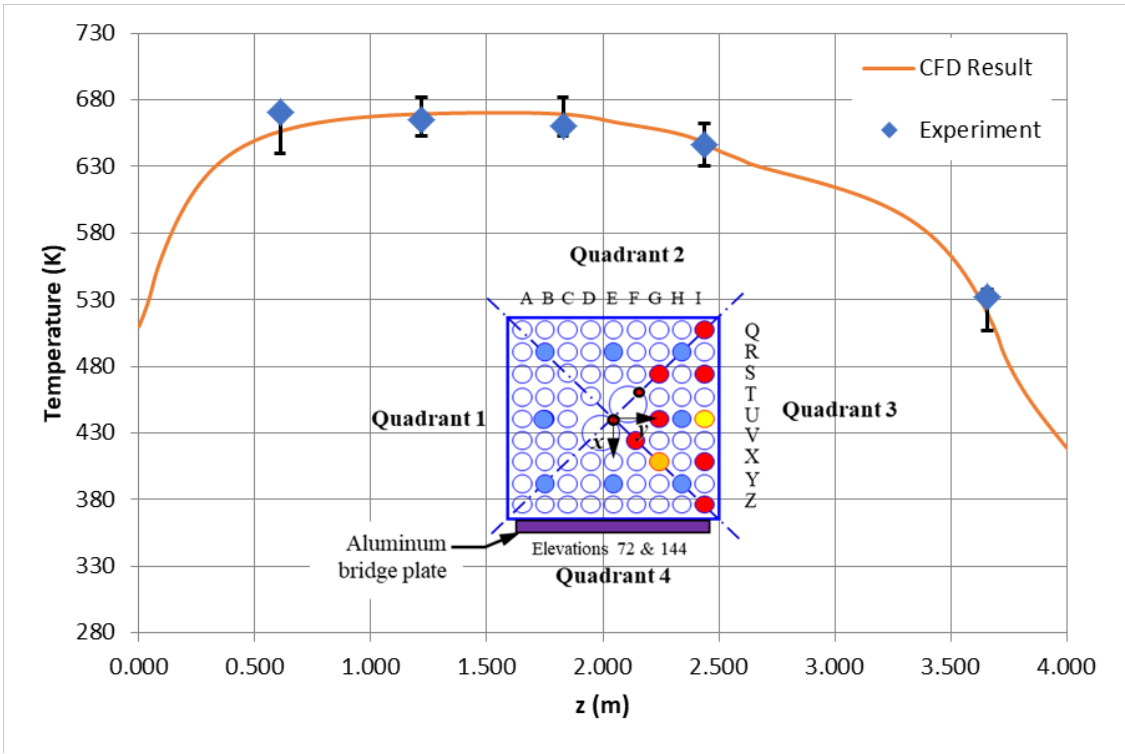

Figure A-16 Axial temperature profile for the 5.0-kW, 800-kPa, helium test (blind)

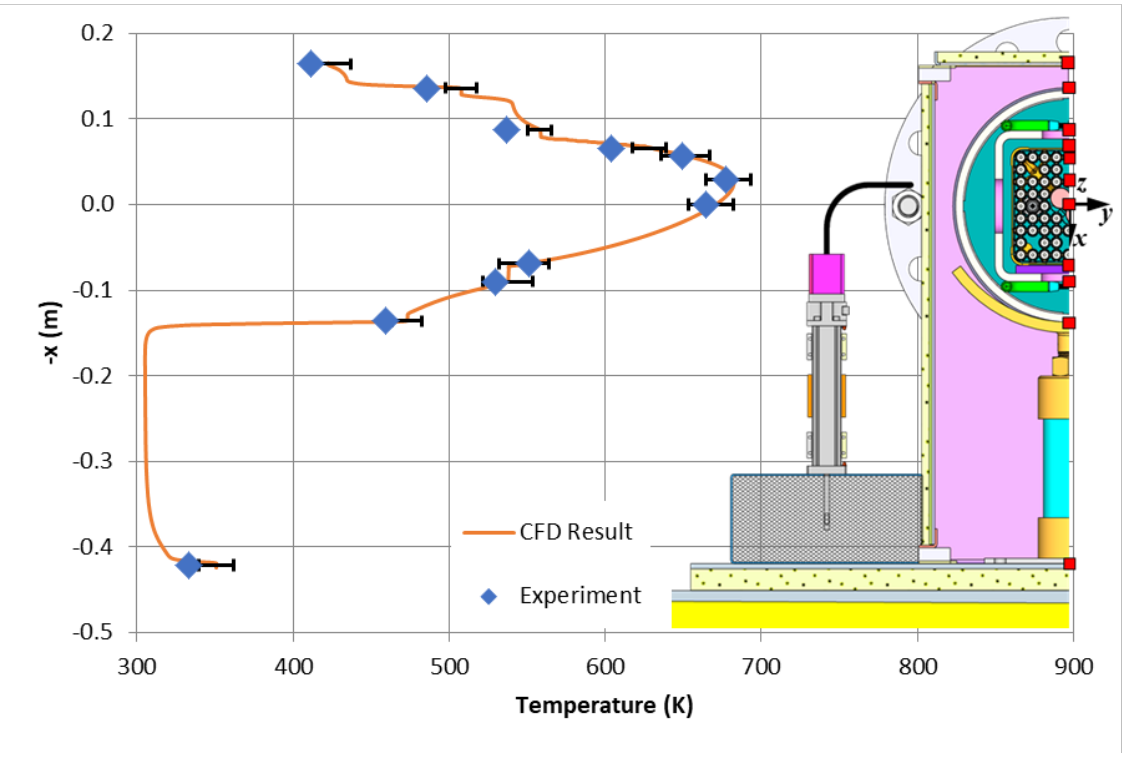

Figure A-17 Vertical temperature profile for the 5.0-kW, 800-kPa, helium test (blind)

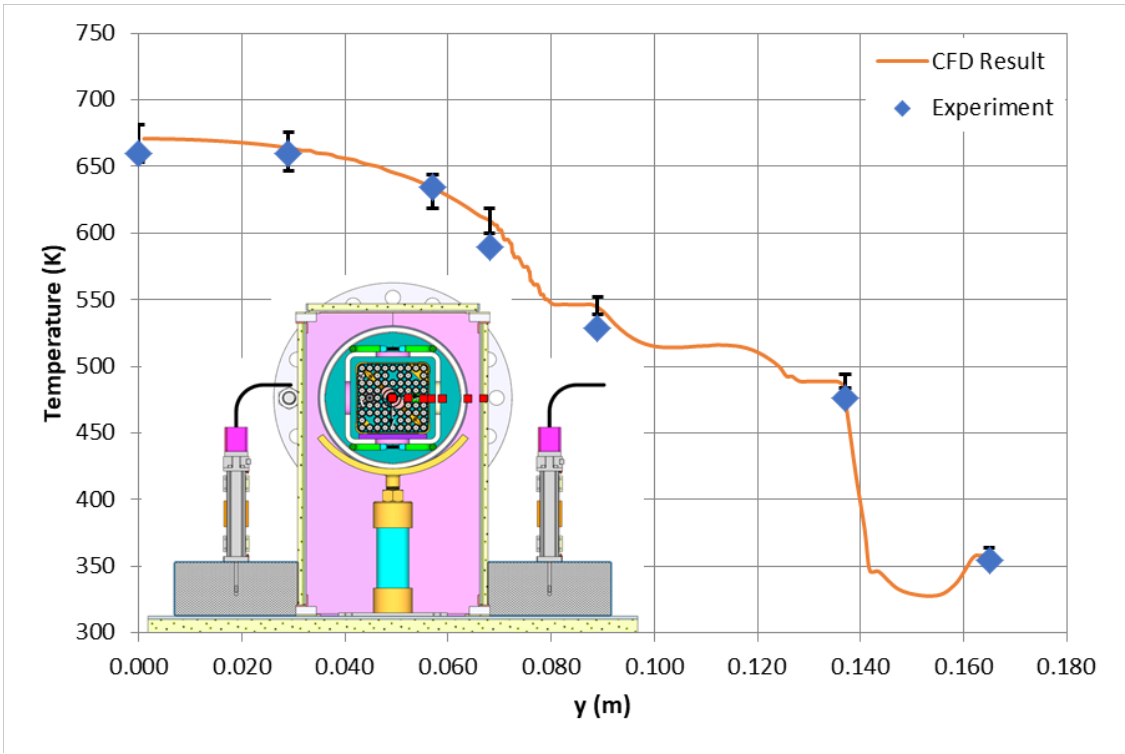

Figure A-18 Horizontal temperature profile for the 5.0-kW, 800-kPa, helium test (blind)

Table A-7 Blind Test Results for 0.5-kW, 100-kPa, Air

Parameter	Test Result	CFD Result	Positive Uncert.	Negative Uncert.	Compare Error, E	Valid?
Airflow Rate (kg/s)	0.0141	0.0136	0.0011	-0.0010	0.0004	YES
PCT Location						
X value (m)		-0.031	0.036	-0.033		
Y value (m)		0.000	0.047	-0.047		
Z value (m)	1.22	1.517	0.625	-0.915	-0.297	YES
PCT Value (K)	426.6	414.9	8.2	-11.2	11.7	NO
WEU (x = 0, y = 0)						
z = 0.610 m (K)	421	402.2	7.6	-10.8	18.8	NO
z = 1.219 m (K)	421	406.5	7.9	-10.5	14.1	NO
z = 1.829 m (K)	418	406.2	8.0	-10.5	11.5	NO
z = 2.438 m (K)	412	398.7	9.7	-11.5	13.0	NO
z = 3.658 m (K)	373	359.7	9.4	-10.2	13.1	NO
Vertical (y = 0 m, z = 1.219 m)						
x = -0.169 m (K)	315	314.2	4.2	-4.9	0.9	YES
x = -0.137 m (K)	331	332.5	4.9	-5.0	-1.1	YES
x = -0.090 m (K)	354	351.9	4.9	-5.1	1.8	YES
x = -0.068 m (K)	386	388.0	7.1	-7.7	-2.3	YES
x = -0.057 m (K)	415	400.9	9.4	-11.0	13.8	NO
x = -0.029 m (K)	427	414.5	8.1	-11.4	12.1	NO
x = 0.000 m (K)	421	406.5	7.9	-10.5	14.1	NO
x = 0.068 m (K)	367	353.0	7.1	-8.6	14.4	NO
x = 0.090 m (K)	354	347.9	6.4	-6.5	5.7	YES
x = 0.137 m (K)	328	332.3	4.9	-5.1	-4.2	YES
x = 0.421 m (K)	302	305.3	4.5	-4.5	-2.8	YES
Horizontal (x = 0 m, z = 1.829 m)						
y = 0.000 m (K)	418	406.2	8.0	-10.5	11.5	NO
y = 0.029 m (K)	419	403.7	8.5	-10.5	14.9	NO
y = 0.057 m (K)	401	389.7	8.9	-9.7	11.4	NO
y = 0.068 m (K)	379	377.4	6.5	-6.7	2.0	YES
y = 0.089 m (K)	353	350.2	5.0	-5.1	2.8	YES
y = 0.137 m (K)	331	332.4	4.7	-4.7	-1.8	YES
y = 0.165 m (K)	306	306.0	4.5	-4.5	0.4	YES

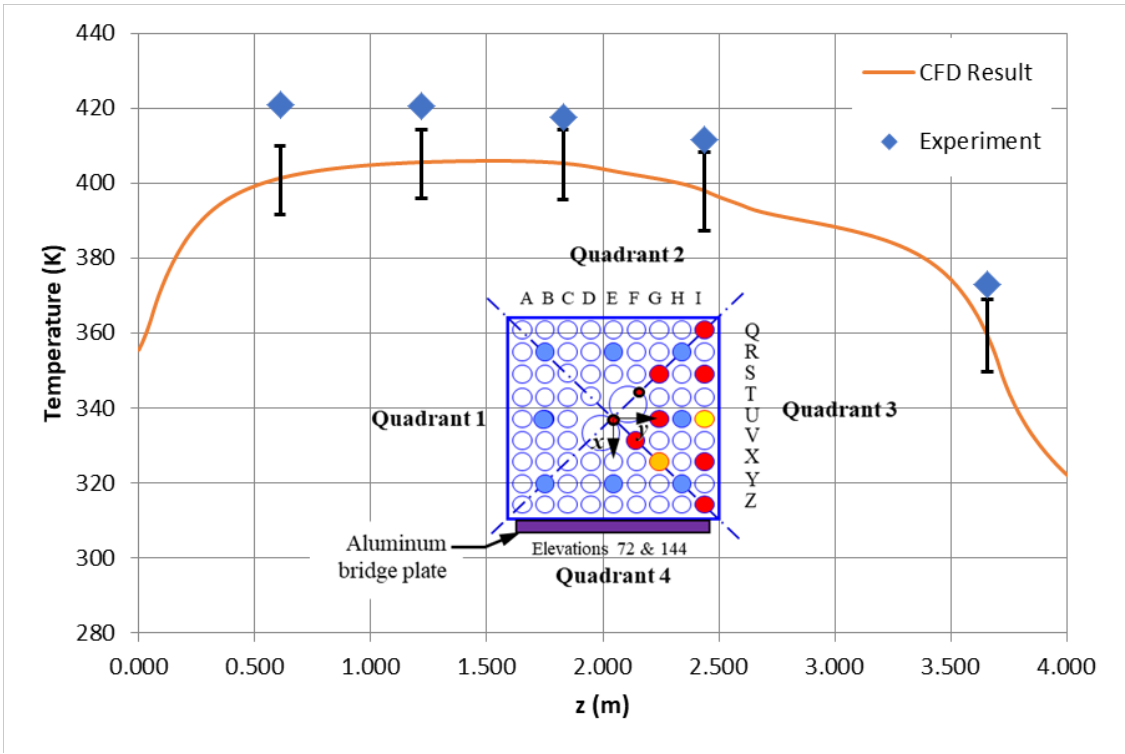

Figure A-19 Axial temperature profile for the 0.5-kW, 100-kPa, air test (blind)

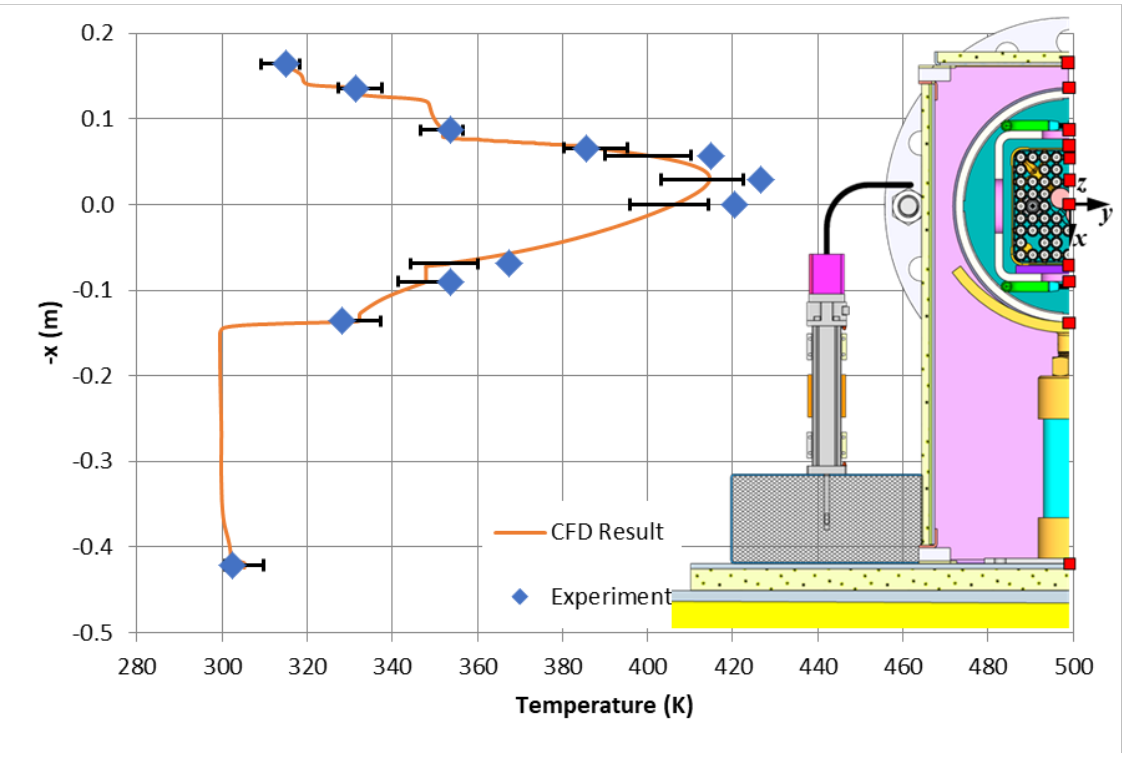

Figure A-20 Vertical temperature profile for the 0.5-kW, 100-kPa, air test (blind)

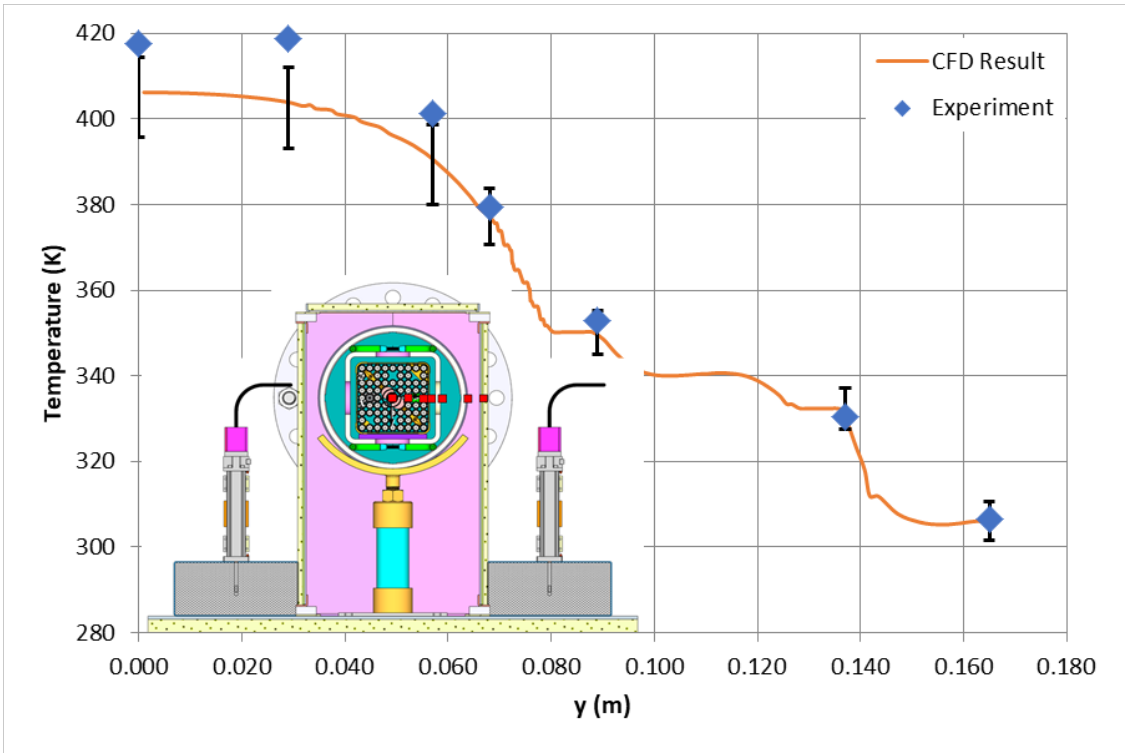

Figure A-21 Horizontal temperature profile for the 0.5-kW, 100-kPa, air test (blind)

Table A-8 Blind Test Results for 1.0-kW, 100-kPa, Air

Parameter	Test Result	CFD Result	Positive Uncert.	Negative Uncert.	Compare Error, E	Valid?
Airflow Rate (kg/s)	0.0194	0.0183	0.0011	-0.0011	0.0011	YES
PCT Location						
X value (m)		-0.027	0.035	-0.033		
Y value (m)		0.000	0.042	-0.042		
Z value (m)	1.22	1.517	0.541	-0.900	-0.297	YES
PCT Value (K)	501.4	491.1	11.1	-15.8	10.2	YES
WEU (x = 0, y = 0)						
z = 0.610 m (K)	496	476.4	10.5	-15.2	19.5	NO
z = 1.219 m (K)	494	482.2	10.8	-15.1	11.3	NO
z = 1.829 m (K)	489	481.7	10.9	-15.1	7.4	YES
z = 2.438 m (K)	481	469.5	13.7	-16.8	11.4	YES
z = 3.658 m (K)	427	404.8	22.6	-23.4	22.1	YES
Vertical (y = 0 m, z = 1.219 m)						
x = -0.169 m (K)	329	327.2	6.3	-6.7	2.0	YES
x = -0.137 m (K)	357	358.3	5.2	-5.3	-1.7	YES
x = -0.090 m (K)	393	392.1	5.8	-6.1	1.3	YES
x = -0.068 m (K)	442	448.0	9.6	-10.2	-5.8	YES
x = -0.057 m (K)	484	467.3	12.8	-14.9	16.3	NO
x = -0.029 m (K)	501	490.6	11.1	-15.9	10.7	YES
x = 0.000 m (K)	494	482.2	10.8	-15.1	11.3	NO
x = 0.068 m (K)	417	394.8	10.0	-13.8	22.7	NO
x = 0.090 m (K)	393	385.0	8.8	-8.8	8.3	YES
x = 0.137 m (K)	351	356.8	5.4	-5.4	-6.1	NO
x = 0.421 m (K)	307	310.6	4.7	-4.8	-3.3	YES
Horizontal (x = 0 m, z = 1.829 m)						
y = 0.000 m (K)	489	481.7	10.9	-15.1	7.4	YES
y = 0.029 m (K)	491	476.4	12.3	-15.5	14.6	NO
y = 0.057 m (K)	467	452.1	12.5	-13.8	14.8	NO
y = 0.068 m (K)	433	432.9	8.8	-8.9	0.3	YES
y = 0.089 m (K)	392	388.9	5.9	-6.0	2.7	YES
y = 0.137 m (K)	354	357.1	5.0	-5.0	-2.7	YES
y = 0.165 m (K)	313	311.7	4.6	-4.7	1.5	YES

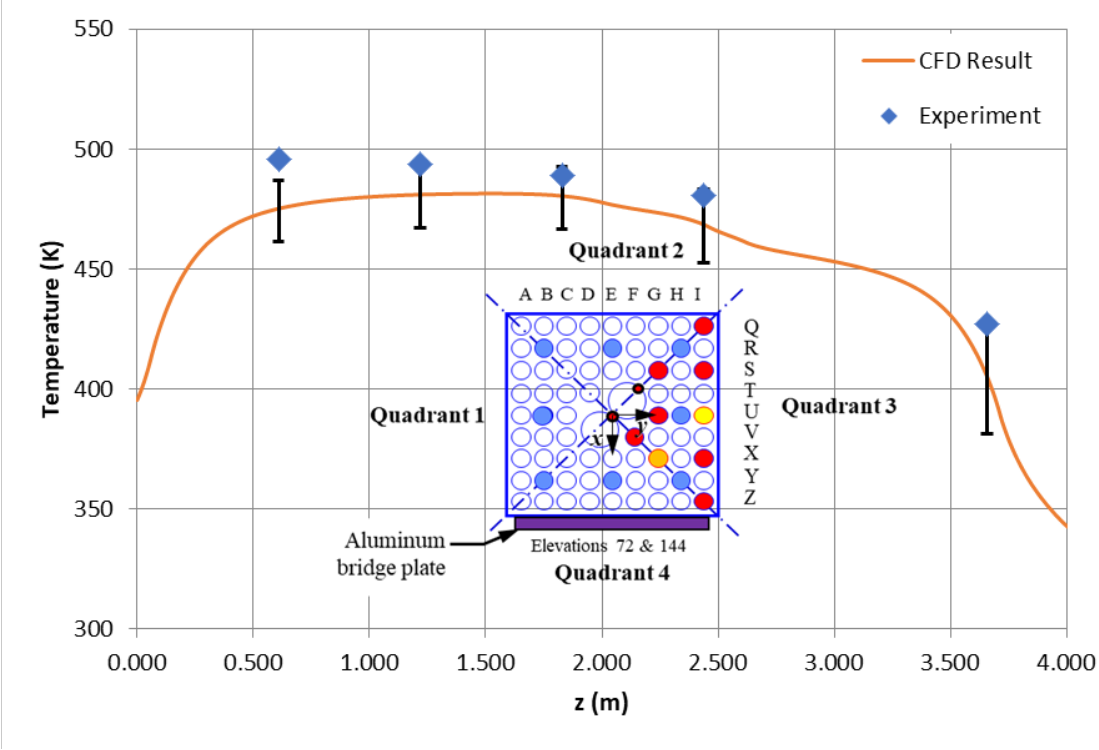

Figure A-22 Axial temperature profile for the 1.0-kW, 100-kPa, air test (blind)

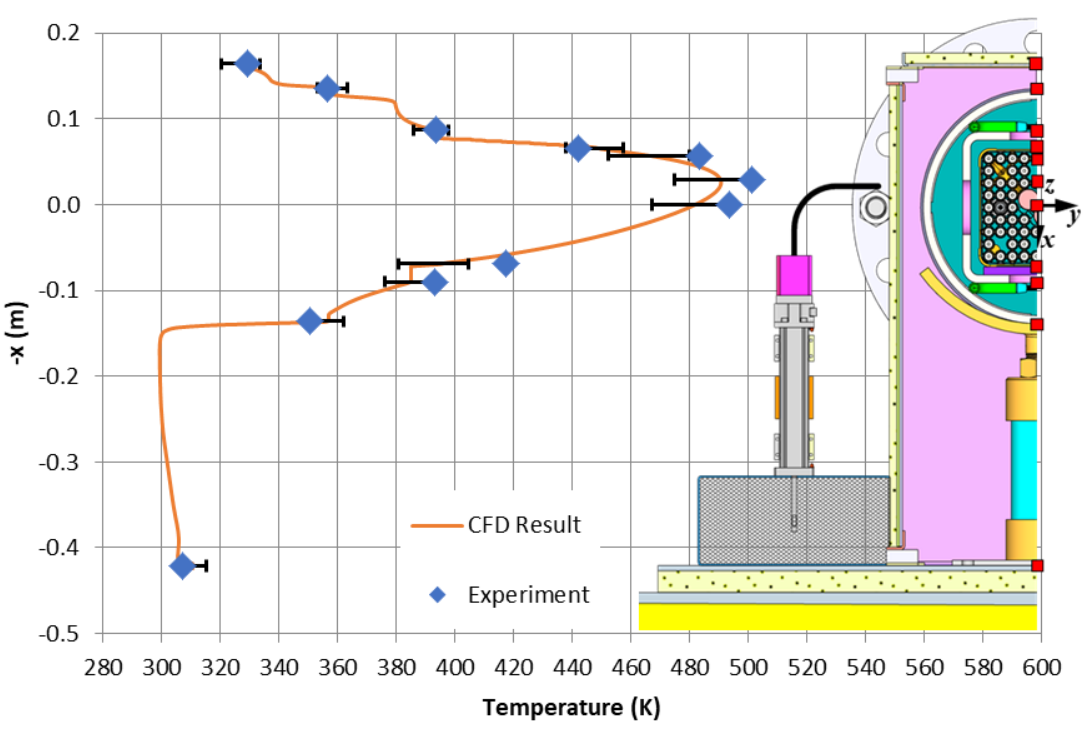

Figure A-23 Vertical temperature profile for the 1.0-kW, 100-kPa, air test (blind)

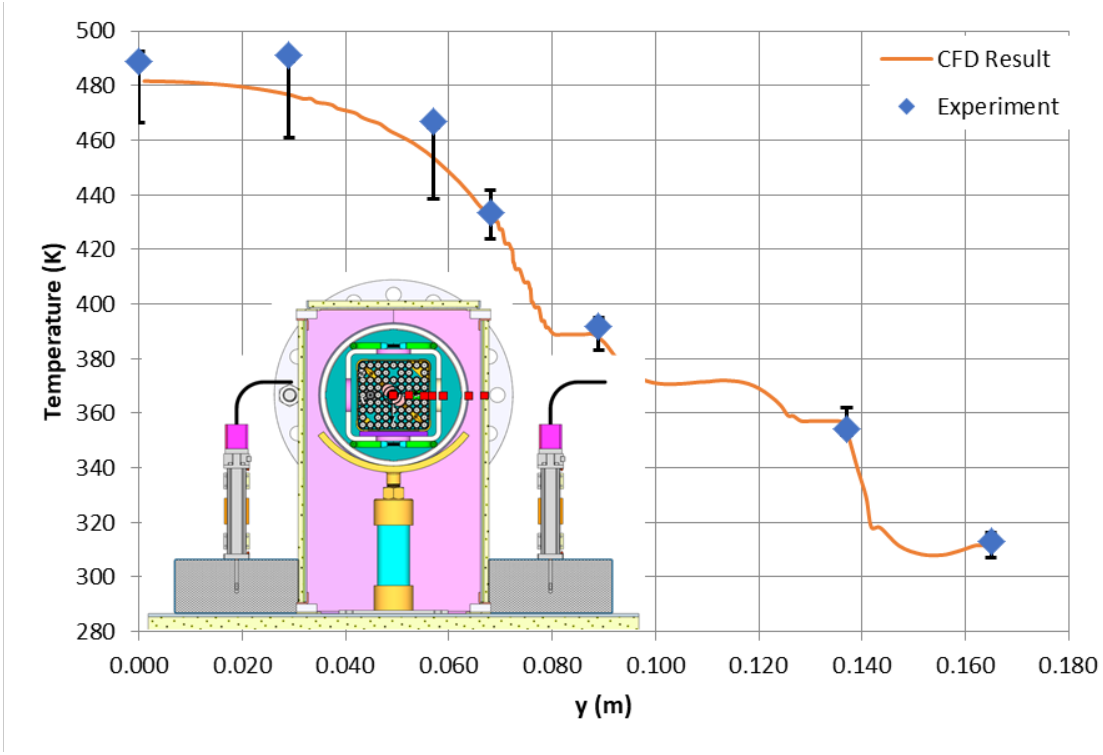

Figure A-24 Horizontal temperature profile for the 1.0-kW, 100-kPa, air test (blind)

Table A-9 Open Test Results for 2.5-kW, 100-kPa, Air

Parameter	Test Result	CFD Result	Positive Uncert.	Negative Uncert.	Compare Error, E	Valid?
Airflow Rate (kg/s)	0.0277	0.0263	0.0011	-0.0011	0.0014	NO
PCT Location						
X value (m)		-0.017	0.035	-0.034		
Y value (m)		0.000	0.037	-0.037		
Z value (m)	0.61	1.557	0.465	-0.986	-0.947	YES
PCT Value (K)	647.0	639.4	20.0	-29.5	7.6	YES
WEU (x = 0, y = 0)						
z = 0.610 m (K)	645	628.3	19.3	-28.8	16.3	YES
z = 1.219 m (K)	637	634.4	19.5	-29.0	3.0	YES
z = 1.829 m (K)	630	633.7	19.4	-28.9	-3.5	YES
z = 2.438 m (K)	615	613.7	22.6	-30.2	1.0	YES
z = 3.658 m (K)	527	513.6	26.9	-29.2	13.9	YES
Vertical (y = 0 m, z = 1.219 m)						
x = -0.169 m (K)	367	368.3	6.3	-6.3	-1.1	YES
x = -0.137 m (K)	420	423.8	6.7	-6.9	-3.7	YES
x = -0.090 m (K)	486	486.1	8.9	-9.2	-0.3	YES
x = -0.068 m (K)	562	568.1	17.1	-17.3	-6.6	YES
x = -0.057 m (K)	617	595.5	21.2	-24.8	21.4	NO
x = -0.029 m (K)	645	635.7	20.2	-29.3	9.0	YES
x = 0.000 m (K)	637	634.4	19.5	-29.0	3.0	YES
x = 0.068 m (K)	534	497.2	18.6	-29.4	37.0	NO
x = 0.090 m (K)	484	473.3	16.2	-15.9	11.2	YES
x = 0.137 m (K)	408	416.2	8.8	-8.4	-7.9	YES
x = 0.421 m (K)	321	330.1	6.1	-6.4	-9.1	NO
Horizontal (x = 0 m, z = 1.829 m)						
y = 0.000 m (K)	630	633.7	19.4	-28.9	-3.5	YES
y = 0.029 m (K)	634	622.0	22.8	-29.8	11.8	YES
y = 0.057 m (K)	607	579.3	21.2	-24.0	27.7	NO
y = 0.068 m (K)	552	550.8	15.6	-15.5	1.3	YES
y = 0.089 m (K)	481	479.9	9.0	-8.9	1.3	YES
y = 0.137 m (K)	414	418.7	6.8	-6.9	-4.3	YES
y = 0.165 m (K)	333	332.6	5.7	-5.8	0.0	YES

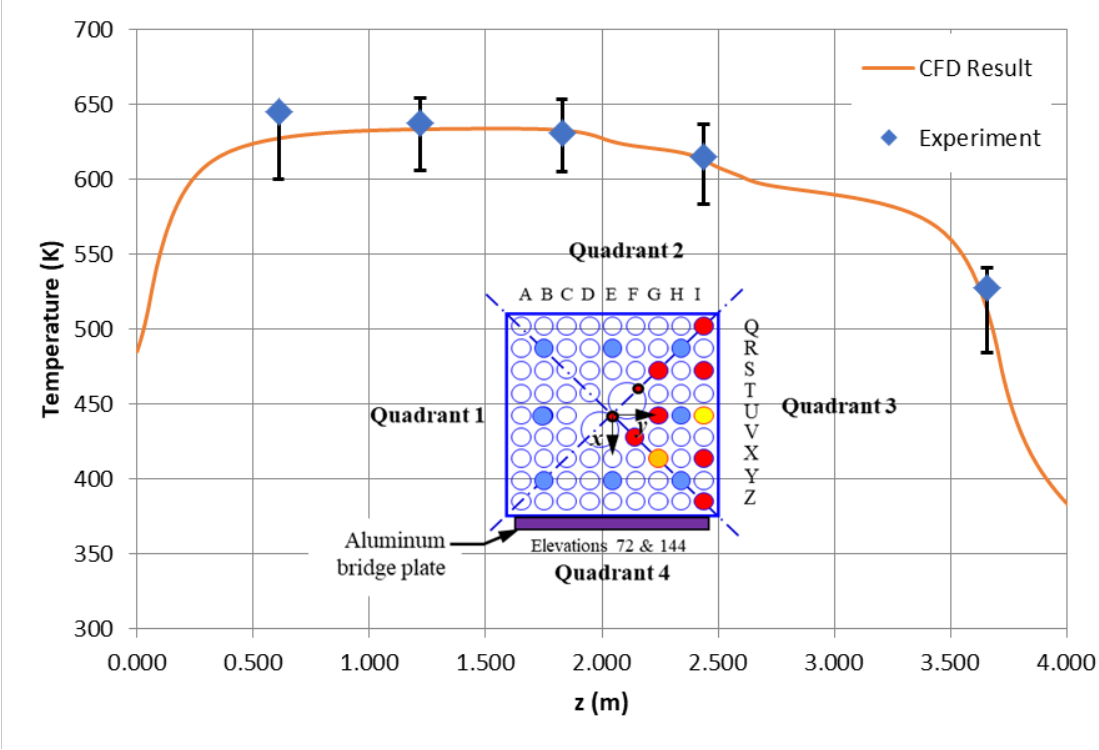

Figure A-25 Axial temperature profile for the 2.5-kW, 100-kPa, air test (open)

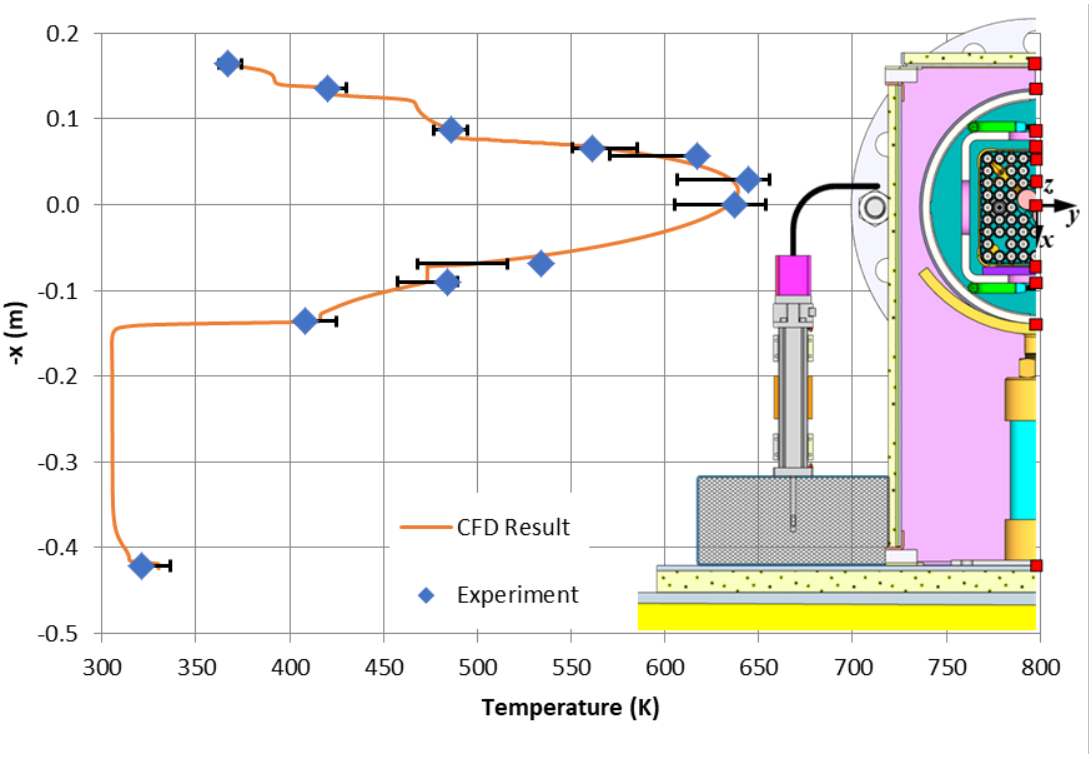

Figure A-26 Vertical temperature profile for the 2.5-kW, 100-kPa, air test (open)

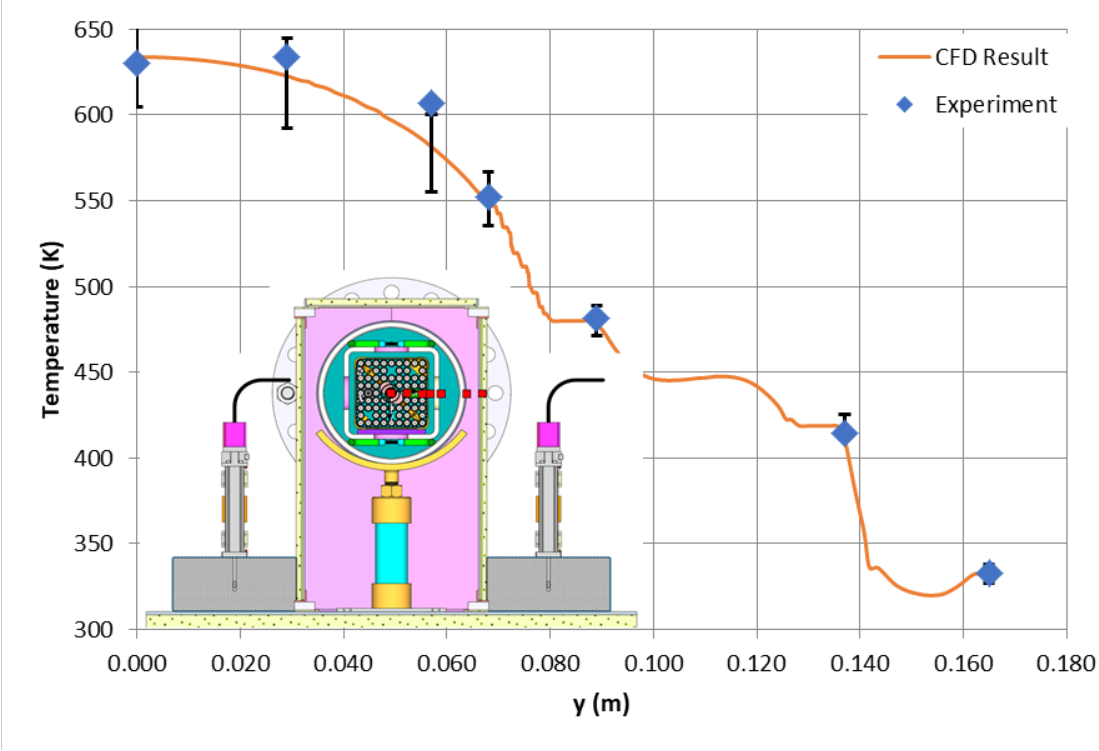

Figure A-27 Horizontal temperature profile for the 2.5-kW, 100-kPa, air test (open)

Table A-10 Blind Test Results for 5.0-kW, 100-kPa, Air

Parameter	Test Result	CFD Result	Positive Uncert.	Negative Uncert.	Compare Error, E	Valid?
Airflow Rate (kg/s)	0.0359	0.0339	0.0015	-0.0014	0.0020	NO
PCT Location						
X value (m)		-0.010	0.035	-0.035		
Y value (m)		0.000	0.036	-0.036		
Z value (m)	0.61	1.589	0.427	-1.065	-0.979	YES
PCT Value (K)	781.9	787.5	28.3	-39.9	-5.6	YES
WEU (x = 0, y = 0)						
z = 0.610 m (K)	778	779.3	27.7	-39.4	-1.1	YES
z = 1.219 m (K)	769	785.0	28.1	-39.7	-15.7	YES
z = 1.829 m (K)	762	784.4	27.7	-39.5	-21.9	YES
z = 2.438 m (K)	744	757.8	31.0	-41.2	-13.7	YES
z = 3.658 m (K)	651	640.7	32.8	-39.5	9.9	YES
Vertical (y = 0 m, z = 1.219 m)						
x = -0.169 m (K)	421	428.9	17.2	-17.5	-8.0	YES
x = -0.137 m (K)	496	510.1	9.9	-9.4	-13.7	NO
x = -0.090 m (K)	585	596.6	14.6	-14.0	-11.2	YES
x = -0.068 m (K)	676	694.6	24.2	-23.1	-18.8	YES
x = -0.057 m (K)	741	727.5	28.4	-31.6	13.4	YES
x = -0.029 m (K)	777	779.6	28.5	-38.8	-2.5	YES
x = 0.000 m (K)	769	785.0	28.1	-39.7	-15.7	YES
x = 0.068 m (K)	655	621.2	28.0	-48.1	33.8	NO
x = 0.090 m (K)	582	578.6	25.8	-24.9	3.1	YES
x = 0.137 m (K)	476	490.9	11.8	-11.2	-14.7	NO
x = 0.421 m (K)	343	364.2	11.4	-11.5	-20.8	NO
Horizontal (x = 0 m, z = 1.829 m)						
y = 0.000 m (K)	762	784.4	27.7	-39.5	-21.9	YES
y = 0.029 m (K)	763	768.1	31.6	-40.5	-5.6	YES
y = 0.057 m (K)	729	712.5	28.5	-31.5	16.6	YES
y = 0.068 m (K)	665	677.8	22.4	-21.4	-12.8	YES
y = 0.089 m (K)	577	586.7	13.3	-12.6	-9.4	YES
y = 0.137 m (K)	486	496.8	7.7	-7.4	-10.9	NO
y = 0.165 m (K)	366	367.9	6.5	-6.4	-2.0	YES

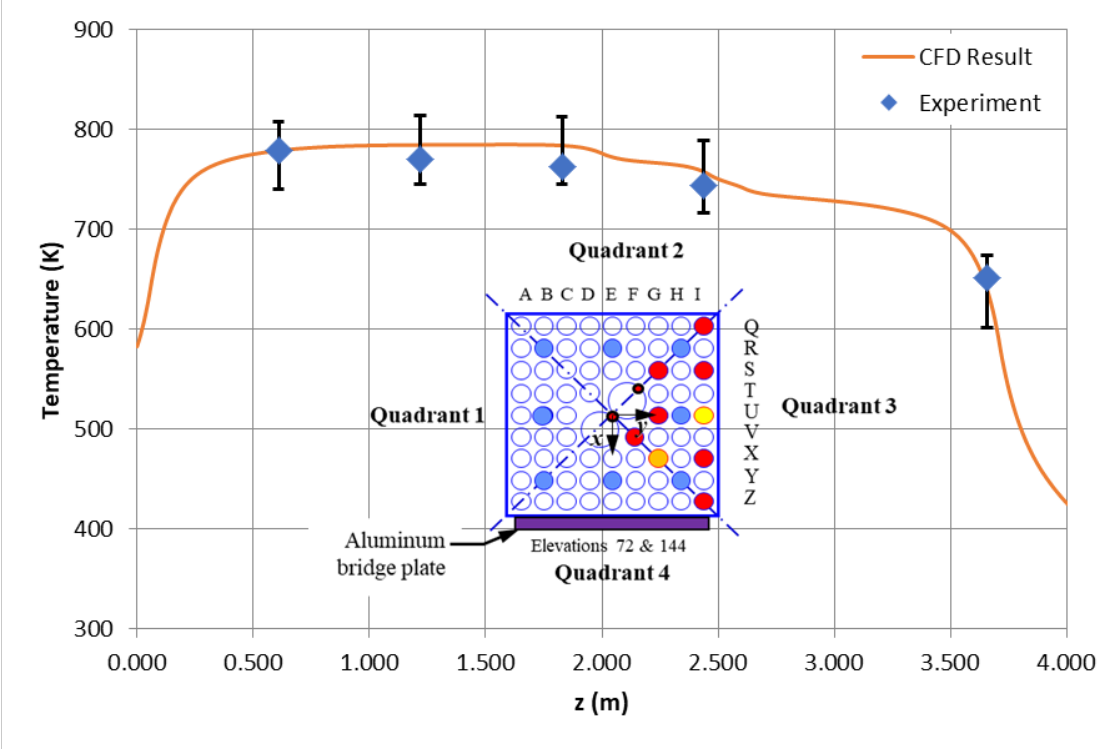

Figure A-28 Axial temperature profile for the 5.0-kW, 100-kPa, air test (blind)

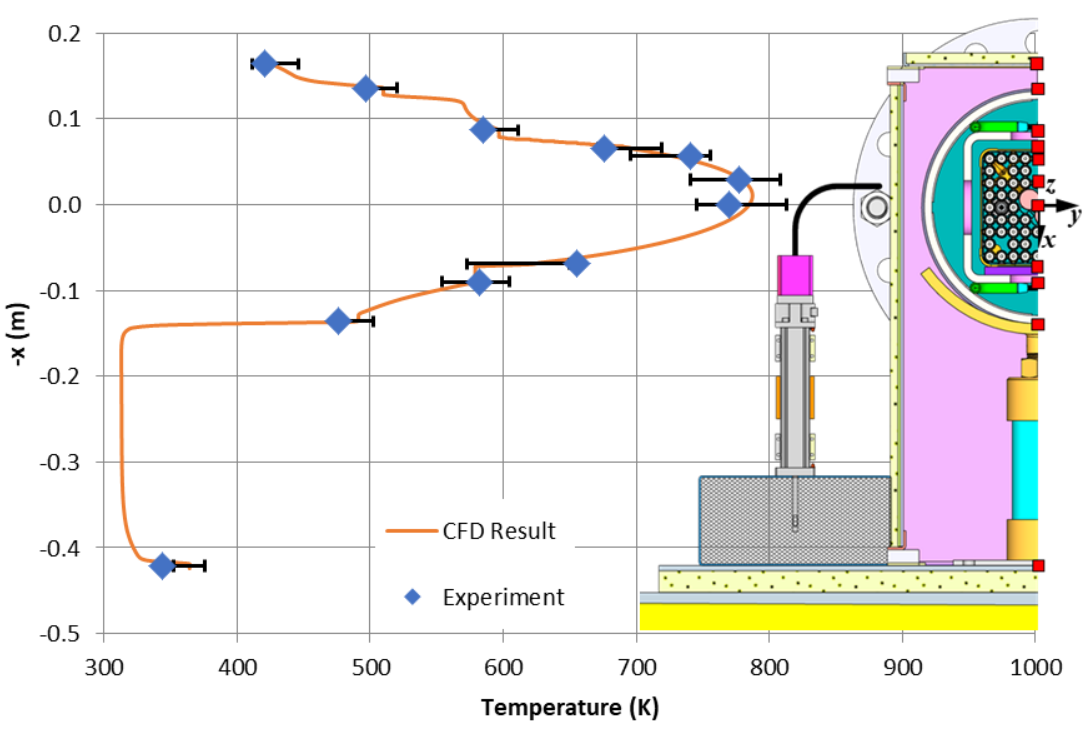

Figure A-29 Vertical temperature profile for the 5.0-kW, 100-kPa, air test (blind)

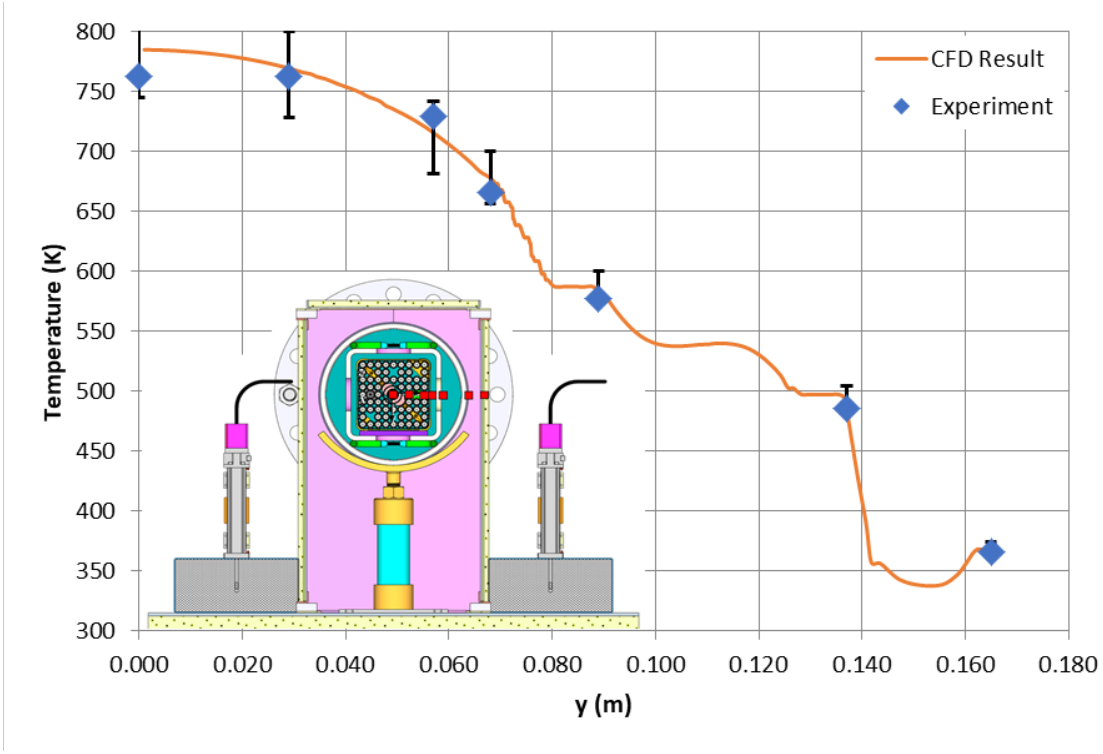

Figure A-30 Horizontal temperature profile for the 5.0-kW, 100-kPa, air test (blind)

NRC FORM 335
(12-2010)
NRCMD 3.7

U.S. NUCLEAR REGULATORY COMMISSION

BIBLIOGRAPHIC DATA SHEET

(See instructions on the reverse)

1. REPORT NUMBER
(Assigned by NRC, Add Vol., Supp., Rev., and Addendum Numbers, if any.)

NUREG/CR-7274

2. TITLE AND SUBTITLE

Validation of a Computational Fluid Dynamics Method Using Horizontal Dry Cask Simulator Data

3. DATE REPORT PUBLISHED

MONTH	YEAR
December	**2020**

4. FIN OR GRANT NUMBER

5. AUTHOR(S)

Kimbal Hall and Abdelghani Zigh

6. TYPE OF REPORT

Technical

7. PERIOD COVERED (Inclusive Dates)

8. PERFORMING ORGANIZATION - NAME AND ADDRESS (If NRC, provide Division, Office or Region, U. S. Nuclear Regulatory Commission, and mailing address; if contractor, provide name and mailing address.)

Alden Research Laboratory
Holden, MA 01520

Office of Nuclear Regulatory Research
U.S. Nuclear Regulatory Commission
Washington, DC 20555-0001

9. SPONSORING ORGANIZATION - NAME AND ADDRESS (If NRC, type "Same as above", if contractor, provide NRC Division, Office or Region, U. S. Nuclear Regulatory Commission, and mailing address.)

Division of System Analysis
Office of Nuclear Regulatory Research
U.S. Nuclear Regulatory Commission
Washington, DC 20555

10. SUPPLEMENTARY NOTES

11. ABSTRACT (200 words or less)

Recent applications have increasingly used thermal-hydraulic analyses using computational fluid dynamics (CFD) codes (e.g., ANSYS-Fluent) to demonstrate the adequacy of the thermal design. The applicants are also seeking to license casks with decay heat close to 50 kilowatts, resulting in a peak cladding temperature (PCT) close to the NUREG-2215 [2] suggested temperature limit of 400 degrees Celsius (752 degrees Fahrenheit). CFD predictions for the PCT or any other target variable should be supported by an uncertainty quantification (UQ) to provide assurance and confidence that the obtained margin is adequate. For this reason, the NRC Office of Nuclear Regulatory Research was part of a dry cask storage system (DCSS) numerical modeling validation study to support regulatory decisions ensuring adequate protection for storage and transportation casks [3]. The NRC recognizes that CFD using finite volume is one of the methods for the applicants to show compliance with the regulations for the thermal response of a DCSS. Additionally, when demonstrating compliance, it is valuable to quantify the uncertainty in the simulation result as a function of the computational mesh and simulation inputs. The NRC led this validation effort to include uncertainty quantification and followed the CFD best practice guidelines in NUREG-2152 [4].

12. KEY WORDS/DESCRIPTORS (List words or phrases that will assist researchers in locating the report.)

Horizontal Dry Cask System (HDCS); HDCS; Spent nuclear fuel; dry storage cask; computational fluid dynamics; validation; verification; CFD-grade experiment; Uncertainty quantification; VVUQ; VV; UQ; ASME V&V 20-2009;

13. AVAILABILITY STATEMENT

unlimited

14. SECURITY CLASSIFICATION

(This Page)
unclassified

(This Report)
unclassified

15. NUMBER OF PAGES

16. PRICE

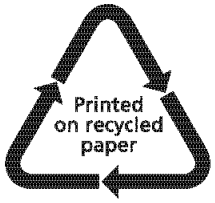

Federal Recycling Program

UNITED STATES
NUCLEAR REGULATORY COMMISSION
WASHINGTON, DC 20555-0001

OFFICIAL BUSINESS